PHILOSOPHICAL TRANSACTIONS OF THE ROYAL SOCIETY A MATHEMATICAL, PHYSICAL & ENGINEERING SCIENCES

Electromagnetic Radiation from a Dipole Source in a Homogeneous Magnetoplasma

Ya. L. Al'pert, K. G. Budden, B. S. Moiseyev and G. F. Stott

Phil. Trans. R. Soc. Lond. A 1983 **309**, 503-557
doi: 10.1098/rsta.1983.0057

Phil. Trans. R. Soc. Lond. A **309**, 503–557 (1983) [503]
Printed in Great Britain

ELECTROMAGNETIC RADIATION FROM A DIPOLE SOURCE IN A HOMOGENEOUS MAGNETOPLASMA

By YA. L. AL'PERT*, K. G. BUDDEN, F.R.S.†, B. S. MOISEYEV* and G. F. STOTT†‡

* *IZMIRAN, p/o Akademgorodok, Moscow Region* 142092, *U.S.S.R.*
† *Cavendish Laboratory, University of Cambridge, Madingley Road, Cambridge CB*3 0*HE, U.K.*

(*Received* 18 *November* 1982)

CONTENTS

‡ Present address: Lloyd's Register of Shipping, London, EC3M 4BS, U.K.

An electric hertzian dipole is immersed in a cold homogeneous magnetoplasma and it is required to calculate the electromagnetic field at a moderate or great distance. Known methods of doing this are reviewed and extended. They all, in effect, express the field as an integral representing an angular spectrum of plane waves or of waves with conical wavefronts. The integral is evaluated by the method of steepest descents and extensions of it. Results are then presented of some calculations for various plasmas containing one or more species of positive ion.

A study is made of the dependence of the radiated field, and of its Poynting vector, on direction and on frequency, when the source dipole is parallel to the superimposed magnetic field. There are three conditions where signals of large or very large amplitude can occur, namely (*a*) enhancement for directions very close to the direction of the superimposed magnetic field, (*b*) resonance cones, in which the signal is large for directions where the refractive index is very large, and (*c*) Storey cones and reversed Storey cones, which may be thought of as conical caustic surfaces where two rays have moved to coalescence and give constructive interference. These three features occur only in certain limited frequency ranges.

The classification of these results is complicated and necessitates discussion of the transition frequencies of the plasma. For a plasma with more than one species of positive ion the phenomenon of crossover occurs, and its effect on the three types of signal enhancement is discussed.

1. INTRODUCTION

The study of the electromagnetic field radiated by an electric hertzian dipole in a cold homogeneous magnetoplasma is important for some radio propagation problems in the ionosphere and magnetosphere and for some problems in laboratory plasmas. Methods of calculating it have been described by Bunkin (1957); Kogelnik (1960); Arbel & Felsen (1963); Mittra & Deschamps (1963); Motz & Kogelnik (1963); Clemmow (1963, 1966); Al'pert & Moiseyev (1980). All these methods in effect express the field as an integral representing an angular spectrum of plane waves, or, in some cases, of waves with conical wavefronts. The integral is then evaluated by the method of steepest descents and extensions of it. These are approximate methods whose accuracy is greatest at large distances, that is in the 'far field'. The results are complicated because of the anisotropy of the plasma. They vary greatly, depending on the type of plasma studied, and on the frequency.

The purpose of this paper is to review and summarize these methods so as to give the essential formulae, and then to present the results of some calculations for various plasmas in which one or more species of positive ion plays an essential part. Most of the results are for a fully ionized proton plasma, but some results for a plasma with three species of positive ion are also included. The calculations were done partly in Moscow, U.S.S.R., and partly in Cambridge, U.K. Where the results overlapped there was satisfactory agreement.

Some results of this kind of calculation for a plasma in which only electrons are effective were given by Arbel & Felsen (1963). Al'pert & Moiseyev (1980) drew attention to three features of

the radiated field which can give rise to signals of large amplitude. These are (*a*) an enhancement of the field for directions very close to the direction of the superimposed magnetic field, (*b*) resonance cones where the signal is large in a narrow range of angle for directions where the refractive index of the principal contributing wave is very large, and (*c*) Storey cones and reversed Storey cones, which may be thought of as conical caustic surfaces where two rays, equivalently two saddle points of the integrand, have moved to coalescence; in a narrow range of angle near these cones the signal has a maximum, often large, because of constructive interference of the two rays. These three features occur only in certain limited frequency ranges. They are discussed in detail in later sections.

In §2 we set out the notation used and summarize the properties of plane waves with a specified direction of the wave normal in a cold homogeneous magnetoplasma. These include the dispersion relation, the refractive indices and the polarizations. They are expressed in terms of the three principal axis elements of the electric permittivity tensor. The main problem is stated in §3. Here the six components of the electromagnetic field are expressed as integrals, when the source is an electric hertzian dipole parallel to the constant magnetic field. The results in this paper apply entirely to this type of source (but see Appendix B).

When the receiver is far enough from the source, the integrals are suitable for evaluation by steepest descents. A method for finding the saddle points, for a given ray direction β, is described in §4. For a saddle point that is far enough from other saddle points and from singularities, the first order formula for steepest descents may be used, and its limitations are reviewed. These techniques are well known, but the present problem has some special points that need discussion. When the refractive index associated with a saddle point approaches infinity, this is called resonance. In §5 it is shown that in many practical cases, when collisions are allowed for, the first order steepest descents formula can still be used. In §6 we deal with the case where two saddle points are close together. This occurs near a Storey cone or reversed Storey cone. It is known that the integral here may be expressed in terms of an Airy integral function and its derivative. Formulae suitable for the present problem are given and their properties are illustrated.

In §7 the fields very close to the axis of the source dipole are considered. It is found (Al'pert & Moiseyev 1980) that for certain forms of the refractive index surface, an enhancement of the field can occur near the axis, and it is dealt with by a modification of the method of steepest descents. Some illustrative results are given and a further possible refinement of the method is described though not used in this paper.

In §8 we describe the method used to classify the results of the later sections. It deals with the possibly controversial question of the meaning to be attached to the terms 'ordinary' and 'extraordinary', and then describes the use of $\beta(\theta)$ curves as a quick and clear way of specifying the topology of the refractive index surfaces. The features of these curves change when the frequency passes through certain transition frequencies which are associated with boundary lines in the C.M.A. diagram. These frequencies are listed in §9 and their properties are summarized.

In §10 we present results for a fully ionized cold proton plasma. It illustrates the dependence of the signal on the ray direction β. The frequency dependence of the enhanced signals for a resonance cone, for Storey cones and reversed Storey cones, and for fields near the axis of the source dipole is then studied. In §11 results are given for a plasma with three species of positive ions. The main new feature here is the appearance of crossover frequencies, which are not present when there is only one species of positive ion. This section is mainly devoted to a study of the

behaviour near crossover, and its effect on resonance cones, Storey cones and axial field enhancement.

In Appendix A a way for dealing with collisions between species is given when allowance is made for the relative velocity of the two colliding species. It is based on a method of Al'pert (1980*b*). In Appendix B we present the formulae for the fields contributed by one saddle point when the source is an electric hertzian dipole perpendicular to the constant magnetic field. Some of their properties have been studied by Stott (1982).

Notation

The following notation is used. The integer subscript $i = 1, 2, 3 \ldots$ is used to number the species of positive ion in order of increasing mass.

$-e$	charge on electron
m, M_i	mass of electron and of ith species of ion
$\boldsymbol{B}$	superimposed magnetic field, magnitude B
$\omega = 2\pi f$	angular frequency of wave
N	concentration of electrons
$\omega_N = (e^2N/\epsilon_0 m)^{\frac{1}{2}}$	angular plasma frequency for electrons (for gaussian units, $\epsilon_0 = 1/(4\pi)$
$\omega_H = eB/m$, $\Omega_i = eB/M_i$	angular cyclotron frequency for electrons and for ith species of ion respectively
ν_e, ν_i	effective collision frequency for electrons and for ith species of ion, respectively, (but see Appendix A)
X	ω_N^2/ω^2
Y_e, Y_i	ω_H/ω, Ω_i/ω
U_e, U_i	$1-i\nu_e/\omega$, $1-i\nu_i/\omega$
C_i	ratio of concentration of ith species of ion to that of electrons
r_i	ratio of mass of electron to mass of ith species of ion.

In the formulae of this paper the various angular frequencies (in rad s^{-1}) ω, Ω are used with appropriate subscripts. But in the presentation of the results, including the figure captions the actual frequencies f, F (in Hz) are used. The subscripts used on f, F are exactly the same as those used on the corresponding ω, Ω.

2. Properties of the plasma

We are concerned with a cold, homogeneous, non-magnetic magnetoplasma. Its properties are conveniently given by its electric permittivity tensor $\boldsymbol{\epsilon}$ which is independent of position. We use both cartesian coordinates x, y, z and cylindrical polar coordinates ρ, ϕ, z. The superimposed magnetic field $\boldsymbol{B}$ is parallel to the z axis. The elements of $\boldsymbol{\epsilon}$ in cartesian coordinates are

$$\boldsymbol{\epsilon} = \begin{bmatrix} \epsilon_{xx} & \epsilon_{xy} & 0 \\ \epsilon_{yx} & \epsilon_{yy} & 0 \\ 0 & 0 & \epsilon_{zz} \end{bmatrix} \tag{1}$$

and from the symmetry of the plasma it follows that

$$\left.\begin{aligned} \epsilon_{xx} &= \epsilon_{yy} = \epsilon_{\rho\rho} = \epsilon_{\phi\phi} \\ \epsilon_{xy} &= -\epsilon_{yx} = \epsilon_{\rho\phi} = -\epsilon_{\phi\rho}. \end{aligned}\right\} \tag{2}$$

It is convenient to diagonalize $\boldsymbol{\epsilon}$ by the unitary transformation (Westfold 1949; Budden 1961).

$$\boldsymbol{\epsilon}_{\mathrm{D}} = \boldsymbol{U}\boldsymbol{\epsilon}\boldsymbol{U}^{-1}, \quad \boldsymbol{U} = 2^{-\frac{1}{2}}\begin{bmatrix} 1 & \mathrm{i} & 0 \\ 1 & -\mathrm{i} & 0 \\ 0 & 0 & 2^{\frac{1}{2}} \end{bmatrix} \tag{3}$$

whence $\boldsymbol{\epsilon}_{\mathrm{D}}$ is 3×3 diagonal with elements ϵ_+, ϵ_-, ϵ_3, given by

$$\epsilon_+ = \epsilon_{xx} - \mathrm{i}\epsilon_{xy}, \quad \epsilon_- = \epsilon_{xx} + \mathrm{i}\epsilon_{xy}, \quad \epsilon_3 = \epsilon_{zz}. \tag{4}$$

The elements of $\boldsymbol{\epsilon}_{\mathrm{D}}$ are

$$\left.\begin{aligned} \epsilon_- &= 1 - X/(U_{\mathrm{e}} + Y_{\mathrm{e}}) - \sum_i C_i r_i X/(U_i - Y_i), \\ \epsilon_+ &= 1 - X/(U_{\mathrm{e}} - Y_{\mathrm{e}}) - \sum_i C_i r_i X/(U_i + Y_i), \\ \epsilon_3 &= 1 - X/U_{\mathrm{e}} - \sum_i C_i r_i X/U_i. \end{aligned}\right\} \tag{5}$$

This is based on a simple treatment of collisions in which it is assumed that each species of ion collides with particles whose average velocity is zero. A better treatment that allows for the relative velocity of colliding particles has been given by Al'pert (1980*b*). It leads to more complicated formulae for ϵ_-, ϵ_+, ϵ_3 given in Appendix A, and to some new properties of the refractive indices.

The dispersion relation of the plasma gives the refractive indices n for a plane wave whose wave normal makes an angle θ with the z axis. The refractive index may be thought of as a vector $\boldsymbol{n}$ with cartesian components

$$n_x = n\sin\theta\cos\varphi, \quad n_y = n\sin\theta\sin\varphi, \quad n_z = m\cos\theta, \tag{6}$$

which define a refractive index space. In this space the vector $\boldsymbol{n}$ always goes through the origin, and it has cylindrical components

$$n_\rho, 0, n_z \quad \text{with} \quad n_\rho = (n_x^2 + n_y^2)^{\frac{1}{2}} = n\sin\theta. \tag{7}$$

One form of the dispersion relation for the plasma is

$$\epsilon_3 n_z^4 + \{n_\rho^2(\epsilon_3 + \epsilon_{xx}) - 2\epsilon_3\epsilon_{xx}\}n_z^2 + \epsilon_{xx}n_\rho^4 - (\epsilon_3\epsilon_{xx} + \epsilon_+\epsilon_-)n_\rho^2 + \epsilon_+\epsilon_-\epsilon_3 = 0. \tag{8}$$

This is a quadratic either for n_ρ^2 or for n_z^2, with the solutions

$$\begin{aligned} n_\rho^2 = \tfrac{1}{2}[&\epsilon_3\epsilon_{xx} + \epsilon_+\epsilon_- - (\epsilon_3 + \epsilon_{xx})n_z^2 \pm \{(\epsilon_{xx} - \epsilon_3)^2 n_z^4 \\ &+ 2(3\epsilon_{xx}^2\epsilon_3 - \epsilon_{xx}\epsilon_3^2 - \epsilon_+\epsilon_-\epsilon_{xx} - \epsilon_+\epsilon_-\epsilon_3)n_z^2 + (\epsilon_{xx}\epsilon_3 - \epsilon_+\epsilon_-)^2\}^{\frac{1}{2}}]/\epsilon_{xx} \end{aligned} \tag{9}$$

$$n_z^2 = \epsilon_{xx} - \tfrac{1}{2}(\epsilon_{xx} + \epsilon_3)n_\rho^2/\epsilon_3 \pm \tfrac{1}{2}\{(\epsilon_{xx} - \epsilon_3)^2 n_\rho^4 + (\epsilon_+ - \epsilon_-)^2\epsilon_3(\epsilon_3 - n_\rho^2)\}^{\frac{1}{2}}/\epsilon_3. \tag{10}$$

Another form of the dispersion relation is

$$n^4(\epsilon_{xx}\sin^2\theta + \epsilon_3\cos^2\theta) - n^2\{\epsilon_+\epsilon_-\sin^2\theta + \epsilon_{xx}\epsilon_3(1 + \cos^2\theta)\} + \epsilon_+\epsilon_-\epsilon_3 = 0. \tag{11}$$

Let the discriminant of this quadratic for n^2 be

$$S = \pm\{\sin^4\theta(\epsilon_+\epsilon_- - \epsilon_{xx}\epsilon_3)^2 + \cos^2\theta\,\epsilon_3^2(\epsilon_+ - \epsilon_-)^2\}^{\frac{1}{2}}. \tag{12}$$

Then the solutions of (11) are

$$n^2 = \frac{\epsilon_+\epsilon_-\sin^2\theta + \epsilon_{xx}\epsilon_3(1 + \cos^2\theta) + S}{2(\epsilon_{xx}\sin^2\theta + \epsilon_3\cos^2\theta)}. \tag{13}$$

The polarization of the wave is defined by

$$\rho = E_\phi / E_\theta \tag{14}$$

where E_ϕ, E_θ are components of the electric field of the wave; E_θ is in the plane ϕ = constant, and perpendicular to the wave normal; E_ϕ is perpendicular to the plane ϕ = constant. Then

$$\mathrm{i}\rho = \frac{\{\epsilon_+\epsilon_- - \tfrac{1}{2}\epsilon_3(\epsilon_+ + \epsilon_-)\}\sin^2\theta + S}{\epsilon_3(\epsilon_- - \epsilon_+)\cos\theta}. \tag{15}$$

The sign of S determines whether the wave is ordinary or extraordinary. This is discussed in § 8.

The two values of n (13), with positive real parts are used, and they are functions of θ and ω. When the notation $n(\theta)$ is used it is here implied that ω is held constant, and similarly $n(\omega)$ implies that θ is held constant.

Let

$$n^2(\epsilon_{xx} + \epsilon_3) + \epsilon_{xx}\epsilon_3 - \epsilon_+\epsilon_- = D. \tag{16}$$

Then, since $n_\rho^2 + n_z^2 = n^2$, it can be shown from (8) that

$$n_\rho^2 = -\epsilon_3(n^2 - \epsilon_-)\,(n^2 - \epsilon_+)/D, \tag{17}$$

$$n_z^2 = (\epsilon_{xx}n^2 - \epsilon_+\epsilon_-)\,(n^2 - \epsilon_3)/D. \tag{18}$$

From (8) it can further be shown that

$$\frac{\mathrm{d}n_z}{\mathrm{d}n_\rho} = n_z' = -\frac{n_\rho}{n_z}\frac{2\epsilon_{xx}n_\rho^2 + (\epsilon_{xx} + \epsilon_3)\,n_z^2 - \epsilon_{xx}\epsilon_3 - \epsilon_+\epsilon_-}{n_\rho^2(\epsilon_{xx} + \epsilon_3) - 2(\epsilon_{xx} - n_z^2)\,\epsilon_3}. \tag{19}$$

These formulae are needed later.

For the above plasma properties, several different notations are in use and some difference between the notation used here and in previous papers is unavoidable. The following table shows the symbols used in the papers most closely related to this.

present paper	Al'pert & Moiseyev (1980)	Budden & Stott (1980)	Stix (1962)
ϵ_-	$\epsilon_1 + \epsilon_2$	ϵ_1	L
ϵ_+	$\epsilon_1 - \epsilon_2$	ϵ_2	R
$\epsilon_3 = \epsilon_{zz}$	ϵ_3	ϵ_3	P
$\epsilon_{xx} = \tfrac{1}{2}(\epsilon_+ + \epsilon_-)$	ϵ_1		S
$\epsilon_{xy} = \tfrac{1}{2}\mathrm{i}(\epsilon_+ - \epsilon_-)$	$-\mathrm{i}\epsilon_2$		$\mathrm{i}D$
n_ρ, n_z	$n_\perp$ $n_\parallel$,	p_x, p_z	

3. Statement of the problem and summary of the formulae

In the homogeneous plasma described in the previous section there is an oscillatory hertzian electric dipole of moment $M\mathrm{e}^{\mathrm{i}\omega t}$ at the origin O. The factor $\mathrm{e}^{\mathrm{i}\omega t}$ will as usual be omitted in future. It is required to find the cartesian components E_x, E_y, E_z and H_x, H_y, H_z of the resulting electric and magnetic fields $\boldsymbol{E}$, $\boldsymbol{H}$ respectively, at a given receiving point P. This may be assumed to be in the plane $y = 0$, with $x \geqslant 0$, since the plasma has rotational symmetry about the z axis. The receiving point is at a distance r from O in a direction at an angle β to the z axis, so that

$$x = r\sin\beta, \quad y = 0, \quad z = r\cos\beta. \tag{20}$$

Since $y = 0$, the components E_x, E_y are the same as E_ρ, E_ϕ and similarly for the components of $\boldsymbol{H}$. For the magnetic field it is convenient to use $\mathscr{H}$ with components

$$\mathscr{H}_j = Z_0 H_j, \quad j = x, y, z, \tag{21}$$

where $Z_0 = (\mu_0/\epsilon_0)^{\frac{1}{2}}$ is the characteristic impedance of free space. Then the $\mathscr{H}_j$ have the same dimensions as the E_j and for a plane wave *in vacuo* $|\mathscr{H}| = |\boldsymbol{E}|$.

This problem can be solved when the source dipole has any of the three orientations parallel to the x, y or z axes. The formulae can then be combined so as to give the fields from a dipole with any orientation. The results in this paper apply only for a dipole parallel to the z axis, but the formulae for the other two orientations are given as well, for completeness, in Appendix B.

Two different but essentially equivalent methods of solving this problem have been used. In the first method Maxwell's equations for the fields are written down including source terms which are known spatial distributions of electric and magnetic currents. Magnetic currents (studied by Motz & Kogelnik 1963) are not included here since they are not needed. The three dimensional spatial Fourier transform of these equations is then taken. This gives six equations for the Fourier transforms of the six field components E_x, E_y, E_z, $\mathscr{H}_x$, $\mathscr{H}_y$, $\mathscr{H}_z$. These equations are solved by inverting the matrix of their coefficients, and the fields are then found by taking the inverse Fourier transform.

Any one Fourier component of the fields can be thought of as a plane wave containing the exponential factor that appears in (22) and (23) where k means ω/c. It is convenient to use the refractive index components (6) as the variables since that is the interpretation they are given later. Let F be a typical one of the six field components and let G be its Fourier transform. Then

$$F(x, y, z) = \iiint G(n_x, n_y, n_z) \exp\{-\mathrm{i}k(xn_x + yn_y + zn_z)\} \mathrm{d}n_x \mathrm{d}n_y \mathrm{d}n_z, \tag{22}$$

$$G(n_x, n_y, n_z) = (k/2\pi)^3 \iiint F(x, y, z) \exp\{\mathrm{i}k(xn_x + yn_y + zn_z)\} \mathrm{d}x \mathrm{d}y \mathrm{d}z. \tag{23}$$

In all these integrals the limits are $\pm\infty$.

The function G, obtained from Maxwell's equations as just described, contains as a factor the Fourier transform $\mathscr{S}$ of the source current distribution. It also contains in the denominator a factor equal to the left hand side of the dispersion relation (8). In simple cases, like those studied here, $\mathscr{S}$ is either independent of n_z, or contains only integer powers of it. Then G is a rational function of n_z, and the n_z integral in (22) can be done by closing the contour with a large semicircle in the lower half of the complex n_z plane. This gives contributions from two poles that occur for two of the solutions (10), and that are associated with two waves with the same n_ρ, both satisfying the dispersion relation (8). The n_x and n_y integrations in (22) can be changed to use n_ρ and φ as the variables. Finally (20) is used and the integral (22) becomes

$$F(r\sin\beta, 0, r\cos\beta) = \sum_{l=1,2} \int_0^\infty \int_0^{2\pi} \mathscr{G}\{n_\rho, n_z^{(l)}, \varphi\} \exp\{-\mathrm{i}kr(n_\rho \sin\beta\cos\varphi + n_z^{(l)}\cos\beta)\} n_\rho \mathrm{d}n_\rho \mathrm{d}\varphi, \tag{24}$$

where the two $n_z^{(l)}$ are the appropriate solutions (10) and $\mathscr{G}$ is $-2\pi\mathrm{i}$ times the residue of G at each pole. The φ dependence of $\mathscr{G}$ is usually simple so that the integral with respect to φ can be expressed in terms of Bessel functions J_m.

This method can be used for any distribution of source currents. For example Motz & Kogelnik (1963) have used it to study the radiation from a modulated ion beam.

The second method (Clemmow 1963, 1966) makes a more direct use of the idea of an angular spectrum of plane waves. It can be used when the source currents are confined to a plane and flow parallel to that plane, which we call the source plane. The two cartesian components of these currents are then expressed as two dimensional Fourier integrals in the source plane. Consider the Fourier component that has wavenumber components k_1, k_2 in the source plane. It gives rise, in the plasma on each side of this plane, to two plane waves travelling outwards. For each of these waves, the six field components are in a fixed ratio which is known and determines the wave polarization and impedance. The amplitudes of the four waves are found from the boundary conditions that apply at the source plane for the four field components parallel to it. The contribution to the fields from the two contributing waves at any point on one side of the source plane are thus found, and the complete fields are then found by taking the inverse Fourier integral with respect to k_1 and k_2.

The authors have used both these methods and have found that they agree. This provides a useful check that the formulae used here are correct.

Results will now be given for the hertzian dipole source with three different orientations, as described at the beginning of this section. The six field components are denoted by

$$E_x, E_y, E_z, \mathscr{H}_x, \mathscr{H}_y, \mathscr{H}_z = F_j, \quad j = 1, \ldots, 6, \tag{25}$$

and the abbreviations

$$kr \sin\beta\, n_\rho = \xi, \quad n^{(l)2} = n_\rho^2 + n_z^{(l)2}, \tag{26}$$

are used. Then for a source dipole parallel to the z axis and for the receiving point $r\sin\beta, 0, r\cos\beta$:

$$F_j = (Mk^3/4\pi\epsilon_0) \sum_{l=1,2} \int_0^\infty \{n_\rho^2(\epsilon_{xx}+\epsilon_3) - 2(\epsilon_{xx} - n_z^{(l)2})\,\epsilon_3\}^{-1} g_j \exp(-ikr\cos\beta\, n_z^{(l)})\, n_\rho^2\, dn_\rho, \tag{27}$$

where the six g_j are

$$\left.\begin{aligned} &(\epsilon_{xx} - n^{(l)2})\,J_1(\xi), \quad \epsilon_{xy} J_1(\xi), \quad i(n_\rho/\epsilon_3 n_z^{(l)})\,(n^{(l)2}\epsilon_{xx} - \epsilon_+\epsilon_-)\,J_0(\xi) \\ &-n_z^{(l)}\epsilon_{xy} J_1(\xi), \quad (\epsilon_+\epsilon_- - n^{(l)2}\epsilon_{xx})\,(n_z^{(l)})^{-1} J_1(\xi), \quad i n_\rho \epsilon_{xy} J_0(\xi). \end{aligned}\right\} \tag{28}$$

When the source dipole is parallel to the x axis, or parallel to the y axis, the field components at the same receiving point are again given by (27) but with different expressions for the g_j. These are not used in the calculations reported in this paper, but for completeness they are set out in Appendix B.

The system of units used here is compatible with the SI, so that if M is in coulomb metres, if k^{-1} and r are in metres and if ϵ_0 has its SI value, then the fields F_j are in volts per metre. The factor $Mk^3/4\pi\epsilon_0$ of (27) appears in all the formulae and will henceforth be omitted for brevity. Thus we write

$$F_i = \mathscr{F}_j\, Mk^3/4\pi\epsilon_0. \tag{29}$$

The $\mathscr{F}_i$ are then the same as the formulae of Al'pert & Moiseyev (1980) who used unrationalized gaussian units.

When the source dipole is parallel to the z axis, the system of fields has complete rotational symmetry about the z axis. The fields (25) and (29) were therefore calculated for the plane $\phi = 0$ and for the range $0 \leqslant \beta \leqslant \frac{1}{2}\pi$. In the discussions, however, it is often necessary to refer to

results with β outside this range. If the fields are known for $\beta = \beta_1$, their values for other related β's are as shown in the following table:

β_1	$-\beta_1$	$\pi-\beta_1$	$\pi+\beta_1$
E_x	$-E_x$	$-E_x$	E_x
E_y	$-E_y$	E_y	$-E_y$
E_ρ	E_ρ	$-E_\rho$	$-E_\rho$

The components of $\mathscr{H}$ with the same subscripts are related in the same way. The components $E_z, \mathscr{H}_z, E_\phi, \mathscr{H}_\phi$ are the same for all four of the cases shown. When the source dipole is not parallel to the z axis, the ϕ dependence of the fields, and the symmetry properties, are more complicated but they are not needed here.

4. Evaluation of the integrals for isolated saddle points

For the integral (27) the integrand is oscillatory because of the exponential factor and of the Bessel functions in (28). Thus it is not easy to evaluate the integral exactly even when a computer is available. But an exact evaluation would be of little use, except in rare cases, because it would be the sum of many different contributions whose relative phases vary rapidly with parameters such as the angle β or the frequency f. It would be a complicated interference pattern and difficult to disentangle. It is therefore best to use the method of steepest descents. This gives separate contributions from the various saddle points or groups of saddle points, and each of these can be given a useful physical interpretation. In a few cases Stott (1982) has evaluated the full integral (27) numerically and has confirmed that it is equal to the sum of the contributions from the saddle points.

In this and the following two sections we consider cases where ξ in (26) is not small, so that the Bessel functions in (28) can be replaced by their asymptotic forms:

$$J_0(\xi) \sim (2\pi\xi)^{-\frac{1}{2}}[\exp\{-\mathrm{i}(\xi-\tfrac{1}{4}\pi)\}+\exp\{\mathrm{i}(\xi-\tfrac{1}{4}\pi)\}], \tag{30}$$

$$J_1(\xi) \sim (2\pi\xi)^{-\frac{1}{2}}\mathrm{i}[\exp\{-\mathrm{i}(\xi-\tfrac{1}{4}\pi)\}-\exp\{\mathrm{i}(\xi-\tfrac{1}{4}\pi)\}], \tag{31}$$

for $|\arg\xi| < \pi$.

If the first terms in each of (30) and (31) are inserted in (28) and if (26) and (29) are used, the integral in (27) gives

$$\mathscr{F}_j = \mathrm{i}e^{\frac{1}{4}\mathrm{i}\pi}(2\pi kr\sin\beta)^{-\frac{1}{2}}\int_0^\infty \{n_\rho^2(\epsilon_{xx}+\epsilon_3)-2(\epsilon_{xx}-n_z^2)\epsilon_3\}^{-1} \times h_j \exp\{-\mathrm{i}kr(n_\rho\sin\beta+n_z\cos\beta)\}n_\rho^{\frac{3}{2}}\,\mathrm{d}n_\rho, \tag{32}$$

where the six h_j are

$$\left.\begin{aligned} &\epsilon_{xx}-n^2, \quad \epsilon_{xy}, \quad (n^2\epsilon_{xx}-\epsilon_+\epsilon_-)\,n_\rho/(\epsilon_3 n_z),\\ &-n_z\epsilon_{xy}, \quad (\epsilon_+\epsilon_- - n^2\epsilon_{xx})/n_z, \quad n_\rho\epsilon_{xy}. \end{aligned}\right\} \tag{33}$$

The superscript (l) has here been omitted. The summation over $l = 1, 2$ in (27) shows that two integrals are implied in (32) but the method for finding the saddle points, described below, finds them for both integrals so that the summation sign is not needed. The integral (32) with (33) is the main formula used for the results in this paper.

If the second terms of (30) and (31) are used instead of the first, the effect in (32) is to replace $\mathrm{i}e^{\frac{1}{4}\mathrm{i}\pi}$ by $-\mathrm{i}e^{-\frac{1}{4}\mathrm{i}\pi}$ and to reverse the sign of n_ρ in the exponent, and to change the signs of the third and sixth terms of (33).

When kr in the exponent of (32) is large enough, the exponential factor is in general a rapidly varying function of n_ρ and is used to find the saddle points. The remaining factors are then treated as slowly varying. The saddle points are given by

$$\sin\beta + \cos\beta\,(\mathrm{d}n_z/\mathrm{d}n_\rho) = 0, \tag{34}$$

which is to be solved for n_ρ.

In a loss free plasma n_ρ and n_z are real for propagated plane waves. The curve of n_ρ against n_z is then a cross section by the plane $\varphi = 0$ of the refractive index surface. This is a surface of revolution about the n_z axis in refractive index space. Equation (34) is the condition that the ray direction $(\sin\beta, 0, \cos\beta)$ shall be an outward normal to the refractive index surface. This property is still true in a plasma with losses, so that it is necessary to use a complex refractive index space, and the solutions of (34) are complex. The theory was given by Budden & Daniell (1965) for a plasma with electrons only, and by Budden & Stott (1980) for a plasma with positive ions. They showed that (34) can be expressed as an equation of degree six for n^2. Each of the six solutions n^2 can then be used to find n_ρ, n_z. The refractive index surface always has two sheets and the method finds the saddle points for both sheets, so that the summation over $l = 1, 2$ in (27) and implied in (32) is taken care of.

The six saddle points do not necessarily all contribute to the integral. To decide which ones contribute it is usually convenient to use physical arguments. It is then useful first to consider a loss free plasma. One method is to construct the refractive index surfaces and the ray surfaces which are reciprocal to them. This method was used by Budden & Daniell (1965). An alternative method used by Al'pert (1980*a*) is to draw curves of β against θ from the formula

$$\beta = \theta - \arctan\,(n^{-1}\,\mathrm{d}n/\mathrm{d}\theta), \tag{35}$$

where β is the angle between the group velocity vector $\mathrm{d}\omega/\mathrm{d}\boldsymbol{k}$ and the magnetic field $\boldsymbol{B}$. Equation (35) is equivalent to (34). Some examples are given in figures 11 and 12. For a given β the values of θ for real saddle points can be read from the curves, and then n, n_ρ, n_z are found from the dispersion relation. These methods show that, at some saddle points, n_ρ is real and negative. They are points of stationary phase on the negative real n_ρ axis. The contour in (32) begins at $n_\rho = 0$ and runs along the positive real axis, which suggests that the saddle points with negative n_ρ should not be included. But when the integral (32) is modified to use the second terms of (30) and (31) the effect is to change the sign of n_ρ in (34). Thus these saddle points occur in the modified integral for positive n_ρ and so they must be retained, with the signs of h_3 and h_6 reversed and with $\mathrm{i}\mathrm{e}^{\frac{1}{4}\mathrm{i}\pi}$ replaced by $-\mathrm{i}\mathrm{e}^{-\frac{1}{4}\mathrm{i}\pi}$.

To complete the evaluation of (32) by steepest descents the value of $\mathrm{d}^2n_z/\mathrm{d}n_\rho^2 = n_z''$ is needed. It can be found from (8) or (10) and is in general complicated, but since it is needed only at the saddle point, (34) can be used and the result is

$$n_z'' = \frac{n_\rho AB}{n_z^2 \sin\beta\cos\beta\,\{n_\rho^2(\epsilon_{xx}+\epsilon_3) - 2(\epsilon_{xx}-n_z^2)\,\epsilon_3\}^2}, \tag{36}$$

where

$$A = 2\epsilon_{xx}n_\rho^2 + (\epsilon_{xx}+\epsilon_3)\,n_z^2 - \epsilon_{xx}\epsilon_3 - \epsilon_+\epsilon_- \tag{37}$$

and

$$B = 4(\epsilon_{xx}+\epsilon_3)\,n_\rho n_z \sin\beta\cos\beta - \{6\epsilon_{xx}n_\rho^2 + (\epsilon_{xx}+\epsilon_3)\,n_z^2 - \epsilon_{xx}\epsilon_3 - \epsilon_+\epsilon_-\}\cos^2\beta$$
$$- \{6\epsilon_3 n_z^2 + (\epsilon_{xx}+\epsilon_3)\,n_\rho^2 - 2\epsilon_{xx}\epsilon_3\}\sin^2\beta. \tag{38}$$

Then the first order steepest descents contribution to (32) from each saddle point is

$$\mathscr{F}_{js} = (kr)^{-1}\,\mathscr{S} n_\rho n_z (AB)^{-\frac{1}{2}}\,h_j \exp\{-\mathrm{i}kr\,(n_\rho\sin\beta + n_z\cos\beta)\}, \tag{39}$$

PHILOSOPHICAL TRANSACTIONS OF THE ROYAL SOCIETY A MATHEMATICAL, PHYSICAL & ENGINEERING SCIENCES

where n_ρ, n_z now take their values at the saddle point, and the h_j are given by (33). The factor $\mathscr{S}$ has modulus unity. It depends on arg (n_z'') and on whether the first or the second asymptotic form in (30) and (31) is used. For a loss free plasma, and for saddle points with real n_ρ and n_z, its values are as follows:

asymptotic term in (30), (31):	first	first	second	second
sign of n_z'':	+	−	+	−
value of $\mathscr{S}$:	i	−1	−1	−i

For a plasma with losses, and for complex saddle points, its value must be decided by studying the direction of the line of steepest descents through the saddle point. When only the moduli or the ratios of the fields are studied, it is not necessary to know $\mathscr{S}$.

In using the contribution (39) it is assumed that the end $n_\rho = 0$ of the contour of integration is not too close to the saddle point. The condition for this is that at the saddle point

$$krn_z''n_\rho^2\cos\beta \geqslant 2, \tag{40}$$

which can be violated if n_ρ^2 is too small. Some properties of the integral (27) in this case are discussed by Stott (1982). It is not violated when $\cos\beta = 0$ because (36) shows that n_z'' has a factor $(\cos\beta)^{-1}$.

The formula (39) was used for many of the calculations reported in later sections. Other versions of it can be derived by using the dispersion relation (8) and equation (34). Various alternatives have been derived independently by the authors in Moscow and in Cambridge and found to be algebraically equivalent.

Apart from the usual approximations of the first order saddle point method, no approximations were used in deriving (39) and therefore there is no restriction on the frequency range for which it is valid. But it does use the asymptotic approximations (30) and (31) for the Bessel functions. Thus when their argument ξ (26), is less than about 2, the formula (39) is not reliable. Methods of dealing with smaller values of ξ are described in §7.

The contribution (39) is proportional to $1/r$ and may be thought of as part of the radiation field of the dipole. The formula is most accurate when r is large and when the saddle point is not too close to any other saddle point; we then say that the saddle point is 'isolated'. The field for two saddle points close together is derived in the following section.

A more accurate expression for the field of an isolated saddle point can be found by taking the method of steepest descents to a higher order. This is equivalent to finding the second term of the asymptotic series that must multiply (39). When this second term is small compared to the first, it is safe to use the expression (39) alone. This second term is proportional to $1/r^2$, and may be thought of as part of the storage field of the dipole source. The second terms of the asymptotic approximations (30) and (31) also lead to contributions proportional to $1/r^2$ and must be included. They are $\pm\frac{1}{8}\mathrm{i}/\xi$ for the two terms in (30) and $\pm\frac{3}{8}\mathrm{i}/\xi$ for the two terms in (31).

If the integral in (32) is written

$$\int_0^\infty \psi(n_\rho)\exp\{-\mathrm{i}kr(n_\rho\sin\beta + n_z\cos\beta)\}\,\mathrm{d}n_\rho, \tag{41}$$

then the second order approximation to (39) is got by multiplying it by

$$1+\frac{\mathrm{i}}{kr\cos\beta}\left\{\frac{n_z''''}{8(n_z'')^2}-\frac{5}{24}\frac{(n_z''')^2}{(n_z'')^3}-\frac{1}{2}\frac{\psi''}{\psi n_z''}+\frac{1}{2}\frac{\psi' n_z'''}{\psi(n_z'')^2}\right\}+\frac{\mathrm{i}R}{kr\sin\beta\, n_\rho}, \tag{42}$$

where R is $+\frac{1}{8}$ for $j = 3$ or 6 and $-\frac{3}{8}$ for $j = 1, 2, 4, 5$. The first two terms in brackets $\{\}$ are given by Morse & Feshbach (1953, part I, p. 442), for the case where $\psi = 1$. The next two terms can be derived from their formulae.

The expression (42) is very complicated to calculate and is different for the six values of j in (32) but it has been used for testing in a few cases. A quicker alternative but less reliable way of assessing the accuracy of (39) is to examine $\mathrm{Re}\{kr(n_\rho \sin\beta + n_z \cos\beta)\}$ at the saddle point. This may be called the phase of the radiation field. For a dipole in free space the storage fields are less than about 5% of the radiation fields for distances exceeding six free space wavelengths, that is when the phase of the radiation field exceeds 12π. Thus if the phase for (39) exceeds about 12π and differs by more than 12π from the phase for other saddle points, it is reasonably safe to assume that (39) can be used with an accuracy of 5% or better. It may be permissible to use a smaller value of the phase for saddle points near a resonance cone (see end of §5).

The result (39) for the six field components (25) can be used to find the time averaged Poynting vector

$$\boldsymbol{\Pi} = \tfrac{1}{4} Z_0^{-1} (\boldsymbol{E}^* \wedge \mathscr{H} + \boldsymbol{E} \wedge \mathscr{H}^*). \tag{43}$$

The ratios of the field components (25), as given by (33), are the same as for a plane wave. It has been shown (Al'pert 1946, 1948) that for a progressive wave with a real n in a loss free medium $\boldsymbol{\Pi}$ has the same direction as the group velocity $\mathrm{d}\omega/\mathrm{d}\boldsymbol{k}$, that is as the ray. In all cases tested this was found to be true. It provides a useful check of the algebra and of the computer programs. For a plasma with losses n is complex, so that the wave is inhomogeneous and the result is no longer exactly true. But Suchy (1972) has shown that when $-\mathrm{Im}(n) \ll \mathrm{Re}(n)$, $\boldsymbol{\Pi}$ has the same direction as $\mathrm{Re}(\mathrm{d}\omega/\mathrm{d}\boldsymbol{k})$. Some examples where $\boldsymbol{\Pi}$ is not parallel to the ray are given later, in §5. For a loss free plasma some solutions of (34) can refer to an evanescent wave so that $\boldsymbol{n}$ is imaginary. It can then be shown from the ratios (33) that $\Pi_x = \Pi_z = 0$. Thus $\boldsymbol{\Pi}$ is perpendicular both to the ray and to the magnetic field $\boldsymbol{B}$. A specific example of this property was given by Budden (1961). This result is illustrated later, at the end of §5.

5. Evaluation of the integrals for resonance

The solution n^2 derived from (34) can be infinite for some values $\theta = \theta_r$ and $\beta = \beta_r$ and this defines a resonance cone. It occurs when the coefficient of n^4 in (11) is zero and this gives

$$\tan^2\theta_r = -\epsilon_3/\epsilon_{xx}. \tag{44}$$

It can be shown from (11) and (35) that, at resonance

$$\theta_r - \beta_r = \pm\tfrac{1}{2}\pi, \tag{45}$$

so that

$$\tan^2\beta_r = -\epsilon_{xx}/\epsilon_3, \tag{46}$$

and when $\tan\beta_r$ and $\tan\theta_r$ are real, they have opposite signs. From (46) it follows that there cannot be more than one resonance in the quadrant $0 \leqslant \beta_r \leqslant \frac{1}{2}\pi$. Here we consider only values of β and β_r in this range. For real β_r and a loss free plasma, the value of n^2 that shows the resonance is real and positive when β is on one side of β_r, and this is called the illuminated side. If it is where $\beta < \beta_r$, then β_r is called a (forward) resonance cone, and this occurs if $\epsilon_3 < 0$ (figure 1*a*). The other side is called the dark side and here n^2 is real and negative. When $\epsilon_3 > 0$ the illuminated side occurs where $\beta > \beta_r$ and then β_r is called a reversed resonance cone (figure 1*b*).

Equations (16)–(18) show that as $n \to \infty$, both n_ρ and n_z are of the same order as n and both $\to \infty$ but their ratio $n_\rho/n_z = \tan\theta$ remains bounded and is found from (44). Equations (36)–(38) show that n_z'' is of order $1/n$ and tends to zero as resonance is approached. This means that the curvature of the refractive index surface approaches zero as illustrated in figure 1. Then some of the terms after the first in (42) become large near resonance, and therefore the first order saddle point method of §4 fails. A more accurate formula than (39) would be needed and a method of deriving it is outlined below.

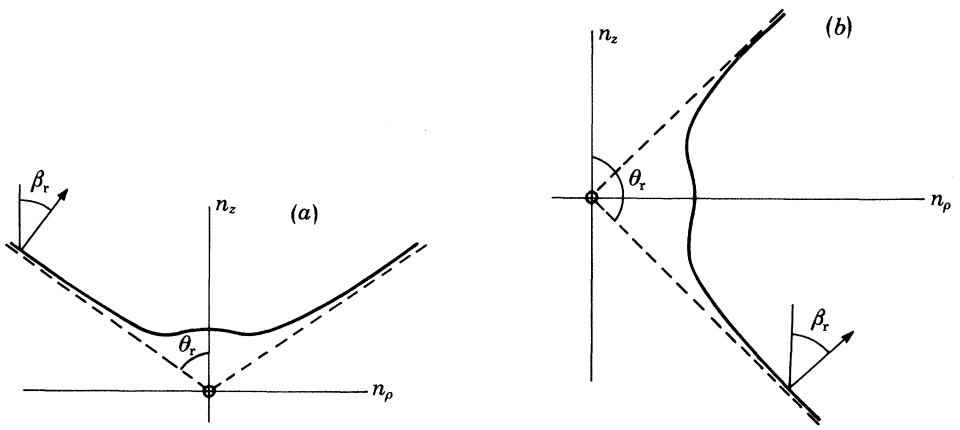

FIGURE 1. Cross sections by a plane ϕ = constant of typical refractive index surfaces for a loss free plasma with a resonance cone. The marked values are only those in the range $0 \leqslant \beta_r \leqslant \frac{1}{2}\pi$. (*a*) Shows a (forward) resonance cone and occurs, for example, for the electron whistler mode. (*b*) Shows a reversed resonance cone and occurs, for example, for the Z mode. The $\beta(\theta)$ curves for both these cases are given in §8.

For the illuminated side of a resonance, the value of n_ρ, found from (34), for the saddle point is real and positive so that it is on the contour of integration and contributes to the integral (32). For the dark side, the value of n_ρ is purely imaginary. It is shown below that this saddle point now gives a very small contribution.

If the effect of collisions is allowed for, ϵ_-, ϵ_+, ϵ_3 are complex and (46) shows that β_r is complex. For real β, therefore, exact resonance is never reached, and the transition from the illuminated to the dark side of resonance is continuous. In the cases discussed later, §§10 and 11, it turns out that the first order saddle point result (39) can be used for all real β going right through the value $\mathrm{Re}(\beta_r)$. The contribution (39) goes to a maximum value for β near $\mathrm{Re}(\beta_r)$ and falls rapidly to zero on the dark side. A demonstration of this is now to be given in outline.

When n_ρ is large, the form (8) of the dispersion relation can be used to express n_z as a series in descending powers of n_ρ and it can be shown that the even powers are zero. Thus

$$n_z = -n_\rho \tan\beta_r + C/n_\rho + O(n_\rho^{-3}), \tag{47}$$

where

$$C = \{\epsilon_{xx}^2 - \tfrac{1}{2}(\epsilon_+\epsilon_- + \epsilon_3\epsilon_{xx})\}/\{(\epsilon_{xx} - \epsilon_3)\tan\beta_r\}. \tag{48}$$

In the example of figure 1*a*, C is negative and in figure 1*b* it is positive. We shall discuss the case of figure 1*b* so that the required integral is (32). For the case of figure 1*a* it would be necessary to reverse the sign of n_ρ in (32) as explained in §4. If (47) is substituted in (32) and if the terms $O(n_\rho^{-3})$ are neglected, the integral takes the form

$$\int_0^\infty T(n_\rho)\exp[-ikr\cos\beta\{n_\rho(\tan\beta - \tan\beta_r) + C/n_\rho\}]\,\mathrm{d}n_\rho. \tag{49}$$

The function $T(n_\rho)$ can also be expanded in descending powers of n_ρ, and (32) and (33) show that the powers are all half an odd integer. Thus we consider the contribution from one term

$$\int_0^\infty n_\rho^M \exp\left[-ikr\cos\beta\{n_\rho(\tan\beta-\tan\beta_r)+C/n_\rho\}\right]\mathrm{d}n_\rho, \tag{50}$$

where M is half an odd integer, and $M \leqslant \frac{3}{2}$. This is a standard integral representation of a Hankel function (Watson 1944, §6.21) and can be shown to be proportional to

$$H^{(2)}_{M+1}(2krE), \tag{51}$$

where

$$E = \cos\beta\{C(\tan\beta-\tan\beta_r)\}^{\frac{1}{2}}. \tag{52}$$

Thus the integral of (32) is expressed as a series of Hankel functions all with the same argument as (51). When exact resonance is approached E tends to zero and the Hankel functions tend to infinity. A small value of krE effectively means that the near field (storage field) of the source extends out to the receiver (Arbel & Felsen 1963). This is illustrated by the small values of the phase when β is near to β_r (see figure 2). The exponent in (39) is $-ikrn\cos(\theta-\beta)$. It was shown by Budden & Stott (1980, §4.3) that $n\cos(\theta-\beta)$ tends to zero as resonance is approached. The wave normal is almost perpendicular to the ray because $\theta-\beta\to\frac{1}{2}\pi$, and this more than compensates for the large n. Thus the rate of change of phase is very small in the direction of the ray.

When E is large enough, the Hankel function (51) can be replaced by its asymptotic form, which contains the exponential factor

$$\exp(-2ikrE). \tag{53}$$

The condition for this to be valid to within about 6% is

$$|krE| \geqslant 1. \tag{54}$$

The exponent in (53) is the same as the exponent in the integrand of (50) at the saddle point of the integral. The resulting expression is then the same as the first order steepest descents value of (49) and very close to the value of (39) at the resonance saddle point. In the calculations reported later the condition (54) was satisfied in nearly all cases, so that (39) was adequate and it was not necessary to use the expression with Hankel functions.

The criterion (54) is much less stringent than the condition, mentioned near the end of §4, that the phase of the wave should exceed about 12π. But that condition was derived from a crude argument based on properties of the radiation and storage fields in free space. The fields near a resonance cone have very different behaviour from the fields in free space or for isolated saddle points not near resonance, so it is not surprising that a different criterion of accuracy is used.

On the illuminated side of resonance, $\tan\beta > \tan\beta_r$ (figure 1*b*) and $\mathrm{Re}(E)$ is positive. The Hankel functions (51) are oscillatory. On the dark side E is almost negative imaginary and (53) shows that the Hankel functions, and thence the value of (49), are small and decrease rapidly as $|\tan\beta-\tan\beta_r|$ increases.

This explanation has been given for a reversed resonance as in figure 1*b*. The behaviour for a forward resonance is similar, except that the illuminated side is where $\beta < \beta_r$.

Some results illustrating these features, for a forward resonance, are shown in figure 2 which is for a cold fully ionized proton plasma. It is seen, as expected, that when the collision frequency is decreased, the resonance cone becomes narrower and more intense. In most of the results reported later a range of 100 km or more and an electron collision frequency $\nu_e = 100\,\mathrm{s}^{-1}$ were

used. For this value in figure 2 (top curve) the phase is never less than about 4 radians so the condition (54) is well satisfied. Results from this example are included in figure 18. Further results similar to those of figure 2 are given by Al'pert & Moiseyev (1980).

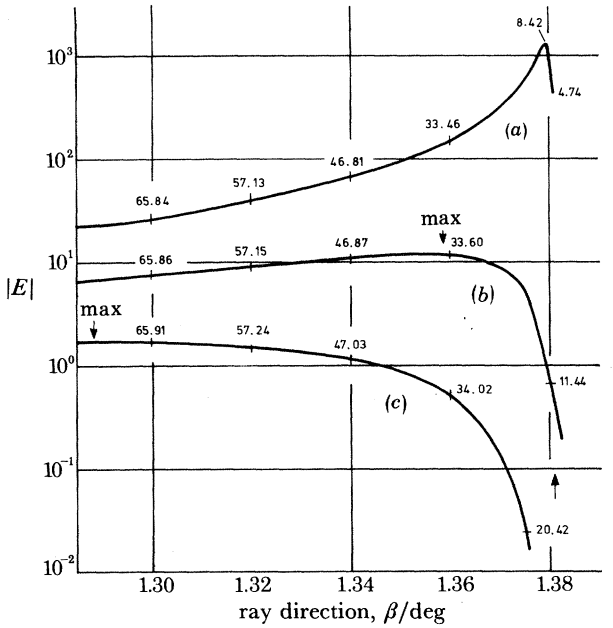

FIGURE 2. Dependence of $|E|$, equation (117) §10, on ray direction β near a forward resonance cone in a cold fully ionized proton plasma. In this example $f_H = 1.1937$ MHz, $f_N = 2.3874$ MHz, the frequency is $f = 3.5811 \times 10^4$ Hz and the receiver is 100 km from the source. For a collisionless plasma the real resonance cone angle would be $\beta_r = 1.381°$. The electron collision frequencies ν_e used for the three curves were (*a*) 100 s^{-1}, (*b*) 500 s^{-1}, (*c*) 1000 s^{-1}. All other collision frequencies were zero. The numbers by the curves are the real part of the phase of the received signal, in radians.

On the illuminated side of a resonance cone in a loss free plasma the formula (39) applies for a progressive wave so that the time averaged Poynting vector $\boldsymbol{\Pi}$ has the direction of the ray (see end of §4). On the dark side the wave is evanescent and $\boldsymbol{\Pi}$ is perpendicular both to the ray and to $\boldsymbol{B}$. When collisions are included, as in figure 2, the wave is never perfectly progressive or perfectly evanescent. The transition from an almost progressive wave to an almost evanescent wave would be expected to be gradual as β moves through β_r. In the example of figure 2 and in other examples studied it was found that for all β the angle

$$\beta' = \arctan(\Pi_x/\Pi_z), \tag{55}$$

was very close to β. The difference was always less than 0.0005°, for the example of figure 2. Thus the projection of $\boldsymbol{\Pi}$ on the x–z plane is always close to the ray direction. But $\boldsymbol{\Pi}$ has a component Π_y which is small for angles β well on the illuminated side, and large on the dark side where the wave is approaching evanescence. The angle γ between $\boldsymbol{\Pi}$ and its projection on the x–z axis plane is given by

$$\gamma = \arctan\{\Pi_y/(\Pi_x^2+\Pi_z^2)^{\frac{1}{2}}\}. \tag{56}$$

Some typical values for the example of figure 2 were as follows.

For curve (*a*), $\nu_e = 100\,s^{-1}$:

β/deg:	1.30	1.32	1.34	1.36	1.37	1.38
γ/deg:	0.34	0.46	0.68	1.34	2.57	25.89.

For curve (*c*), $\nu_e = 1000\,s^{-1}$:

β/deg:	1.30	1.32	1.34	1.36	1.37
γ/deg:	3.42	4.54	6.73	12.72	21.92.

6. Evaluation of the integrals when two saddle points are close together

A value β_s of β where two solutions of (34) are equal defines a cone called a Storey cone (Storey 1953). Here the refractive index surface has a point of inflexion so that

$$d^2 n_z / dn_\rho^2 = 0 \tag{57}$$

and two branches of the ray surface meet in a cusp. The curve of β against θ, figures 11 and 12, has a turning point, and two saddle points of the integrand of (32) coalesce. For directions near this, the fields are expressed in terms of an Airy integral function and its derivative (Arbel & Felsen 1963; Al'pert & Moiseyev 1980) and the formulae are derived in this section. On one side of a Storey cone the values of n at the two saddle points are almost real and close to the value for $\beta = \beta_s$. This is called the illuminated side. The contour of integration must be distorted to go through both saddle points. On the other side, the two values of n are approximately complex conjugates and this is called the dark side. The contour of integration goes through only one of the saddle points, namely the one whose contribution has the smaller modulus. The case where the illuminated side has $\beta > \mathrm{Re}(\beta_s)$ is called a reversed Storey cone.

The contribution from these two saddle points can be found by the method of Chester *et al.* (1957). Consider the integral in the form (32) or (41) and suppose that the exponential has two saddle points where

$$n_\rho = n_{\rho a},\ n_{\rho b}, \tag{58}$$

which are close together in a sense to be explained. On the illuminated side, these are approximately real and it is assumed that $\mathrm{Re}(n_{\rho b}) > \mathrm{Re}(n_{\rho a})$. On the dark side they are approximately complex conjugates and it is assumed that $\mathrm{Im}(n_{\rho b}) > \mathrm{Im}(n_{\rho a})$. Subscripts a, b will henceforth be used to denote values at these two saddle points. Change to a new variable of integration τ so that

$$-ikr(n_\rho \sin\beta + n_z \cos\beta) \equiv -iP = -iA_0 + \eta^2\tau - \tfrac{1}{3}\tau^3. \tag{59}$$

Choose τ and the constants A_0 and η^2 so that the saddle points of the right hand expression are the same as (58). Then

$$\left.\begin{aligned} \text{for} \quad & n_\rho = n_{\rho a}, \quad \tau = \eta, \quad && \text{let } P = P_a, \\ \text{and for} \quad & n_\rho = n_{\rho b}, \quad \tau = -\eta, \quad && \text{let } P = P_b. \end{aligned}\right\} \tag{60}$$

Hence

$$A_0 = \tfrac{1}{2}(P_a + P_b), \quad \tfrac{2}{3}\eta^3 = -\tfrac{1}{2}i(P_a - P_b). \tag{61}$$

The integral (41) becomes

$$\begin{aligned} J &= \fint \psi(n_\rho) \exp(-iP)\, dn_\rho \\ &= \exp(-iA_0) \int_{l_1}^{l_2} \psi(n_\rho)\, (dn_\rho/d\tau) \exp(\eta^2\tau - \tfrac{1}{3}\tau^3)\, d\tau, \end{aligned} \tag{62}$$

where $\fint$ means that the range of integration is restricted so as to include only the contribution from the two saddle points (58). The limits l_1, l_2 are discussed below.

The function $P(n_\rho)$ is approximately a real cubic function of n_ρ. If it were an exact cubic, (59)–(61) show that τ would then be a linear function

$$\tau \approx \eta(2n_\rho - n_{\rho a} - n_{\rho b})/(n_{\rho a} - n_{\rho b}), \tag{63}$$

of n_ρ. Then the two values of

$$\partial^2 P/\partial n_\rho^2 = kS_a, kS_b \tag{64}$$

at the two saddle points (58) would satisfy

$$S_a = -S_b. \tag{65}$$

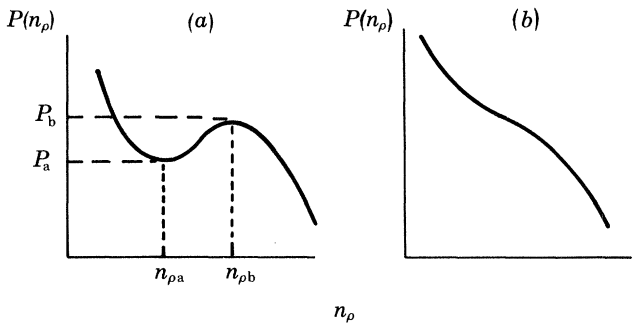

FIGURE 3. The function $P(n_\rho)$ for a loss free plasma. Curve (a) is for the illuminated side of a Storey cone and curve (b) is for the dark side. In this example $S_a = -S_b$ is positive for curve (a), and positive imaginary for curve (b).

In practical cases this is only approximately true and two slightly different values must be used. Figure 3a is a sketch of the function $P(n_\rho)$ for positive S_a on the illuminated side of a Storey cone, and figure 3b is the same function on the dark side. Comparison with (59) and (60) shows that on the illuminated side, approximately

$$\eta^3 \text{ is positive imaginary; } \eta \text{ is negative imaginary; } \eta^2 \text{ is real and negative,} \tag{66}$$

and on the dark side, approximately

$$\eta^3 \text{ is real and negative; } \eta \text{ is real and negative; } \eta^2 \text{ is real and positive.} \tag{67}$$

In both cases, the coefficient $\eta/(n_{\rho a} - n_{\rho b})$ in (63) is almost positive imaginary. Thus the real n_ρ axis contour in (41) maps into the imaginary τ axis in (62).

When $\mathrm{Re}(S_a)$ is negative on the illuminated side, the treatment is similar and need not be given. The only difference is that the sign of η is reversed.

The factor $\psi\, \mathrm{d}n_\rho/\mathrm{d}\tau$ in (62) is now assumed to be a slowly varying function of τ in comparison with the exponential. Its values and derivatives are here used only at the two saddle points. This is equivalent to assuming that for large $\pm \mathrm{i}\tau$ the exponential term dominates and here it makes the integrand very small. This assumption is not always true but then the contributions for large $|\tau|$ are those from other saddle points of (41) and these are evaluated separately. Thus for the Storey cone contribution only, the limits in (62) are set at

$$l_1 = -\mathrm{i}\infty, \quad l_2 = +\mathrm{i}\infty. \tag{68}$$

Now let

$$\psi\, \mathrm{d}n_\rho/\mathrm{d}\tau = G(n_\rho) = p_0 + p_1(\tau^2 - \eta^2) + p_2(\tau^2 - \eta^2)^2 + \ldots + \tau\{q_0 + q_1(\tau^2 - \eta^2) + q_2(\tau^2 - \eta^2)^2 + \ldots\}. \tag{69}$$

Then

$$\left.\begin{aligned} \text{for} \quad \tau = \eta, \quad & p_0 + \eta q_0 = G_a, \\ \text{and for} \quad \tau = -\eta, \quad & p_0 - \eta q_0 = G_b, \end{aligned}\right\} \tag{70}$$

so that

$$p_0 = \tfrac{1}{2}(G_a + G_b), \quad q_0 = \tfrac{1}{2}\eta^{-1}(G_a - G_b). \tag{71}$$

Higher coefficients p_1, q_1 etc. in (69) could be found if needed, but they are not used here. They could be used to find asymptotic series multiplying the two terms in (76) below.

Expand both sides of (59) in powers of $\delta\tau = \tau - \tau_s$ about each saddle point τ_s in turn, as far as the squared terms. Then

$$\left.\begin{aligned} -\tfrac{1}{2}\mathrm{i}kS_a(n_\rho - n_{\rho a})^2 &= -\eta\delta\tau^2, \\ -\tfrac{1}{2}\mathrm{i}kS_b(n_\rho - n_{\rho b})^2 &= \eta\delta\tau^2. \end{aligned}\right\} \tag{72}$$

Hence

$$\mathrm{i}\partial n_\rho/\partial\tau = \begin{cases} (2\mathrm{i}\eta/kS_a)^{\frac{1}{2}} & \text{at} \quad n_\rho = n_{\rho a} \\ (-2\mathrm{i}\eta/kS_b)^{\frac{1}{2}} & \text{at} \quad n_\rho = n_{\rho b} \end{cases} \tag{73}$$

and from (65) with (66) and (67) it can be shown that these are approximately equal, real and positive. From (69), (70), (71):

$$\left.\begin{aligned} \mathrm{i}p_0 &= \tfrac{1}{2}\{\psi_a(2\mathrm{i}\eta/kS_a)^{\frac{1}{2}} + \psi_b(-2\mathrm{i}\eta/kS_b)^{\frac{1}{2}}\}, \\ \mathrm{i}q_0 &= \tfrac{1}{2}\eta^{-1}\{\psi_a(2\mathrm{i}\eta/kS_a)^{\frac{1}{2}} - \psi_b(-2\mathrm{i}\eta/kS_b)^{\frac{1}{2}}\}, \end{aligned}\right\} \tag{74}$$

where ψ_a, ψ_b mean $\psi(n_a)$, $\psi(n_b)$ respectively.

The standard integral representations of the Airy integral function and its derivative are (Miller 1946):

$$\left.\begin{aligned} \int_{-\mathrm{i}\infty}^{\mathrm{i}\infty} \exp(\eta^2\tau - \tfrac{1}{3}\tau^3)\,\mathrm{d}\tau &= 2\pi\mathrm{i}\,\mathrm{Ai}(\eta^2); \\ \int_{-\mathrm{i}\infty}^{\mathrm{i}\infty} \tau\exp(\eta^2\tau - \tfrac{1}{3}\tau^3)\,\mathrm{d}\tau &= 2\pi\mathrm{i}\,\mathrm{Ai}'(\eta^2). \end{aligned}\right\} \tag{75}$$

If p_1, p_2 etc. and q_1, q_2 etc. are neglected in (69), we have from (62), (69), (75):

$$J(\beta) = 2\pi\mathrm{i}\exp(-\mathrm{i}A_0)\{p_0\mathrm{Ai}(\eta^2) + q_0\mathrm{Ai}'(\eta^2)\}, \tag{76}$$

where p_0 and q_0 are given by (74). This is the required result for the field near a Storey cone.

The formula (76) can be used to calculate all six field components (25). The required values of p_0 and q_0 are different for the six. The order of the computer calculations (Cambridge) was as follows.

(*a*) For each given β locate the six saddle points by solving the 6th degree equation (34) for n^2 as described in § 4.

(*b*) Select the two that contribute to the Storey cone. This was done by including in the data a value of $\mathrm{Re}(n^2)$ found previously using the method of Budden & Stott (1980, Appendix B) to locate the Storey cone. The two solutions with $\mathrm{Re}(n^2)$ nearest to the given value were selected.

(*c*) For these two saddle points calculate n_ρ^2 from (17), n_z^2 from (18), n_ρ, n_z, then P from the first equation (59), and A_0 from (61).

(*d*) Calculate η, η^2 from (61) and thence Ai and Ai' in (76).

These four steps are the same for all six field components.

(*e*) Calculate the six values of G_a and of G_b from (73) and the first equation (69). Here by comparison of (32) and (41), and use of (33):

$$\psi = h_j \mathrm{i} e^{\frac{1}{4}\mathrm{i}\pi} R(2\pi kr \sin\beta)^{-\frac{1}{2}} \tag{77}$$

where

$$R(= R_a \text{ or } R_b) = n_\rho^{\frac{3}{2}}\{n_\rho^2(\epsilon_{xx}+\epsilon_3) - 2(\epsilon_{xx} - n_z^2)\,\epsilon_3\}^{-1}. \tag{78}$$

Note that ψ and R and each of the six h_j, has different values at the two saddle points.

(*f*) Calculate p_0 and q_0 from (71) and finally $\mathscr{F}_j = J$ from (76).

These steps can be combined into the formula, valid when $0 < \beta < \frac{1}{2}\pi$:

$$\mathscr{F}_j = \pi^{\frac{1}{2}} e^{-\frac{1}{4}\mathrm{i}\pi}(kr)^{-\frac{5}{6}}(\cos\beta)^{-\frac{1}{3}}(\sin\beta)^{-\frac{1}{2}} \exp(-\mathrm{i}A_0)\{P_j \mathrm{Ai}(\eta^2) + \mathrm{i}Q_j(kr\cos\beta)^{-\frac{1}{3}}\mathrm{Ai}'(\eta^2)\}, \tag{79}$$

where

$$\left.\begin{aligned} P_j &= \chi^{\frac{1}{4}}[R_a\{h_j(n_z'')^{-\frac{1}{2}}\}_a + R_b\{h_j(-n_z'')^{-\frac{1}{2}}\}_b] \\ Q_j &= \chi^{-\frac{1}{4}}[R_a\{h_j(n_z'')^{-\frac{1}{2}}\}_a - R_b\{h_j(-n_z'')^{-\frac{1}{2}}\}_b]. \end{aligned}\right\} \tag{80}$$

Here n_z'' means $\partial^2 n_z/\partial n_\rho^2$, R_a, R_b are given by (78) and

$$\chi = -\eta^2(kr\cos\beta)^{-\frac{2}{3}}. \tag{81}$$

The functions Ai and Ai′ in (79) are oscillatory when $\mathrm{Re}(\eta^2)$ is negative. It can be shown, either from (61) or by a simpler approximate treatment of the integral (32) or (41), that when $\beta - \beta_s$ is small, η^2 is approximately proportional to $(\beta - \beta_s)r^{\frac{2}{3}}$. Hence the period of the oscillations, as β varies, is proportional to $r^{-\frac{2}{3}}$. Note also that χ (81), is approximately independent of r. The oscillations of the terms with Ai and Ai′ in (79) are approximately in quadrature both in time, and when β varies. Thus when the Ai′ term is large, the oscillations of the combination may have only a small amplitude (figure 4, upper continuous curve), or may not appear at all (figure 5, upper continuous curve).

The r dependence of the term containing Ai in (79) is $r^{-\frac{5}{6}}$. Thus this contribution decreases more slowly with range r than the normal radiation field, given by (39), which is proportional to r^{-1}. This shows that the field near the edge of a Storey cone should be enhanced, especially at great ranges r, but in many practical cases, studied in later sections, this tends to be masked by the effects of attenuation. The r dependence of the term containing Ai′ in (79) is $r^{-\frac{7}{6}}$ so that this decreases faster than r^{-1}.

Some typical results are shown in figures 4 and 5 for a (forward) Storey cone in a fully ionized proton plasma. The continuous curves are for ranges r of 200 km and 2000 km. The chain curves show the fields from the two saddle points (58), computed with the first order steepest descents formula (39) with $r = 200$ km, and ignoring the failure of this formula near the Storey cone. The upper continuous curve where $\beta < \beta_s$ can be thought of as an interference pattern from these two fields. For $\beta > \beta_s$ the larger of these fields does not contribute. The oscillations in figure 4 have a shorter period for the larger range, with the correct ratio $10^{\frac{2}{3}} = 4.64$. For $r = 2000$ the minima are more pronounced because the Ai′ term is relatively much smaller. The association of this behaviour with the curvature of the refractive index surface near the Storey cone angle θ_s has been discussed by Stott (1982). The results in figure 4 are for an electron collision frequency $\nu_e = 100\,\mathrm{s}^{-1}$. In this example the attenuation is small. For a collisionless plasma the fields are only about 0.7% greater for $r = 200$ km. The frequency, 560 Hz, is near to the proton gyro frequency 649.8 Hz. Thus there is a small but appreciable difference between the electron

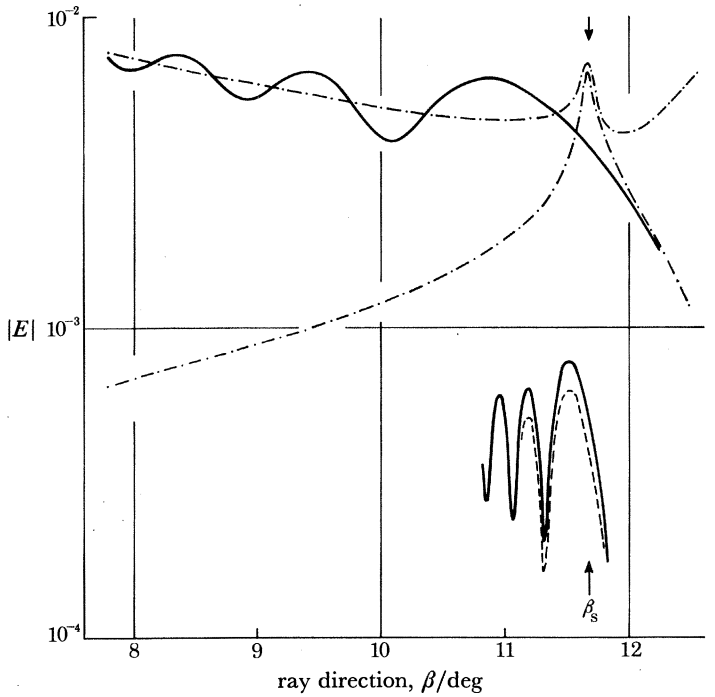

FIGURE 4. Dependence of $|E|$, equation (117) §10, on ray direction β near a Storey cone in a fully ionized cold proton plasma with $f_H = 1.1937$ MHz, $f_N = 2.3874$ MHz and for frequency $f = 5.6 \times 10^2$ Hz. For a collisionless plasma the real Storey cone angle would be $\beta_S = 11.68°$ as shown by the arrows. The two continuous curves are for ranges $r = 200$ km, upper curve, and $r = 2000$ km, lower curve. The chain curves show the separate contributions from the two saddle points (58) for $r = 200$ km. For these four curves the electron collision frequency was $\nu_e = 100\ s^{-1}$. The broken curve is for $r = 2000$ km and $\nu_{ei} = 100\ s^{-1}$ so as to allow for the movement of the protons in collisions with electrons.

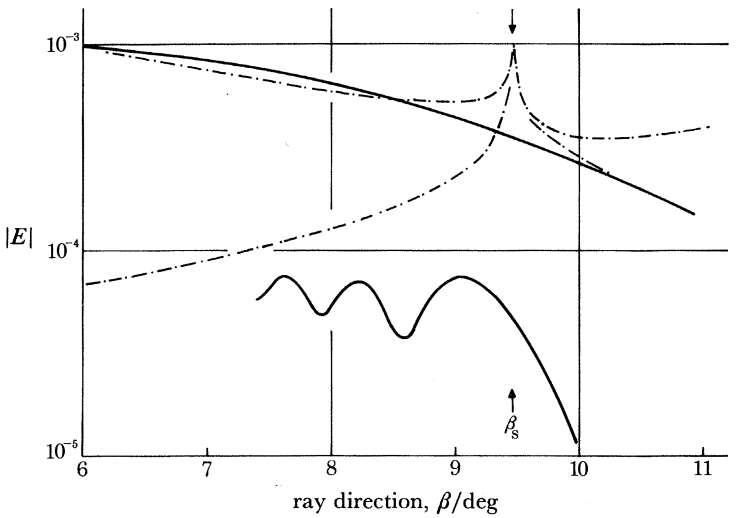

FIGURE 5. The same as figure 4 except that the frequency is 3.0×10^2 Hz and there is no curve for $\nu_{ei} = 100\ s^{-1}$. Oscillations do not occur for $r = 200$ km, upper continuous curve, because the Ai′ term is too large. They do occur for $r = 2000$ km, lower continuous curve, because the Ai′ term is relatively smaller. For a collisionless plasma the real Storey cone angle would be $\beta_S = 9.46°$ as shown by the arrows.

collision frequency $\nu_e = 100\,s^{-1}$ used for the continuous curves, and a collision frequency $\nu_{ei} = 100\,s^{-1}$ between electrons and moving protons (see Al'pert 1980*b*, Appendix A). For $r = 200$ km the fields are about 2.2% less, too small to show clearly on the scale of figure 4, but for $r = 2000$ km the fields are about 20% less and are shown as a broken curve.

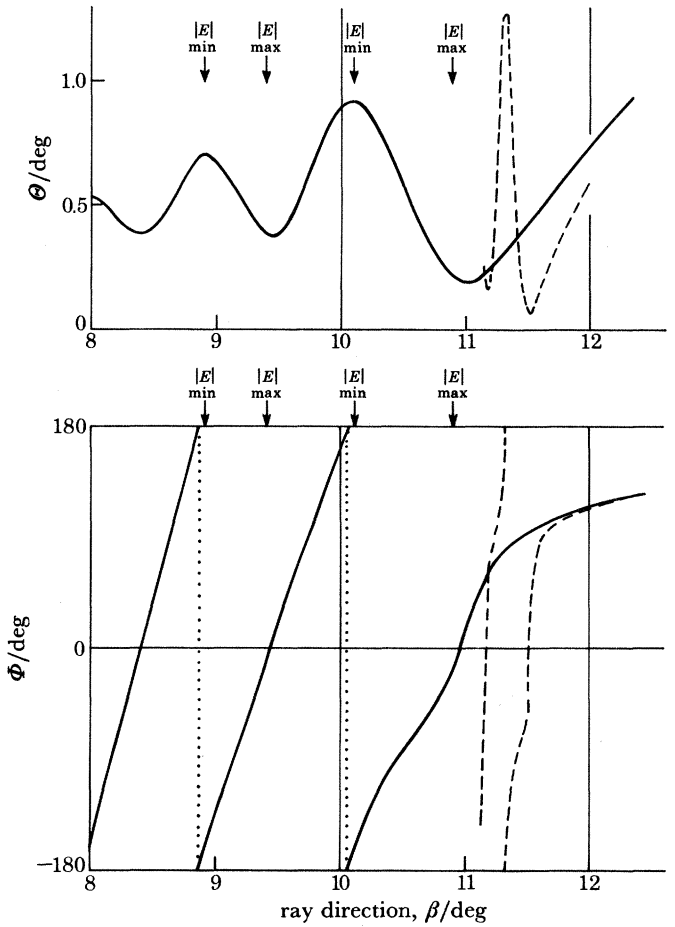

FIGURE 6. Shows how the direction of the time averaged Poynting vector $\boldsymbol{\Pi}$ depends on ray direction β near a Storey cone, for the example of figure 4. The continuous curve is for range $r = 200$ km and the broken curve is for range $r = 2000$ km. The polar angles Θ, Φ of $\boldsymbol{\Pi}$ are defined in the text. The arrows show where $|E|$ is a maximum or a minimum for $r = 200$ km.

The time averaged Poynting vector $\boldsymbol{\Pi}$, (43) was calculated from (79) for ray directions near the edge of a Storey cone. Since the fields on the illuminated side are now effectively composed of two waves associated with the two contributing saddle points (58), it is no longer expected that $\boldsymbol{\Pi}$ is approximately parallel to the ray, as it was for a single saddle point (end of §4). Figure 6 shows how the direction of $\boldsymbol{\Pi}$ changes when β changes, for the example of figure 4. The behaviour in other cases studied was very similar to this example. The direction of $\boldsymbol{\Pi}$ is specified by its polar angles Θ measured from the ray direction as polar axis, and azimuth angle Φ measured from the plane $y = 0$. The Poynting vector has a y component Π_y which changes sign roughly at those values of β where $|\boldsymbol{E}|$ is a maximum ($\Phi \approx 0°$ and Θ approximately a minimum in figure 6), or a minimum ($\Phi \approx 180°$ and Θ approximately at a maximum).

7. Evaluation of the integrals for fields near the axis

We now consider the evaluation of the integral (27) when ξ (26), is so small that the asymptotic forms (30) and (31) for the Bessel functions cannot be used. It is convenient to rewrite (27), with the cylindrical coordinates

$$\rho = r\sin\beta, \quad z = r\cos\beta, \tag{82}$$

of the receiving point and with the use of (29), thus

$$\mathscr{F}_j = \int_0^\infty \{n_\rho^2(\epsilon_{xx}+\epsilon_3) - 2(\epsilon_{xx}-n_z^2)\,\epsilon_3\}^{-1} g_j \exp(-\mathrm{i}kzn_z)\, n_\rho^2 \,\mathrm{d}n_\rho \tag{83}$$

where the summation over $l = 1, 2$ has been omitted as explained in §4. The six g_j contain the Bessel functions and are given by (28).

The argument $\xi = k\rho n_\rho$ of the Bessel functions can be small for either of two reasons. First, at a saddle point of (83), n_ρ may be small. Then the saddle point is near the end $n_\rho = 0$ of the contour of integration and (40) is violated. A form of the steepest descents integral can be derived in this case. It uses an error function and is complicated. But the integral of (83) contains the small factor n_ρ^2, so that the contribution from this saddle point is necessarily small. This is just an expression of the property that a dipole does not radiate in the direction of its axis. Thus this case is not of great interest for a dipole source parallel to the z axis. It would be important for other orientations of the dipole as given in Appendix B, but no results for these are given here.

The second reason for a small ξ is that ρ is small so that the receiver is very near the dipole axis, but n_ρ is not small. This is a most interesting case first described by Al'pert & Moiseyev (1980). To see when it is likely to be important, consider the special case $\rho = 0$, $\beta = 0$. The refractive index surface must have a normal parallel to the z axis where $n_\rho \neq 0$. Well known cases, for a plasma with electrons only, are the whistler mode and the Z mode, as sketched in figure 7. Since these surfaces are surfaces of revolution about the z axis, there is an infinite number of normals meeting the surface on a circle. There is no single normal of the kind that was associated with each saddle point given by (34).

Since ξ is small, the Bessel functions in the g_j of (83) are slowly varying functions of n_ρ. In applying the method of steepest descents to (83) it may therefore be assumed that the saddle points are determined by the exponential alone. Thus they are given by

$$\mathrm{d}n_z/\mathrm{d}n_\rho = 0, \tag{84}$$

which is the same as (34) with $\beta = 0$. The equation of degree six for n^2, to which (34) leads, can be factorized in this special case (Budden & Stott 1980). Two of its solutions are $n^2 = \epsilon_+, \epsilon_-$, but these both give $n_\rho^2 = 0$ so that the first order steepest descents contribution to (83) is zero. The remaining four solutions are in two equal pairs (Budden & Stott 1980, equation (A 7) with $\beta = 0$) and they satisfy the quadratic equation for n^2:

$$\begin{aligned}(\epsilon_+ + \epsilon_-)(\epsilon_+ + \epsilon_- - 2\epsilon_3)\,n^4 + 2(\epsilon_+ + \epsilon_-)\{\epsilon_3(\epsilon_+ + \epsilon_-) - 2\epsilon_+\epsilon_-\}n^2 \\ + 4(\epsilon_+\epsilon_-)^2 - 2\epsilon_+\epsilon_-\epsilon_3(\epsilon_+ + \epsilon_-) - \{(\epsilon_+ - \epsilon_-)\,\epsilon_3\}^2 = 0.\end{aligned} \tag{85}$$

The solutions, when used in (16), (17), (18) give

$$n_\rho^2 = \frac{-2\epsilon_{xy}^2\epsilon_3}{(\epsilon_{xx}-\epsilon_3)^2}\left[1 \pm \mathrm{i}\frac{\epsilon_{xx}+\epsilon_3}{2\epsilon_{xy}}\left\{-\frac{\epsilon_{xy}^2 + (\epsilon_{xx}-\epsilon_3)^2}{\epsilon_{xx}\epsilon_3}\right\}^{\frac{1}{2}}\right], \tag{86}$$

$$n_z^2 = \frac{1}{(\epsilon_{xx}-\epsilon_3)^2}[(\epsilon_+\epsilon_- - \epsilon_3\epsilon_{xx})(\epsilon_{xx}-\epsilon_3) + 2\epsilon_3\epsilon_{xy}^2] \pm \frac{2\mathrm{i}\epsilon_{xy}}{(\epsilon_{xx}-\epsilon_3)^2}[-\epsilon_3\epsilon_{xx}\{\epsilon_{xy}^2 + (\epsilon_{xx}-\epsilon_3)^2\}]^{\frac{1}{2}}. \tag{87}$$

PHILOSOPHICAL TRANSACTIONS OF THE ROYAL SOCIETY A MATHEMATICAL, PHYSICAL & ENGINEERING SCIENCES

The value (36) of n_z'' cannot be used when $\beta = 0$ because its numerator and denominator are both zero, but an alternative expression valid when (84) is true, is

$$n_z'' = -\frac{6\epsilon_{xx} n_\rho^2 + (\epsilon_{xx} + \epsilon_3) n_z^2 - \epsilon_{xx}\epsilon_3 - \epsilon_+\epsilon_-}{n_z\{n_\rho^2(\epsilon_{xx} + \epsilon_3) - 2(\epsilon_{xx} - n_z^2)\epsilon_3\}}. \tag{88}$$

Then the first order steepest descents evaluation of (83) gives for the contribution at one saddle point

$$\mathscr{F}_j \sim e^{\mp\frac{1}{4}i\pi} g_j n_\rho^2 (2\pi n_z/kz)^{\frac{1}{2}} \exp(-ikzn_z) \times [\{(\epsilon_{xx} + \epsilon_3) n_\rho^2 + 2\epsilon_3(n_z^2 - \epsilon_{xx})\}\{-6\epsilon_{xx} n_\rho^2 - (\epsilon_{xx} + \epsilon_3) n_z^2 + \epsilon_{xx}\epsilon_3 + \epsilon_+\epsilon_-\}]^{-\frac{1}{2}}, \tag{89}$$

where the g_j are given by (28), and n, n_ρ, n_z take their values at the saddle point. The sign in the exponential is opposite to the sign of $\mathrm{Re}(\mathrm{d}^2 n_z/\mathrm{d}n_\rho^2)$. The square root with positive real part is used.

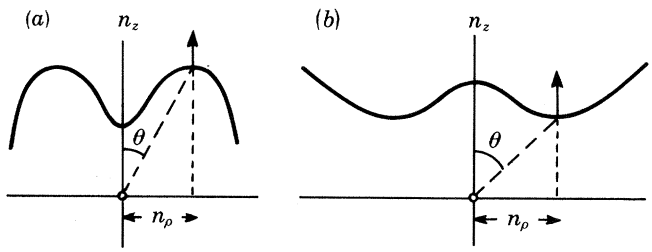

FIGURE 7. Some examples of forms of the refractive index surface which give solutions with $n_\rho \neq 0$ when $\beta = 0$. The arrow is the direction of the ray and for $\beta = 0$ it is parallel to the z axis. Example (a) is for the Z mode and example (b) is for the whistler mode, in an electron plasma.

The fields (89) are proportional to $z^{-\frac{1}{2}}$, that is to $r^{-\frac{1}{2}}$ ($\beta = 0$). Thus, at great distances from the source, they can be much larger than the fields (39) or (76) which are proportional to r^{-1} and $r^{-\frac{5}{6}}$ respectively. Some examples of this field enhancement near the axis are given later in §§ 10 and 11.

It is necessary to decide whether or not the contour of integration goes through a saddle point given by (85). For a loss free plasma, a solution n_ρ^2 which is real and positive gives a saddle point on the real positive half of the n_ρ axis, and it is a point of stationary phase for this contour. This occurs for the examples of figure 7. Thus when the solution n_ρ is real and positive, or nearly so for a plasma with losses, it would be expected on physical grounds that the contribution (89) must be included.

For a solution n_ρ^2 which is real and negative, the saddle point n_ρ is imaginary and does not lie near the original contour. The argument ξ of the Bessel functions in (28) is imaginary, so that these functions are modified Bessel functions $I_0(\zeta)$, $I_1(\zeta)$ where $\zeta = i\xi$, which increase very rapidly as ξ increases. This suggests that these saddle points cannot contribute to the field.

The transition between these two cases occurs, for a loss free plasma, when (85) has a solution $n_\rho^2 = 0$, that is when the last term of (85) is zero. For conditions near this a more elaborate treatment of the integral (83) would be needed.

From the six field components (89), the time averaged Poynting vector $\boldsymbol{\Pi}$, (43) can be calculated. Some examples of results obtained with the formula (89) are given in figures 8 and 9 which show how $|E|$ and the three components of $\boldsymbol{\Pi}$ depend on distance x ($= \rho$) from the z axis, for a receiving point in the plane $y = 0$ at a fixed distance z. Since the fields have cylindrical symmetry

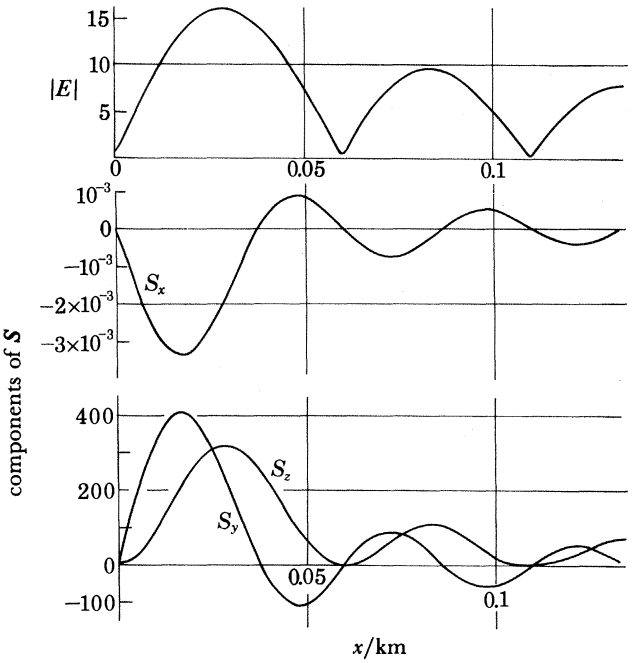

FIGURE 8. Dependence of $|E|$, equation (117) §10, and of the components of $\boldsymbol{S} = 4Z_0\boldsymbol{\Pi}$, equation (43), on distance x from the axis of the dipole source. This example is for a fully ionized proton plasma with $f_H = 1.1937$ MHz, and $f_N = 2.3874$ MHz. The frequency is $f = 2.984 \times 10^4$ Hz, the electron collision frequency is $\nu_e = 100\ s^{-1}$ and the receiver is at a distance $z = 100$ km from the plane $z = 0$ containing the source. Here $\boldsymbol{\Pi}$ is the time averaged Poynting vector. These results are for the electron whistler wave, that is the ordinary wave, for which the refractive index surface has the shape of figure 7*b*.

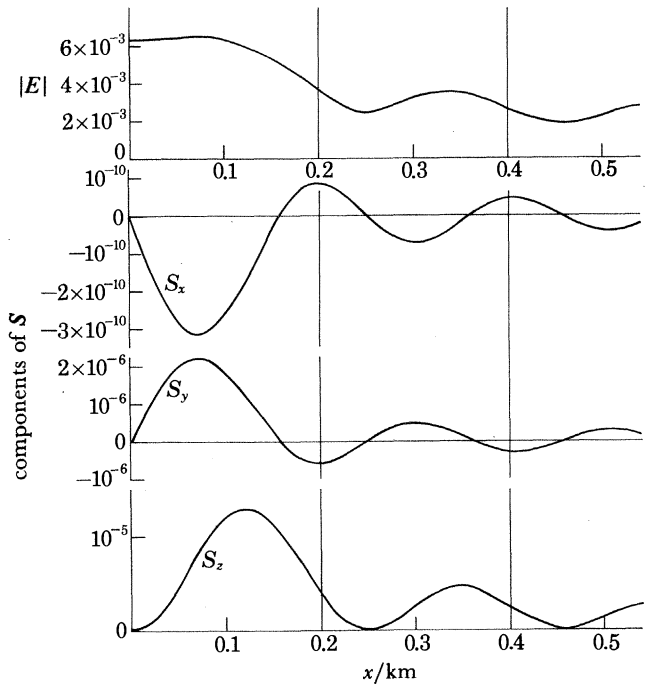

FIGURE 9. Similar to figure 8 and for the same plasma, but the frequency is $f = 2.268$ MHz, and the distance of the receiver from the plane of the source is $z = 200$ km. These results are for the Z mode, that is the extraordinary wave, where there is a Storey cone but no resonance cone. The refractive index surface has the shape of figure 7*a*.

about the z axis, Π_x is the same as Π_ρ and Π_y is the same as Π_ϕ for $x > 0$. Since the argument ξ, (26) of the Bessel functions in (28) depends only on $x = r\sin\beta$, and not on z, the form of the x dependence of the fields and of $\boldsymbol{\Pi}$ is independent of z. Thus the curves like those of figures 8 and 9 are the same shape for all z, and only the ordinate scales would change when z is changed.

Formula (28) shows that for a loss free plasma the four field components E_x, E_y, $\mathscr{H}_x$, $\mathscr{H}_y$ are all in phase or in antiphase with each other, and E_z, $\mathscr{H}_z$ are in quadrature with them. Then Π_x is zero. This is not strictly accurate. Since all field components decrease as $z^{-\frac{1}{2}}$, the electromagnetic wave energy stored within any cylinder, $\rho =$ constant, must decrease as z^{-1} and there ought, therefore, to be a radially outward flow of energy. Thus $\Pi_x = \Pi_\rho$ should have a small positive value for all x. The discrepancy arises because of the assumption, made in using (84), that the Bessel functions in (83) are slowly varying and do not influence the determination of the saddle point. A more accurate method that does not use this restriction is given in outline below.

For the plasma studied in figures 8 and 9, collisions are allowed for and Π_x has a small but non-zero value. For small x, Π_x is negative so that there is a radially inward flow to replace the energy being absorbed by the plasma near the axis. The rate of absorption per unit volume is $-\operatorname{div}\boldsymbol{\Pi}$ and it is easily checked that this is everywhere non-negative. It is interesting to note that Π_y $(= \Pi_\phi)$ is comparable with Π_z. Thus the energy flux has a large component around the axis.

The more accurate treatment mentioned above is as follows. Instead of treating the Bessel functions in (28) as slowly varying functions of n_ρ in the integrand of (83), they are written in terms of Hankel functions thus:

$$J_m(\xi) = \tfrac{1}{2}\{H_m^{(1)}(\xi) + H_m^{(2)}(\xi)\} = L_m^{(1)}(\xi)\,\mathrm{e}^{\mathrm{i}\xi} + L_m^{(2)}(\xi)\,\mathrm{e}^{-\mathrm{i}\xi}, \tag{90}$$

where, from (26)

$$\xi = kxn_\rho, \tag{91}$$

and where $m = 1, 2$ in the present application. When ξ is large enough, the functions L are simply the factors that include $\xi^{-\frac{1}{2}}$ in (30) and (31), but for smaller ξ they are more complicated. Integral representations of them have been given (Watson 1944, §6.12, and other standard texts) but these are not needed here. Now the exponentials in (90) are included with the exponential factor in (83) and the saddle points are found for the combined exponential

$$\exp\{-\mathrm{i}k(zn_z \mp xn_\rho)\}. \tag{92}$$

This is exactly the same as was done in §4 when the saddle points of (32) were found by using (34). The result gives two saddle point values $n_{\rho\mathrm{A}}$, $n_{\rho\mathrm{B}}$. If $x = 0$ these values are equal and are the solutions (86) of (85) previously used in (89). But if $x \neq 0$, the values are slightly different. They are now inserted in the contributions, analogous to (39), from the saddle point of each term in (90). These contributions therefore contain factors

$$L_m^{(1)}(kxn_{\rho\mathrm{A}})\exp(\mathrm{i}kxn_{\rho\mathrm{A}}) = \tfrac{1}{2}H_m^{(1)}(kxn_{\rho\mathrm{A}}),$$

and

$$L_m^{(2)}(kxn_{\rho\mathrm{B}})\exp(-\mathrm{i}kxn_{\rho\mathrm{B}}) = \tfrac{1}{2}H_m^{(2)}(kxn_{\rho\mathrm{B}}), \tag{93}$$

for $m = 1, 2$. In this process the functions $L(\xi)$ are treated as slowly varying and therefore do not affect the determination of the saddle points. But they are finally recombined with the exponential factors in (93) to give Hankel functions. The result is that the formula (89), for each of the six

field components, is replaced by two terms derived from the two Hankel functions in each of the Bessel functions of (28). Thus, for example, the result for $j = 1$ is

$$\mathscr{F}_1 \sim \mathrm{e}^{\mp\frac{1}{4}\mathrm{i}\pi}(\pi/2kz)^{\frac{1}{2}}[n_{\rho\mathrm{A}}^2 n_{z\mathrm{A}}^{\frac{1}{2}} V(n_{\rho\mathrm{A}})\,(\epsilon_{xx}-n_{\mathrm{A}}^2)\,H_1^{(1)}(kxn_{\rho\mathrm{A}})\exp(-\mathrm{i}kzn_{z\mathrm{A}}) + n_{\rho\mathrm{B}}^2 n_{z\mathrm{B}}^{\frac{1}{2}} V(n_{\rho\mathrm{B}})\,(\epsilon_{xx}-n_{\mathrm{B}}^2)\,H_1^{(2)}(kxn_{\rho\mathrm{B}})\exp(-\mathrm{i}kzn_{z\mathrm{B}})], \quad (94)$$

where V is the factor $[\ldots]^{-\frac{1}{2}}$ in (89) and where subscripts A, B denote values at the two saddle points $n_{\rho\mathrm{A}}$, $n_{\rho\mathrm{B}}$. Formulae for the other five field components are constructed in a similar way. These formulae have not been tested or used for any of the results presented in this paper.

The results of this section and of §§ 5 and 6 are summarized by the schematic diagram figure 10 which shows the possible arrangements of the regions of enhancement in the radiation polar diagram for various conditions. It applies for a very large range, in a homogeneous plasma with very small losses so that the enhancements are large. In the results studied later, for ranges of only a few hundred kilometres and for a plasma with losses allowed for, the enhancements are seldom so marked as is suggested by figure 10.

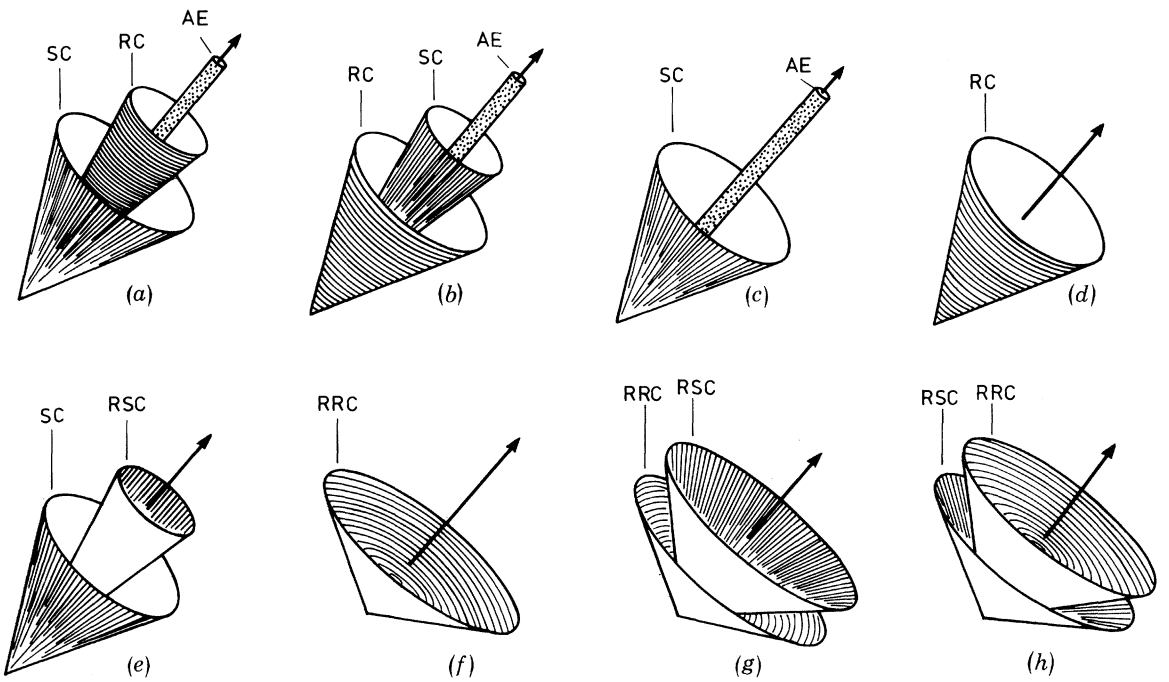

FIGURE 10. Schematic diagrams showing the possible arrangements of the regions of signal enhancement. The meaning of the symbols is: SC Storey cone, RC resonance cone, AE axial enhancement, RSC reversed Storey cone, RRC reversed resonance cone. The shading on the cones indicates the dark side. The arrow shows the direction of the superimposed magnetic field $\boldsymbol{B}$. For a given plasma, the frequency ranges where a given type of enhancement is present can be found from the charts such as figures 15, 20, 22, and these can be used to find which of the above diagrams applies for a given wave, ordinary or extraordinary, at a specified frequency.

For any plasma there are eight different types of arrangement of the cones and the axial enhancement, as shown in figure 10 (*a–h*). Some of their properties that apply for the range $0 < \beta < \frac{1}{2}\pi$ are summarized as follows:

(*a*) there can be at most one resonance cone *or* one reversed resonance cone;

(*b*) there are no cases where more than two cones are present;

(*c*) a resonance cone never occurs with a reversed Storey cone; a reversed resonance cone never occurs with a (forward) Storey cone.

(*d*) when axial enhancement is present there *must* be a Storey cone, and there *may* also be a resonance cone, figure 10*a*, *b or* no other cone, figure 10*c*;

(*e*) for a frequency range where a Storey cone and a resonance cone are both present, the the Storey cone is outside (greater β) for the smaller frequencies, figure 10*a*, and inside for the greater frequencies, figure 10*b*; (thus there is some frequency for which the two cones have the same ray direction β (not shown in figure 10) and here their wave normal directions θ have opposite signs.)

(*f*) similarly, for a frequency range where a reversed Storey cone and a reversed resonance cone are both present, the reversed resonance cone is outside for the smaller frequencies, figure 10*g* and inside for the greater frequencies figure 10*h*; (again there is some frequency for which the two cones have the same ray direction, and the complements $\frac{1}{2}\pi - \theta$ of their wave normal directions θ then have opposite signs.)

(*g*) when a Storey cone and a reversed Storey cone are both present, figure 10*e*, the reversed Storey cone has the smaller value of β.

8. The two wave types and their $\beta(\theta)$ curves

(*a*) *The terms 'ordinary' and 'extraordinary'*

The results given in previous sections for the radiated field of a dipole depend on the properties of the homogeneous plasma and these are completely determined by the three numbers ϵ_-, ϵ_+, ϵ_3, of (5), which are functions of the frequency ω. For a plasma with losses they are, in general, complex, and this applies to the results presented here, which are for a plasma with collisions included. To classify the results, however, it is useful to consider a loss-free plasma so that collisions are ignored and ϵ_-, ϵ_+, ϵ_3 are all real. This is done throughout this and the following section.

We now consider the range $0 < \theta < \frac{1}{2}\pi$. The behaviour in other ranges of θ is similar. When θ is not equal to 0 or $\frac{1}{2}\pi$, the square root S of (12) can never be zero. It is infinite, because it has simple poles in the ω plane, where either ϵ_- or ϵ_+ is infinite, that is when ω is equal to any of the gyro frequencies Ω_i or ω_H, but then the two refractive indices are unequal and not infinite. Thus these two values of $n(\omega)$, given by (13), can never be equal for any real ω. One of them, but only one, is infinite at a resonance frequency where the denominator of (13) is zero. Apart from this, the two values of $n(\omega)$ are continuous distinct functions of ω for all real ω, provided that the sign of S is reversed each time ω passes through a gyro frequency Ω_i or ω_H. This reversal of sign occurs automatically if the real axis path in the complex ω-plane is indented on the negative imaginary side near each pole $\omega = \Omega_i, \omega_H$.

The refractive index of the wave for which S is positive when $\omega_H < \omega$ and when $\Omega_{i+1} < \omega < \Omega_i$ with i odd, is denoted by n_1 and this wave is here called the ordinary wave. Similarly the value with the other sign of S is denoted by n_2 and the wave is called the extraordinary wave. This choice of the terms is made here purely for convenience of description and is not necessarily the best for general use. Some authors use a different convention (see below).

Consider, now, an 'electrons only' plasma, that is, one in which the positive ions are assumed all to be infinitely massive so that they do not affect the dispersion relation. Then it can be shown that, for all ω:

$$n_1^2(\theta) \to \epsilon_3 \quad \text{when} \quad \theta \to \tfrac{1}{2}\pi. \tag{95}$$

Now ϵ_3 is independent of $\boldsymbol{B}$ and it is for this reason that the wave is called 'ordinary'. Similarly, for the extraordinary wave it can be shown that

$$n_2^2(\theta) \to \epsilon_+\epsilon_-/\epsilon_{xx} \quad \text{when} \quad \theta \to \tfrac{1}{2}\pi. \tag{96}$$

These results also apply for any cold collisionless plasma at frequencies much greater than the greatest ion cyclotron frequency. This use of 'ordinary' and 'extraordinary' is adopted by most ionospheric physicists who use high frequencies and are not concerned with the effects of positive ions of finite mass. At lower frequencies, however, where the non-infinite ion mass is important, the results (95) and (96) are not always true.

The two refractive indices n_1 and n_2 can only be equal when the square root (12) is zero, and this can occur only in the following three conditions (r is any integer):

(i) crossover (§§ 8 (viii), 9 (i)): $\omega = \omega_{cr}$

$$\theta = r\pi, \quad \epsilon_- = \epsilon_+ = n_1^2 = n_2^2; \tag{97}$$

(ii) Window frequency (§ 9 (*d*)): $\omega = \omega_0$

$$\theta = r\pi, \quad \epsilon_3 = 0; \tag{98}$$

(iii) O–E transition: $\omega = \omega_T$

$$\theta = (r+\tfrac{1}{2})\pi, \quad \epsilon_3 = \epsilon_+\epsilon_-/\epsilon_{xx}. \tag{99}$$

When positive ions of non-infinite mass are present, the number of real bounded values of ω_T is equal to the number of such positive ion species. If ω is decreased to just less than the greatest ω_T, it can be shown that

$$n_2^2(\theta) \to \epsilon_3 \quad \text{and} \quad n_1^2(\theta) \to \epsilon_+\epsilon_-/\epsilon_{xx} \quad \text{when} \quad \theta \to \tfrac{1}{2}\pi. \tag{100}$$

Some authors, for example Booker (1975), then interchange the names ordinary and extraordinary, so that a wave of fixed type changes its name when the frequency ω is changed and passes through one of the values ω_T. This can be inconvenient, especially when there are more than one ion species. For the description of the results of the present paper we prefer to be able to use the terms ordinary and extraordinary unambiguously without specifying the frequency.

The change from (95) and (96) to (100) occurs each time ω passes through one of the values ω_T. Thus the number of frequency ranges where (100) is true is equal to the number of positive ion species of non-infinite mass.

(*b*) *Curves of* $\beta(\theta)$

A curve $n(\theta)$ with n as radius and θ as polar angle is a cross section of the refractive index surface, which is formed by rotating the curve about the z axis, $\theta = 0$. The direction β of the ray, that is the radius from the source to the receiving point, is related to θ by (35). This shows that the ray direction is normal to the refractive index surface (Al'pert 1948, 1967, 1980*a*; Bremmer 1949; Rawer & Suchy 1967; Budden 1961). It is also useful to consider a curve with the ray velocity

$$V = c/(n\cos\alpha), \quad \alpha = \theta - \beta \tag{101}$$

plotted as radius with β as polar angle. This is a cross section of the ray surface which has the shape of the wave front that has travelled some distance from the source (Budden 1961; Walker 1977*a*).

Refractive index surfaces $n(\theta)$ and their associated ray surfaces $V(\beta)$ are often classified by means of the C.M.A. diagram (Clemmow & Mullaly 1955; Allis 1959; Walker 1977*a*). It is here convenient to use a simpler method in which curves of β against θ are studied (Al'pert 1980*a*), and some typical curves are shown in figures 11 and 12. Crossing a line in the C.M.A. diagram

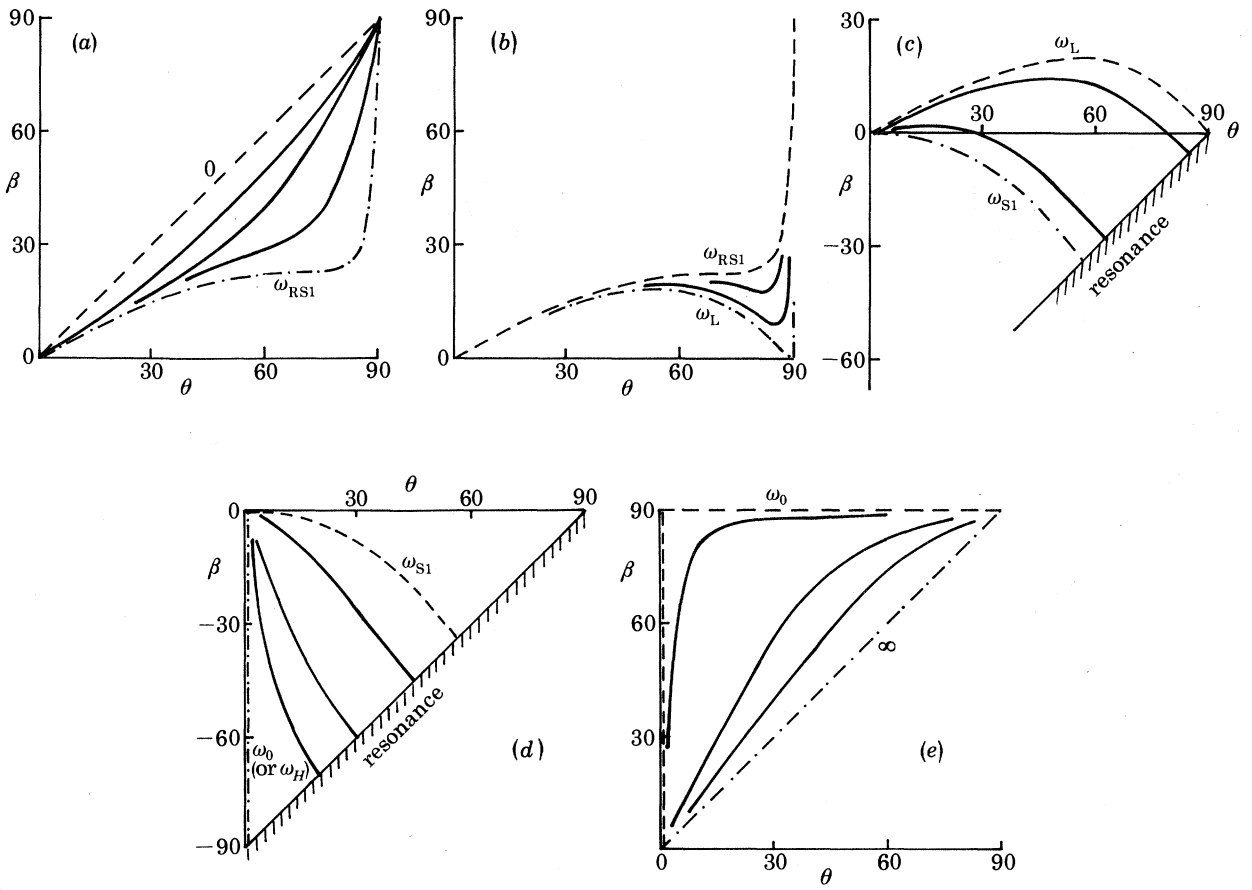

FIGURE 11. Some examples of curves of β against θ. This sequence is for the ordinary wave (defined in §8) in a collisionless plasma with one species of positive ion. The diagrams are in order of increasing frequency, and in each diagram the limiting curve at the lowest frequency is a broken line, and at the greatest frequency it is a chain line. The symbols by these curves are the transition frequencies defined in §9 and apply when $\omega_0 < \omega_H$. If $\omega_0 > \omega_H$ the sequence is the same but in (*d*) the symbol ω_0 must be replaced by ω_H. Then in the frequency range $\omega_H < \omega < \omega_0$ the ordinary wave is evanescent for all θ, so there are no curves for this range. Typical curves are shown as continuous lines, and in each diagram they have the same general shape. Thus each diagram corresponds to a single region of the C.M.A. diagram and therefore to a fixed topology of the refractive index surface. In curves (*a*) and (*e*) there are no Storey cones nor reversed Storey cones nor resonance cones. In (*b*) there is a Storey cone and a reversed Storey cone. In (*c*) there is a Storey cone and a resonance cone. In (*d*) there is a resonance cone but no other cones. Curves (*c*), (*d*), (*e*) would apply also to the ordinary wave in a plasma in which only electrons are effective. Then the curve for zero frequency would be very close to the curve marked ω_L in (*c*).

indicates a change in the topology of the $n(\theta)$ curve and there is a corresponding change in the curve $\beta(\theta)$. The main properties of these curves are as follows.

(i) From the dispersion relation (11) it can be shown that $\partial n/\partial\theta = 0$ when $\theta = 0$, or $\pm\frac{1}{2}\pi$. Hence from (34) it follows that the $\beta(\theta)$ curves always go through the points $\theta = 0$, $\beta = 0$, and $\theta = \frac{1}{2}\pi$, $\beta = \frac{1}{2}\pi$ provided that n is real there.

(ii) The refractive index surface is symmetrical about the lines $\theta = 0$, and $\theta = \pm\frac{1}{2}\pi$, and hence the $\beta(\theta)$ curve has a centre of symmetry at $\theta = 0$, $\beta = 0$ and at $\theta = \frac{1}{2}\pi$, $\beta = \frac{1}{2}\pi$.

(iii) One value of the refractive index $n(\theta)$ is zero for all θ when $\epsilon_+ = 0$, or $\epsilon_- = 0$, and this is called 'cut-off'. It occurs for the frequencies $\omega = \omega_+, \omega_-$ respectively. When ω is greater than the

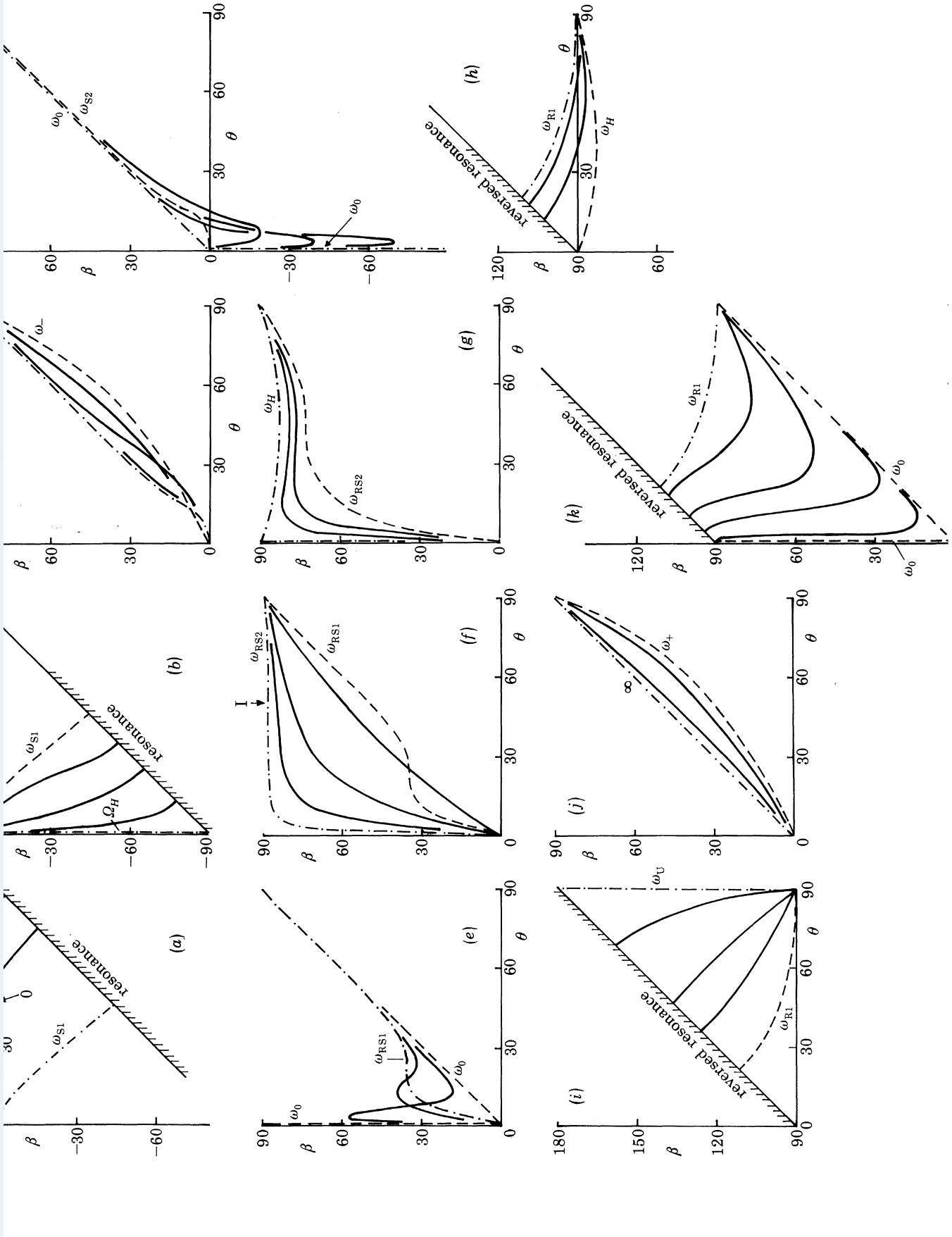

cut-off value and very close to it, one of the functions $n(\theta)$ is real and small, and it can be shown from (8) that $\beta(\theta)$ approaches the limiting form given by

$$\tan\beta = \tfrac{1}{2}\tan\theta \tag{102}$$

(Budden & Stott 1980). Examples can be seen in figures 12*c* (curve ω_-), 12*j* (curve ω_+) and in figures given by Al'pert (1980*a*).

(iv) Both functions $n_1(\theta)$ and $n_2(\theta)$ are single valued for $0 < \theta < \frac{1}{2}\pi$. Thus the two $\beta(\theta)$ curves are each single valued, and also continuous, except at resonance (see (v) below).

(v) One refractive index curve $n(\theta)$ can sometimes be an open curve with n going to infinity at some value $\theta = \theta_r$, as described in §5, and this defines a resonance cone where $\beta = \beta_r$. The conditions for this are (44), (45), (46). Thus, at a resonance, the $\beta(\theta)$ curve ends on one of the lines (45), which will be called resonance lines. It can further be shown that on these lines

$$\partial\beta/\partial\theta = -1, \tag{103}$$

so that the curves always meet the resonance lines at right angles.

(vi) The $\beta(\theta)$ curve may cross the line $\beta = 0$ at some value $\theta = \theta_2 \neq 0$, as for example in figures 11*c* and 12*a*, *d*. There is then, in refractive index space, a cone of directions $\theta = \theta_2$, where the ray, that is the normal to the refractive index surface, is parallel to the z axis, as in figure 7, and the conditions for field enhancement on the z axis, §7, are satisfied.

(vii) The refractive index surface may have a point of inflexion. The condition for this is discussed by Clemmow & Mullaly (1955); Walker (1977); Budden & Stott (1980); Al'pert (1980*a*). It is given by (57) which can be shown, from (34), to lead to $\partial\beta/\partial\theta = 0$. It occurs where $\beta = \beta_s$, $\theta = \theta_s$, and here the $\beta(\theta)$ curve has a turning point, and the ray surface $V(\beta)$ has a cusp. If β and $\partial^2\beta/\partial\theta^2$ here have opposite signs, there is a Storey cone at $\beta = \beta_s$, with the illuminated side where $|\beta| < |\beta_s|$. If β and $\partial^2\beta/\partial\theta^2$ have the same sign there is a reversed Storey cone at $\beta = \beta_s$.

(viii) The special case given by (97) is called 'crossover' and ω_{cr} is the (angular) crossover frequency. The number of different values of ω_{cr} is one less than the number of positive ion species of finite mass. Thus crossover cannot occur in a plasma with a single positive ion species, and so there are no examples of it in figures 11–14. At crossover the $\beta(\theta)$ curves are simple. One refractive index surface is a sphere $n^2 = \epsilon_-$ so that the $\beta(\theta)$ curve is just the straight line $\beta = \theta$. The other refractive index surface is a conicoid given by

$$n^2(\epsilon_-\sin^2\theta + \epsilon_3\cos^2\theta) = \epsilon_-\epsilon_3, \tag{104}$$

and $\beta(\theta)$ is given by

$$\tan\beta = (\epsilon_-/\epsilon_3)\tan\theta. \tag{105}$$

FIGURE 12. Similar to figure 11 but for the extraordinary wave in a collisionless plasma with one species of positive ion. This wave is evanescent for all θ when ω is in the ranges $\Omega_H < \omega < \omega_-$ and $\omega_U < \omega < \omega_+$. When $\omega_0 < \omega_H$ the sequence is consecutively (*a*)–(*j*). When $\omega_H < \omega_0$ the sequence is (*a*), (*b*), (*c*), (*d*), (*k*), (*h*), (*i*), (*j*). In (*f*) the symbol I indicates a point of inflexion where the gradient is zero. In (*g*) the curves have been distorted to show the shape; in practical cases the limiting curve marked ω_H is very close to the line $\beta = 90°$, and the limiting curve ω_{RS2} is actually the same as in (*f*). Curves 12(*c*) and 12(*j*) are similar to 11(*a*) and have no cones. Curves 12(*f*) are similar to 11(*e*) and also have no cones. Curves 12(*a*) are similar to 11(*c*) and have a Storey cone and a resonance cone. Curves 12(*b*) are similar to 11(*d*) and have a resonance cone. Curves 12(*e*) and 12(*g*) are similar to 11(*b*) and have a Storey cone and a reversed Storey cone. Curves 12(*i*) have a reversed resonance cone and do not appear in figure 11. Curves 12(*h*) and 12(*k*) are similar to each other; they have a reversed resonance cone and a reversed Storey cone and they do not appear in figure 11. Curves 12(*d*) have a Storey cone and do not appear in figure 11.

In practical cases, at crossover, ϵ_- is positive and ϵ_3 is negative so that (104) is a hyperboloid with a resonance where

$$\tan\theta = \pm(-\epsilon_3/\epsilon_-)^{\frac{1}{2}}, \quad \tan\beta = \mp(-\epsilon_-/\epsilon_3)^{\frac{1}{2}}. \tag{106}$$

The $\beta(\theta)$ curve (105) has negative slope, and its shape is as in figure 11*d* or 12*b*. The hyperboloid will be called the outer refractive index surface and the sphere will be called the inner refractive index surface.

Near crossover, when $\epsilon_+ - \epsilon_-$ is small but not exactly zero, the two surfaces separate and cannot intersect. It can be shown that if $\epsilon_{xx} + \epsilon_3 > 0$, the $\beta(\theta)$ curve for the inner surface has points $\theta = \pm\theta_s$, where $\mathrm{d}\beta/\mathrm{d}\theta = 0$, and points $\theta = \pm\theta_1$ where $\beta = 0$ (see, for example, figures 7*a*, 12*d*). Further, $\theta_1 > \theta_s$ and both tend to zero when $|\epsilon_+ - \epsilon_-| \to 0$. This occurs for either sign of $\epsilon_+ - \epsilon_-$. Thus the inner surface has a real Storey cone at $\beta(\theta_s)$ and shows field enhancement near the axis (§7). For the outer surface $\beta(\theta)$ is monotonic near $\theta \approx 0$.

If $\epsilon_{xx} + \epsilon_3 < 0$ the behaviour is similar but the real Storey cone and the field enhancement occur for the outer surface (see figures 7*b*, 11*c*, 12*a*) and the $\beta(\theta)$ curve for the inner surface is monotonic near $\theta \approx 0$. This is the most commonly occurring case.

If $\epsilon_{xx} + \epsilon_3 = 0$ both $\beta(\theta)$ curves are monotonic, and neither surface shows a Storey cone nor field enhancement near the axis.

(ix) At extremely low frequency, less than the least of the ion-cyclotron frequencies, it can be shown from (5) that, if collisions are neglected

$$\left.\begin{aligned} \epsilon_- \\ \epsilon_+ \end{aligned}\right\} = 1 + \rho/\epsilon_0 B^2 \pm N_e M^2 \omega/(\epsilon_0 e B^3) + O(\omega^2)$$
$$\epsilon_3 = 1 - \omega_0^2/\omega^2 \tag{107}$$

where ρ is the density of the medium and $M^2 = \sum_i C_i M_i^2 - m_e^2$. Thus in the limit $\omega \to 0$, the condition (97) for crossover is satisfied. One of the two refractive index surfaces is the two parallel planes

$$n^2 = \epsilon_- \sec^2\theta, \tag{108}$$

which is the limiting form of the hyperboloid (104). The $\beta(\theta)$ curve is the line $\beta = 0$. For small $\omega \neq 0$ this curve acquires a positive slope where $\beta = 0$, figure 12*a*. It can be shown from (34) and (19) that it crosses the line $\beta = 0$ where

$$\tan^2\theta \approx \pm(\epsilon_+ - \epsilon_-)(-2\epsilon_3)^{\frac{1}{2}}(\epsilon_+ + \epsilon_-)^{-\frac{3}{2}}, \tag{109}$$

and (44) shows that it meets the resonance line where θ is slightly less than $\frac{1}{2}\pi$ and $\beta < 0$. It has a maximum, corresponding to a Storey cone, at values θ_s, β_s which decrease when ω decreases. It can be shown from Budden & Stott (1980, equation (B 5)) that they move to $\theta_s \to 0$, $\beta_s \to 0$ when $\omega \to 0$. The other refractive index surface is the sphere

$$n^2 = \epsilon_-. \tag{110}$$

These two waves are sometimes called Alfvén waves by analogy with the waves studied in magnetohydrodynamics for a conducting fluid of density ρ in a constant magnetic field B. For both waves when $\theta = 0$, the wave velocity is

$$c(\epsilon_-)^{-\frac{1}{2}} \approx B(\mu_0\rho)^{-\frac{1}{2}} \quad \text{provided that} \quad \rho/\epsilon_0 B^2 \gg 1. \tag{111}$$

This is the same as the Alfvén velocity in a fluid.

For the wave (108) the θ dependence of the refractive index is the same as for an Alfvén wave in a fluid. It can be shown from (33) that when $\omega \to 0$ the only non zero component of the wave's

magnetic field is $\mathscr{H}_\phi$. In the fluid analogy the fluid displacement would also be in the ϕ direction, that is perpendicular both to the wave normal and to B. This wave is sometimes called the shear Alfvén wave (Stix 1962); its propagation is unaffected by the compressibility of the fluid. In figures 15, 20 and 22 it is called simply the Alfvén wave.

For the wave (110) there is no close analogy with Alfvén waves in a fluid, but it is sometimes called the 'modified Alfvén wave'. The only non-zero component of its electric field is E_ϕ. This wave is not generated by a dipole source parallel to the superimposed magnetic field.

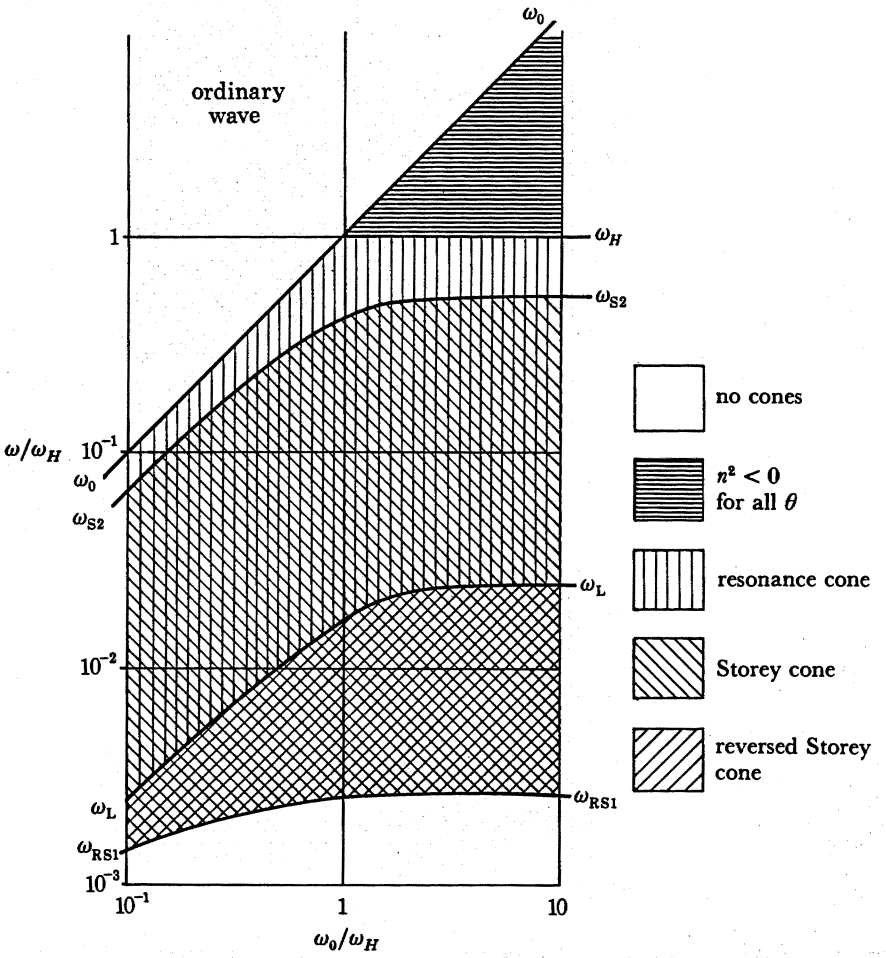

FIGURE 13. Diagram similar to C.M.A. diagram, for the ordinary wave in a cold collisionless plasma with one species of positive ion. This example is approximately correct for a fully ionized proton plasma. For a plasma with 'electrons only', the transition curves marked ω_L and ω_{RS1} would be absent and the region with a resonance and a Storey cone, that applies to the whistler wave, would extend down to zero frequency.

9. CLASSIFICATION OF RESULTS: TRANSITION FREQUENCIES

Either of the two $\beta(\theta)$ curves, and its associated refractive index surface and ray surface, changes its form when ω passes through certain transition frequencies. These correspond to boundary lines in the C.M.A. diagram. Their behaviour will first be described for a fully ionized proton plasma, since this is typical of a plasma with a single positive ion species. Thus there is only one ion cyclotron (angular) frequency Ω_i, and it will here be written Ω_H.

For a given type of plasma it is usual to draw just one C.M.A. diagram. But since the ordinary and extraordinary waves are separate systems, unconnected when $\theta \neq \frac{1}{2}r\pi$, as explained in §8,

it proves helpful to use separate diagrams for the two waves. Figure 13 is such a diagram for the ordinary wave, but the ordinates and abscissae are different from those normally used. The abscissa is ω_0/ω_H and is independent of ω so that each vertical line represents a plasma of fixed composition. The ordinate is ω/ω_H. Figure 14 is a similar diagram for the extraordinary wave.

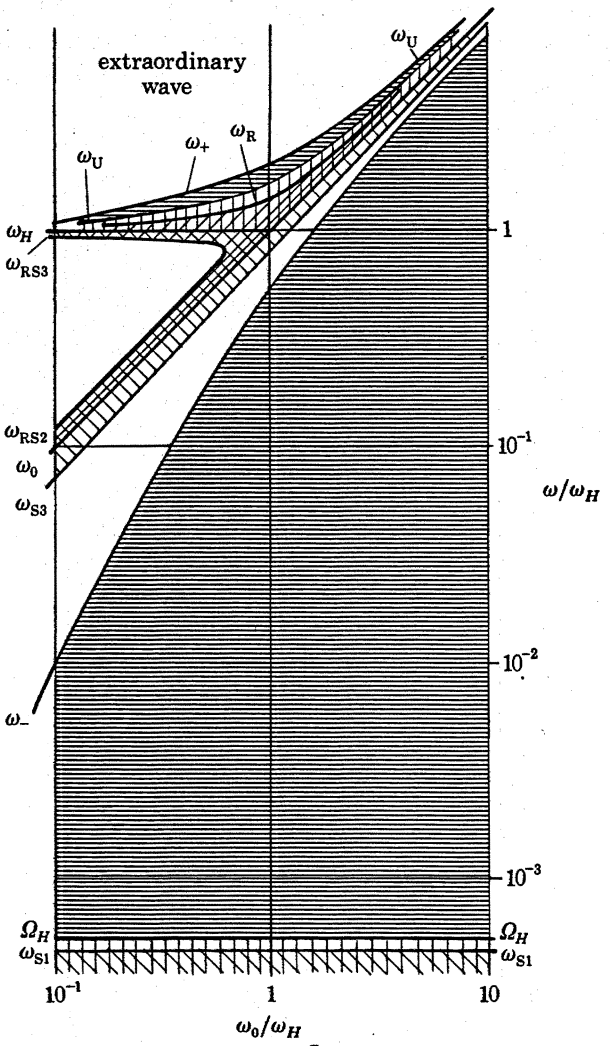

FIGURE 14. Similar to figure 13 but for the extraordinary wave. For a plasma with 'electrons only', the transition curves marked Ω_H and ω_{S1} would be absent and the region of evanescence would extend down to zero frequency. The curves Ω_H and ω_{S1} are actually extremely close together. They have been deliberately separated here, so as to show their form. Similarly, the curve ω_{RS3} has been distorted. It is actually extremely close to the line ω_H.

Figure 11 shows the types of $\beta(\theta)$ curve that occur for the ordinary wave, and should be studied in comparison with figure 13. In each diagram of figure 11 the curves are of the same type. The limiting curve at the lowest frequency is shown as a broken line and at the greatest frequency it is a chain line. These limiting curves occur at the transition frequencies which are listed below. For the lowest frequency range, figure 11*a*, the $n(\theta)$ curve is closed and has no points of inflexion. In the limit of zero frequency it is a sphere and the $\beta(\theta)$ curve is the straight line $\beta = \theta$. This is the modified Alfvén wave mentioned at the end of §8. As the frequency is increased its properties are given consecutively by figures 11 (*a*–*d*). For the greater frequencies in this sequence the wave

is known as the 'electron whistler wave'. The upper frequency limit for this wave is either ω_0 when $\omega_0 < \omega_H$, or ω_H when $\omega_H < \omega_0$. When $\omega > \omega_0$, figure 11*e*, the wave is known simply as the 'ordinary wave' and is then the one commonly used for probing the ionosphere at high frequency.

Similarly figure 12 shows the $\beta(\theta)$ curves for the extraordinary wave and should be studied in comparison with figure 14. The sequence here is more complicated and depends on whether $\omega_H < \omega_0$ or $\omega_H > \omega_0$, as explained in the legend for figure 12, but in both cases there are three types of wave in three frequency ranges separated by the two ranges $\Omega_H < \omega < \omega_-$ and $\omega_U < \omega < \omega_+$ where the wave is evanescent for all θ. The wave for the lowest frequency range, $\omega < \Omega_H$, is the Alfvén wave, figures 12*a* and *b*. The wave for the range $\omega_- < \omega < \omega_U$ is known as the Z mode. This range includes the two curves labelled ω_{RS2} and ω_{RS3} which join where their tangent is vertical at $\omega_0/\omega_H = g$ say $(g < 1)$. If $\omega_0 < g\omega_H$ the sequence of $\beta(\theta)$ curves for the Z mode is 12$(c, \ldots, i)$. If $\omega_0 > \omega_H$ the sequence is 12(c, d, k, i). If $g\omega_H < \omega_0 < \omega_H$ the sequence is not shown in figure 12. Another diagram is then needed for the frequency range $\omega_0 < \omega < \omega_H$. Its curves would have the same shape as in figures 11*e* and *g* but there would be no limiting curves ω_{RS2} or ω_{RS3}.

Transition frequencies are denoted by Ω (for ion cyclotron frequencies) or by ω with a subscript, for example ω_+, ω_0, ω_{RS} as used earlier. When a given type of transition occurs at more than one frequency, for the same plasma, the various values of the transition frequency are given an additional integer subscript, 1, 2, 3, ... in order of increasing frequency, regardless of whether the transition occurs for the ordinary or the extraordinary wave. Thus for a plasma with only one species of positive ion, there are three values of ω_S, of which ω_{S1} and ω_{S3} apply for the extraordinary wave, figure 14, and ω_{S2} for the ordinary wave, figure 13. For some hybrid frequencies two integer subscripts are used as explained under (*c*) below.

The following list gives the main properties of the various transition frequencies.

(*a*) *Cut-off frequencies*

When ω decreases and passes through one of the cut-off frequencies ω_+ or ω_-, §8(iii), one of the refractive index surfaces shrinks to zero and becomes imaginary. For any cold plasma there is only one value ω_+ which is the greatest cut-off frequency for the extraordinary wave. The number of values of ω_- is equal to the number of positive ion species, including ions of infinite mass, if any are assumed to be present. For a plasma with only one positive ion species the one value of ω_- gives cut-off for the extraordinary wave, figure 14. For a plasma with more than one positive ion species, the ordinary wave can also show cut-off of this kind. See, for example, figure 22.

It can be proved that each cut-off frequency must always be at the lower end of a frequency range where $n(\theta)$ is real.

(*b*) *Cyclotron frequencies*

The ion cyclotron frequencies are usually denoted by Ω_i (§2) but when there is only one, Ω_H is sometimes used, or when reference is made to a specific ion then, for example, $\Omega(He^+)$ may be used.

When $\omega = \omega_H$ equation (5) shows that ϵ_+ is infinite, and when $\omega = \Omega_i$ $(= \Omega_H)$ then ϵ_- is infinite. In all these cases (44) and (45) show that there is a resonance where $\theta = 0$, $\beta = \pm\frac{1}{2}\pi$. When ω changes and passes through a cyclotron frequency, two different types of behaviour can occur. The first is for the extraordinary wave when ϵ_3 is positive. It can only happen at the

electron cyclotron frequency ω_H and only when $\omega_0 < \omega_H$, figure 12*g*. Then when ω is slightly less than ω_H and close to it, the refractive index surface is closed and has the large value $n = (\epsilon_+)^{\frac{1}{2}}$ where $\theta = 0$. It has a Storey cone at $\theta = \theta_{s1}$, $\beta = \beta_{s1}$, where θ_{s1} is small and β_{s1} is near $\frac{1}{2}\pi$. It also has a reversed Storey cone at $\theta = \theta_{s2}$, $\beta = \beta_{s2}$. When $\omega \to \omega_H$ then $\theta_{s1} \to 0$ and $\beta_{s1} \to \frac{1}{2}\pi$. The $\beta(\theta)$ curve moves to a limiting curve shown as a chain line in figure 12*g*. This is made up of the line segment $\theta = 0$, $0 \leqslant \beta \leqslant \frac{1}{2}\pi$, together with the curve marked ω_H in figures 12*g* and *h*. The equation of this curve can be found from (35) and the dispersion relation. When ω slightly exceeds ω_H, this refractive index surface is open and has a real reversed resonance θ_r which is small, with β_r slightly greater than $\frac{1}{2}\pi$, and the Storey cone has disappeared, but the reversed Storey cone remains, figure 12*h*. The $\beta(\theta)$ curve crosses the line $\beta = \frac{1}{2}\pi$ where θ is small and meets the resonance line at θ_r, β_r. Thus the transition of ω through the electron cyclotron frequency is where a reversed resonance appears, and a Storey cone disappears.

The second type of transition occurs when ϵ_3 is negative at a cyclotron frequency. When there is only one positive ion species it occurs only for the extraordinary wave, but for more than one it occurs also for the ordinary wave. When ω is less than this cyclotron frequency and close to it, the refractive index surface has a resonance cone with small θ_r and with $\beta_r = -\frac{1}{2}\pi + \theta_r$. The associated branch of the $\beta(\theta)$ curve, figure 12*b*, runs steeply from $\theta = 0$, $\beta = 0$ to the resonance line where $\theta = \theta_r$, $\beta = -\frac{1}{2}\pi + \theta_r$. When ω equals the cyclotron frequency this branch moves to coincide with the line segment $\theta = 0$, $-\frac{1}{2}\pi \leqslant \beta \leqslant 0$. When ω exceeds the cyclotron frequency the refractive index surface and the $\beta(\theta)$ curve are no longer real. This type of transition occurs at $\omega = \omega_H$ only if $\omega_0 > \omega_H$ and then for the ordinary wave. It occurs also at all ion cyclotron frequencies Ω_i. For the greatest Ω_i it is for the extraordinary wave and for successively smaller Ω_i it is alternately for ordinary and extraordinary.

(*c*) *Hybrid frequencies*

Frequencies for which $\epsilon_+ + \epsilon_- = 0$ are called hybrid frequencies. The greatest of them ω_U is the upper hybrid frequency. It is mainly associated with the electrons and is given approximately by

$$\omega_U \approx (\omega_H^2 + \omega_N^2)^{\frac{1}{2}}. \tag{112}$$

For this frequency, $\epsilon_3 > 0$. The next greatest is denoted by ω_L and is called the lower hybrid frequency. It satisfies $\Omega_i \ll \omega_L < \omega_H$ for all ion species i, and it is given approximately by

$$\omega_L = \{(\sum_i C_i r_i)\, \omega_N^2 \omega_H^2 / (\omega_N^2 + \omega_H^2)\}^{\frac{1}{2}} \tag{113}$$

(notation as in §1). The other hybrid frequencies are denoted by $\omega_{L1,2}$, $\omega_{L2,3}$, ... and are called ion–ion hybrid frequencies. It can be shown that $\omega_{Lj,j+1}$ is between Ω_j and Ω_{j+1}. Thus the total number of hybrid frequencies is equal to the number of ion species, including electrons. At all of them (44) and (46) show that there is a resonance where $\theta = \pm\frac{1}{2}\pi$, $\beta = 0$ or π. All of them except ω_U occur where $\epsilon_3 < 0$.

When ω is slightly less than the upper hybrid frequency ω_U, the refractive index surface for the extraordinary wave, figure 12*i* has reversed resonance cones where $\theta = \frac{1}{2}\pi \pm \psi$ and $\beta = \psi, \pi - \psi$ where ψ is a small angle. One branch of the $\beta(\theta)$ curve runs steeply from $\theta = \frac{1}{2}\pi$, $\beta = \frac{1}{2}\pi$ to the resonance line where $\theta = \frac{1}{2}\pi - \psi$, $\beta = \pi - \psi$. When $\omega = \omega_U$, the whole of this branch moves to coincidence with the line segment $\theta = \frac{1}{2}\pi$, $\frac{1}{2}\pi \leqslant \beta \leqslant \pi$. When ω is greater than ω_U, this $\beta(\theta)$ curve is no longer real.

PHILOSOPHICAL TRANSACTIONS OF THE ROYAL SOCIETY A MATHEMATICAL, PHYSICAL & ENGINEERING SCIENCES

For the lower hybrid resonances, the behaviour is different. When there is only one positive ion species, it occurs only for the ordinary wave. When ω is on one side of ω_L where $\epsilon_+ + \epsilon_- < 0$, and close to it, one refractive index surface is closed and has the large value $n = \{2\epsilon_+\epsilon_-/(\epsilon_+ + \epsilon_-)\}^{\frac{1}{2}}$ (see §8) where $\theta = \frac{1}{2}\pi$. It has a reversed Storey cone at $\theta = \theta_{s1}$, $\beta = \beta_{s1}$ where θ_{s1} is near $\frac{1}{2}\pi$ and β_{s1} is near 0. It also has a Storey cone at $\theta = \theta_{s2}$, $\beta = \beta_{s2}$. When $\omega \to \omega_L$ then $\theta_{s1} \to 0$ and $\beta_{s1} \to \frac{1}{2}\pi$, and $\beta(\theta)$ moves to a limiting curve, figure 11*b*, running from $\theta = 0$, $\beta = 0$, to $\theta = \frac{1}{2}\pi$, $\beta = 0$ (Al'pert 1980*a*, equation (37)) together with the line segment $\theta = \frac{1}{2}\pi$, $0 \leqslant \beta \leqslant \frac{1}{2}\pi$. When ω is on the other side of ω_L this refractive index surface has a real resonance θ_r slightly less than $\frac{1}{2}\pi$, with β_r negative and small, and the real reversed Storey cone has disappeared, but the Storey cone remains. The $\beta(\theta)$ curve, figure 11*c*, crosses the line $\beta = 0$ where θ is nearly $\frac{1}{2}\pi$, and it then meets the resonance line at θ_r, β_r.

(*d*) *The window frequency*

The window frequency ω_0 is where $\epsilon_3 = 0$. Here the properties of the refractive index surfaces and of $\beta(\theta)$ are determined mainly by the electrons. When ω slightly exceeds ω_0, the $\beta(\theta)$ curve for the ordinary wave figure 11*e* is monotonic and has no resonance. When ω decreases to ω_0, this curve approaches the two straight line segments $\theta = 0$, $-\frac{1}{2}\pi \leqslant \beta \leqslant \frac{1}{2}\pi$ and $\beta = \frac{1}{2}\pi$, $0 < \theta \leqslant \frac{1}{2}\pi$. When $\omega < \omega_0$ the ordinary refractive index is real only if $\omega_0 < \omega_H$, figure 11*d*, and the wave is then the electron whistler mode. There is a resonance where $\theta = \theta_r$ is small and β is close to $-\frac{1}{2}\pi$. The $\beta(\theta)$ curve has a large negative slope at $\theta = 0$, and runs steeply down to the resonance line. For $\theta > \theta_r$ the refractive index n is imaginary.

For the extraordinary wave, when $\omega < \omega_0$, the $\beta(\theta)$ curve is as shown in figure 12*d*. There is no resonance, but there is one turning point corresponding to a Storey cone where $n < 1$. When ω increases to ω_0 the $\beta(\theta)$ curve approaches the two straight line segments $\theta = \beta$, and $\theta = 0$, $-\frac{1}{2}\pi \leqslant \beta \leqslant \frac{1}{2}\pi$. When $\omega > \omega_0$ the behaviour depends on ω_H. If $\omega_H > \omega_0$ the $\beta(\theta)$ curve is as in figure 12*e*. There is no resonance, but there are two turning points giving a Storey cone and a reversed Storey cone, both where $n > 1$. If $\omega_H < \omega_0$ the $\beta(\theta)$ curve is as in figure 12*k*. There is a reversed resonance at θ_r, β_r and $\theta_r \to 0$, $\beta_r \to \frac{1}{2}\pi$ when $\omega \to \omega_0$. There is also one turning point giving a reversed Storey cone with $n > 1$.

(*e*) *Storey cone appears at* $\theta = 0$

It was shown by Walker (1977*b*) that when ω passes through a value ω_S which makes

$$(\epsilon_3 + \epsilon_+)(\epsilon_3 + \epsilon_-) = 0, \tag{114}$$

one of the refractive index surfaces $n(\theta)$ has a point of inflexion at $\theta = 0$. When ω is on one side of ω_S there are no real points of inflexion. When it is on the other side there are two real points of inflexion for equal and opposite values $\pm\theta_s$ of θ, and these lie on a Storey cone, where $\beta = \pm\beta_s$. If $\partial\beta/\partial\theta$ is negative where $\theta = 0$, then β_s and θ_s have opposite signs as in figure 12*d*. If it is positive, β_s and θ_s have the same sign, as in figure 11*c*.

(*f*) *Reversed Storey cone appears at* $\theta = \frac{1}{2}\pi$

It was further shown by Walker (1977*b*) that when ω passes through a value ω_R which makes

$$(\epsilon_3 - \epsilon_{xx})\{\epsilon_+\epsilon_-(\epsilon_3 + \epsilon_{xx}) - 2\epsilon_3\epsilon_{xx}^2\} = 0, \tag{115}$$

one of the refractive index surfaces $n(\theta)$ has a point of inflexion where $\theta = \frac{1}{2}\pi$. When ω is on one side of ω_R there are no real points of inflexion. When it is on the other side there are two real

points of inflexion for equal and opposite values of $\frac{1}{2}\pi - \theta$ and these lie on reversed Storey cones where $\beta = \beta_s$ and $\frac{1}{2}\pi - \beta_s$. The behaviour of the $\beta(\theta)$ curves is shown in figures 12 (h, i, k). For the proton plasma there is only one example of this transition. It occurs for the extraordinary wave, figure 14 and there it is the second factor of (115) that is zero. There is another real frequency, where the first factor is zero but the associated point of inflexion occurs in the $n(\theta)$ curve for which n is imaginary when $\theta \to \frac{1}{2}\pi$.

(*g*) *Storey cone and reversed Storey cone appear where* $\theta \neq 0$ *or* $\frac{1}{2}\pi$

One of the refractive index surfaces $n(\theta)$ can have two coincident real points of inflexion at some θ in the range $0 < \theta < \frac{1}{2}\pi$, when ω has a value ω_{RS}. There is no simple formula for this condition. When ω is on one side of ω_{RS} there is a real Storey cone and a real reversed Storey cone for values of θ_s in the same quadrant of the refractive index surface. These move to coincidence when $\omega \to \omega_{RS}$, and become complex when ω is on the other side of ω_{RS}. At this transition the $\beta(\theta)$ curve has a point of inflexion where the gradient is zero. Examples appear in figures 11 *a*, *b* and 12 (*e*–*g*).

(*h*) *Field enhancement on the axis*

If enhancement of the field on the z axis is to occur, as described in § 7, it is necessary that the refractive index surface shall have a normal parallel to the z axis for $\theta \neq 0$. Thus the $\beta(\theta)$ curve must cross the line $\beta = 0$ where $\theta \neq 0$. This means that (85) must have a solution that leads to a real non-zero value of θ. The transition to this state occurs when (85) has a solution giving $\theta = 0$, namely $n^2 = \epsilon_+$ or ϵ_-. Hence the transition occurs when

$$\epsilon_3 = \pm\epsilon_+ \quad \text{or} \quad \epsilon_3 = \pm\epsilon_-. \tag{116}$$

These conditions with the $-$ signs are the same as conditions (114). The $+$ signs are of no practical interest because then (116) is only satisfied when ϵ_+ or ϵ_- is negative so that n is imaginary. The transition could also occur when (85) has two equal solutions both giving a real non-zero value of θ. This requires that the discriminant of the quadratic (85) shall be zero, but this is only possible if $\theta = 0$, or if $\epsilon_3 = 0$, that is at the window frequency. Thus the transition only occurs when ω is ω_S or ω_0.

(*i*) *Crossover*

The crossover frequency $\omega = \omega_{cr}$ is where $\epsilon_+ = \epsilon_-$ (97). No examples of it appear in figures 11–14 because these apply to a plasma with only one positive ion species. It was shown in § 8 (viii) that one refractive index surface does not change its topology when ω passes through ω_{cr}. The other has a Storey cone at $\theta = \theta_s(\omega)$ for both $\omega > \omega_{cr}$ and $\omega < \omega_{cr}$. In the limit $\omega \to \omega_{cr}$, θ_s tends to zero and the Storey cone is then absent, but the $n(\theta)$ curve does not have a point of inflexion at $\theta = 0$ and the $\beta(\theta)$ curve has non-zero gradient at $\theta = 0$. If this surface is the outer refractive index surface (§ 8 (viii)), the $\beta(\theta)$ curves are of the form in figure 11 *c*. If it is the inner refractive index surface, they are of the form in figure 12 *d*. This applies in both cases for ω less than or greater than ω_{cr}. But the limiting curves are not the same as the curves ω_{S1}, ω_{S2} respectively. Thus ω_{cr} is not a real transition frequency. The $\beta(\theta)$ curves move to a limiting form but do not pass through it.

The foregoing theory has shown that the topology of the refractive index surface and the ray surface, and the form of the $\beta(\theta)$ curve, change when ω goes through any of the transition frequencies ω_+, ω_-, ω_H, Ω_i, ω_U, ω_L, ω_0, ω_S, ω_R, ω_{RS}. For a homogeneous plasma there is only one

value of each of $\omega_+, \omega_H, \omega_U, \omega_0$ but the other six may have more than one value, depending on the number of ion species and their concentrations. The ascending order of these transition frequencies is not the same for all plasmas. Some examples are given in later sections.

10. Results for a fully ionized cold proton plasma

Results will now be given to illustrate some of the main properties of the formulae derived in earlier sections. The curves given here show the dependence of

$$|E| = \{|E_x|^2 + |E_y|^2 + |E_z|^2\}^{\frac{1}{2}}, \tag{117}$$

on frequency f and on ray direction β. They were computed from $\mathscr{F}_j$ $(j = 1, 2, 3)$ as given by the formulae (79) for β near a Storey cone or reversed Storey cone, by (89) for the enhanced fields near the axis, and by (39) when β is not near either of these field enhanced regions. When β is near a resonance or reversed resonance cone (39) can still be used (§5). In the expressions the factor $Mk^3/4\pi\epsilon_0$ is omitted for simplicity (see §3). For the same dipole source in free space the corresponding radiation field, again with the factor $Mk^3/4\pi\epsilon_0$ omitted, would be

$$E_\theta = (kr)^{-1} \sin\beta \, \mathrm{e}^{-\mathrm{i}kr}; \quad |E| = (kr)^{-1} \sin\beta, \tag{118}$$

which is useful for comparison.

The properties of a plasma are different for the two cases $\omega_N > \omega_H$ and $\omega_N < \omega_H$. Results are therefore presented for $\omega_N/\omega_H = 2.0$ and $\omega_N/\omega_H = 0.3$. The properties of either of these two proton plasmas can be summarized by constructing a chart which is a cross section of figure 13, ordinary wave, and figure 14, extraordinary wave, for a fixed ω_N. The chart for $\omega_N/\omega_H = 2$ is shown in figure 15, and for $\omega_N/\omega_H = 0.3$ in figure 20. These charts apply for a collisionless plasma. The results that follow are for a plasma with collisions, but the charts are still useful.

(a) *Proton plasma with* $\omega_N/\omega_H = 2$

An example of how $|E|$ depends on β at a fixed frequency, $f = 2.4 \times 10^5$ Hz, is shown in figure 16, which combines features already shown separately in figures 2, 4, 5, 8 and 9. Figure 15 shows that at this frequency the extraordinary wave is cut off (evanescent) for all ray directions β. The ordinary wave is the electron whistler mode and it too is cut off for all β greater than the resonance cone angle $\beta_r \approx 13°$. The $\beta(\theta)$ curve is of the form shown in figure 11*c* or 12*a*. There are three (or less) contributing saddle points, and where they are well separated in the complex n_ρ plane, their contributions are shown separately as long dash lines. Where two of them are close together, their contributions are combined to give the field enhancement near the axis, or the Storey cone. These are shown as continuous lines. The effect of the collision frequency $\nu_e = 100\,\mathrm{s}^{-1}$ on these curves is very small. Part of the curve for no collisions is shown as a short-dash line.

Also shown, as a chain line, is the field (118) that would be observed at the same range for a dipole source with the same moment M in free space. This shows that there is a field amplitude enhancement of about 10 times at the maximum of the Storey cone, and about 5×10^4 times at the resonance maximum. It should be remembered, however, that this dipole in free space requires very much less power input than a dipole with the same moment M in the plasma. This is because immersion in the plasma greatly increases its radiation resistance. For the example of

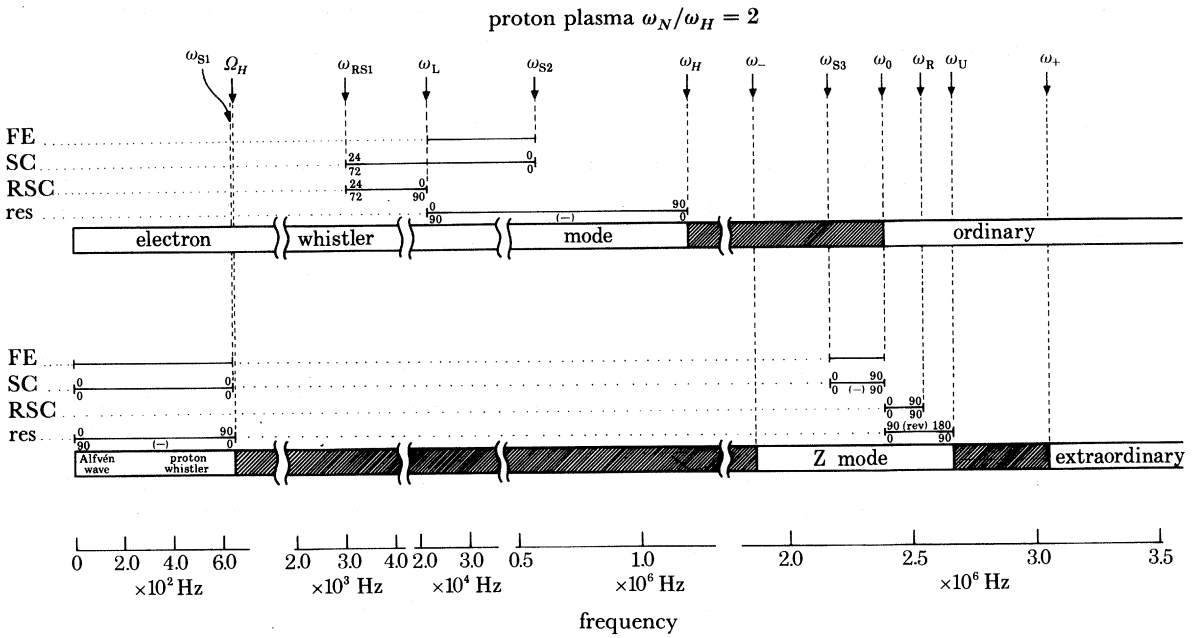

FIGURE 15. Chart for a cold, fully ionized, loss free proton plasma with $\omega_N/\omega_H = 2.0$. The upper and lower strips refer to the ordinary and extraordinary waves respectively, and the shaded parts show where these waves are cut off (evanescent) for all real wave normal and ray directions. The transition frequencies marked at the top are defined in §9. The frequency scale is divided into sections and is linear in each section. The horizontal lines show the frequency ranges where the various features of the field (FE: field enhancement on axis; res: resonance) as indicated at the left, are present. The numbers above and below them give the values in degrees of β and θ respectively at the ends of the ranges.

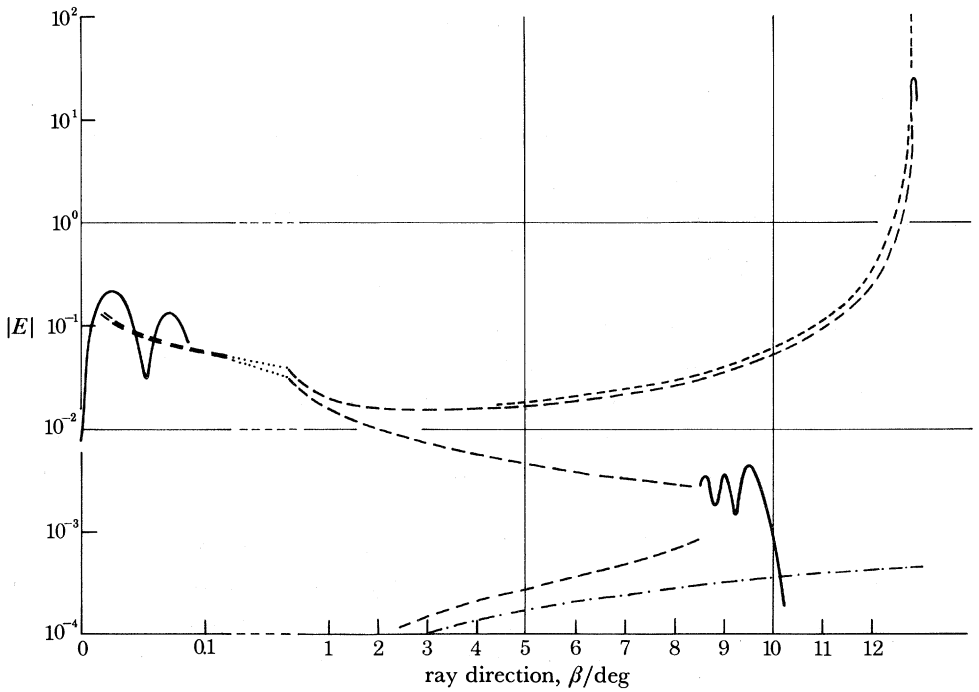

FIGURE 16. Dependence of $|E|$, equation (117), on ray directions β for a frequency $f = 2.4 \times 10^5$ Hz, in a proton plasma with $f_N = 2.3874$ MHz, $f_H = 1.1937$ MHz and electron collision frequency $\nu_e = 100\ s^{-1}$. The short dash curve shows results for no collisions. The chain line shows the comparison value of $|E|$ in free space, equation (118), for a source with the same dipole moment M.

figure 16, the radial component Π_ρ of the time averaged Poynting vector was calculated as explained in §§4–6, and a rough graphical evaluation of the integral

$$P = 4\pi \int_0^{\frac{1}{2}\pi} \Pi_\rho \sin\beta \, \mathrm{d}\beta \tag{119}$$

was used to estimate the power input P. It was found that if the comparison dipole in free space was fed with a power P, its moment M would have to be increased by a factor of approximately 40, and the ordinates of the chain line in figure 16 would have to be increased by this factor. The field enhancement factor at the resonance would then be only of order 10^3, and the field at the maximum of the Storey cone would be less than one third of the value in free space.

Another example of the β dependence of $|E|$ for the same plasma is shown in figure 17. This also is for the electron whistler mode, at a frequency $f = 1.1937 \times 10^4$ Hz and figure 15 shows that here again the extraordinary wave is cut off for all β. The ordinary wave is not cut off for

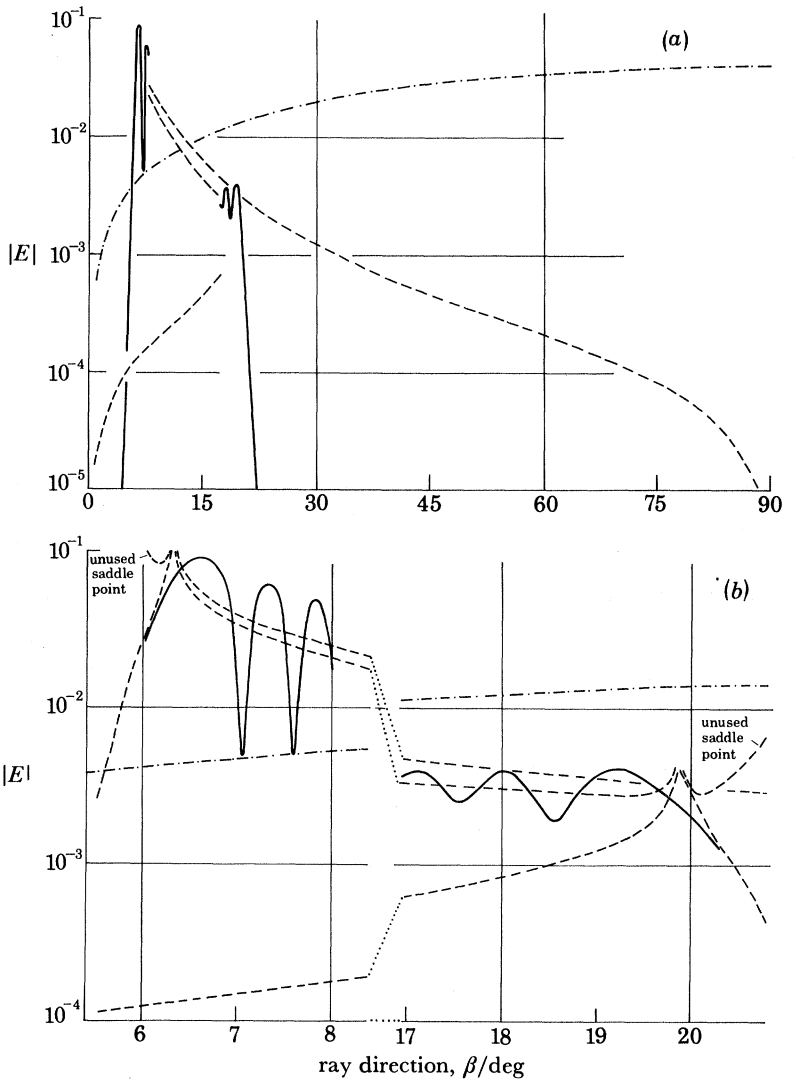

FIGURE 17. Results for the same plasma as in figure 16 but for a frequency 1.1937×10^4 Hz. Here there is no resonance, but there is a Storey cone at $\beta = 19.88°$ and a reversed Storey cone at $\beta = 6.34°$. Figure 17 (*a*) shows the general behaviour and figure 17 (*b*) shows the details near the cones. The meaning of the various curves is as given in the legend for figure 16.

any β. The $\beta(\theta)$ curve has the form of figure 11*b*. There is no resonance cone, but there is a Storey cone and a reversed Storey cone. The smallness of $|E|$ as β approaches 90° occurs because the refractive index surface there has a very large curvature, so that the slope of the $\beta(\theta)$ curve is large there.

Further curves for this plasma showing the β dependence of $|E|$ near a Storey cone are given in figures 4 and 5. The behaviour of the time averaged Poynting vector near a Storey cone is illustrated in figure 6.

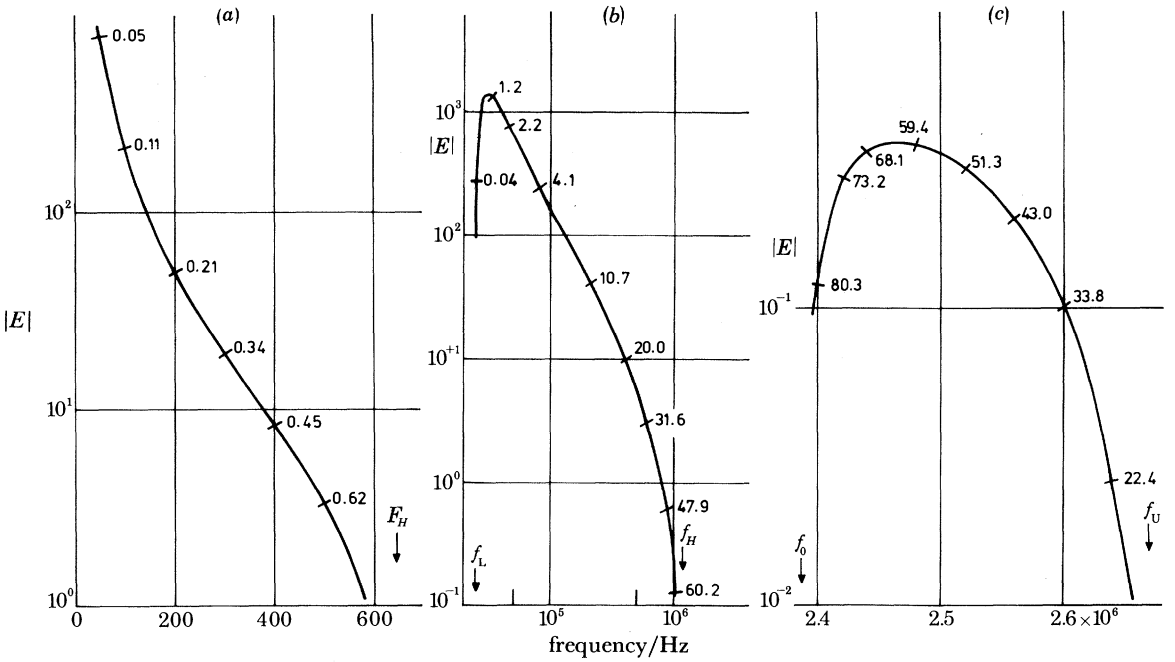

FIGURE 18. Dependence of $|E|$, equation (117), on frequency f at the maxima of resonance cones in a proton plasma with $f_N = 2.3874$ MHz, $f_H = 1.1937$ MHz and electron collision frequency $\nu_e = 100\ s^{-1}$. In (*a*) and (*c*) the frequency scale is linear and in (*b*) it is logarithmic. The numbers by the curves are the values in degrees of the ray direction β at the maxima of the cones. The marked frequencies are the proton gyro frequency F_H, the electron gyro frequency f_H, the lower and upper hybrid frequencies f_L, f_U, respectively and the window frequency f_0. Curve (*a*) is for the extraordinary wave: the Alfvén wave or proton whistler, (*b*) is for the ordinary wave: the electron whistler, and (*c*) is a reversed resonance for the extraordinary wave, Z mode. For (*a*) the range from source to receiver is 200 km. For (*b*) and (*c*) is it 100 km. Comparison values of $|E|$ in free space, equation (118) are as follows. For (*a*) $4.4–5.2\times10^{-3}$. For (*b*) $4.0–4.5\times10^{-4}$. For (*c*) $1.0–1.9\times10^{-4}$.

Figure 15 shows that there are three frequency ranges where a resonance cone is present. One is for the ordinary wave in the range $\omega_L < \omega < \omega_H$ and this is the electron whistler mode. The other two are for the extraordinary wave. One of these is for $\omega < \Omega_H$, the Alfvén wave or proton whistler. The other is a reversed resonance for the Z mode where $\omega_0 < \omega < \omega_U$. Figure 18 shows the frequency dependence of $|E|$ at the maximum of the resonance cone for these three waves. The values from (118) for a dipole in free space are also given, in the caption, for comparison. It should be remembered that the factor $Mk^3/4\pi\epsilon_0$, proportional to the cube of the frequency, is omitted. For any practical study the source dipole moment M would probably depend on frequency in a complicated way depending on the exact type of transmitting aerial used, and on its radiation resistance. The chief interest of the curves of figure 18 is to show the behaviour near the ends of the frequency ranges, and for comparison with other plasmas, figures 23 and 24. Thus figure 18*a* shows that the amplitude enhancement factor is large, about 10^5 at extremely low

frequencies and decreases to 10^2 or less as f approaches the proton gyro frequency F_H. In figure 18*b* the enhancement factor is 5×10^2 to 5×10^6 and decreases at both ends of the frequency range $f_L < f < f_H$. Figure 18*c* is similar with an enhancement factor 10^2 to 2×10^3, showing a decrease at the ends of the range $f_0 < f < f_U$.

Figure 15 also shows that there are three frequency ranges where a Storey cone, a reversed Storey cone, or both are present. These are for the same waves as in figure 18 but for slightly different frequency ranges as follows:

ordinary wave: $\omega_{RS} < \omega < \omega_{S2}$. This range contains the lower hybrid frequency ω_L.

extraordinary wave (Alfvén wave): $\omega < \omega_{S1}$. Here ω_{S1} is less than but very close to Ω_H. The values in the example of figure 19 are: $\omega_{S1} = 257.227\,\mathrm{rad\,s^{-1}}$; $\Omega_H = 257.253\,\mathrm{rad\,s^{-1}}$.

extraordinary wave (Z mode): $\omega_{S3} < \omega < \omega_R$. This range contains the window frequency ω_0. Figure 19 shows the frequency dependence of $|E|$ at the maximum of the cones for these waves.

Where the abscissa f in figure 19 is near to f_{RS} (ω near to ω_{RS}), the ray direction β at the maximum of the Storey cone and reversed Storey cone are close together. This means that there are three saddle points close together in the n_ρ plane. The formula (79) used for figure 19 makes use of two of these saddle points and it is implied that there is no other nearby saddle point. This assumption fails when f is near to f_{RS}, so that the curves at this point must be treated as approximate only. Similar caution is necessary near the other transition frequencies $f_{S1}, f_L, f_{S2}, f_{S3}, f_0$ and f_R. In these regions the curves are shown as dotted lines.

Figure 19 shows that the amplitude enhancement factors for Storey cones and reversed Storey cones are much less than for resonance cones (figure 18) and often they are less than unity. But the decrease at the ends of the frequency ranges is less marked or absent. When the frequency approaches the lower hybrid resonance f_L, the signal amplitude $|E|$ for the reversed Storey cone tends to a large value and the dipole radiation in free space is weak because $\beta \to 0$. These two effects together mean that the enhancement factor is of order 10^5.

Figure 16 shows at $\beta \approx 0.025°$, an example of the enhanced value of $|E|$ near the direction of the magnetic field $\boldsymbol{B}$, that is, in this case, near the axis $\beta = 0$ of the dipole source. Other examples for the same plasma were given in figures 8 and 9. These two figures also show the behaviour of the time averaged Poynting vector.

Resonance cones, Storey cones and reversed Storey cones occur at values of β which are approximately independent of the range from source to receiver. For them it is useful to compare the values of $|E|$ with the values for the same dipole and the same direction in free space, as has been done earlier. But the axial enhancement of $|E|$ occurs at a roughly constant distance from the z axis and therefore with a ray direction $\beta = \beta_v$ say, which is inversely proportional to the range. It is misleading to compare the axially enhanced $|E|$ with the value in free space at this variable value β_v. Instead we compare it with the $|E|$ in free space at the same range and in the direction of the dipole's maximum radiation (that is, in the present example, at $\beta = 90°$). The enhancement factors for the three examples mentioned above are then as follows:

	frequency, f/Hz	range from source to receiver, z/km	distance of maximum from axis, x/m	amplitude enhancement factor
figure 8	2.984×10^4	100	30	1000
figure 9	2.268×10^6	200	80	67
figure 16	2.4×10^5	100	44	100

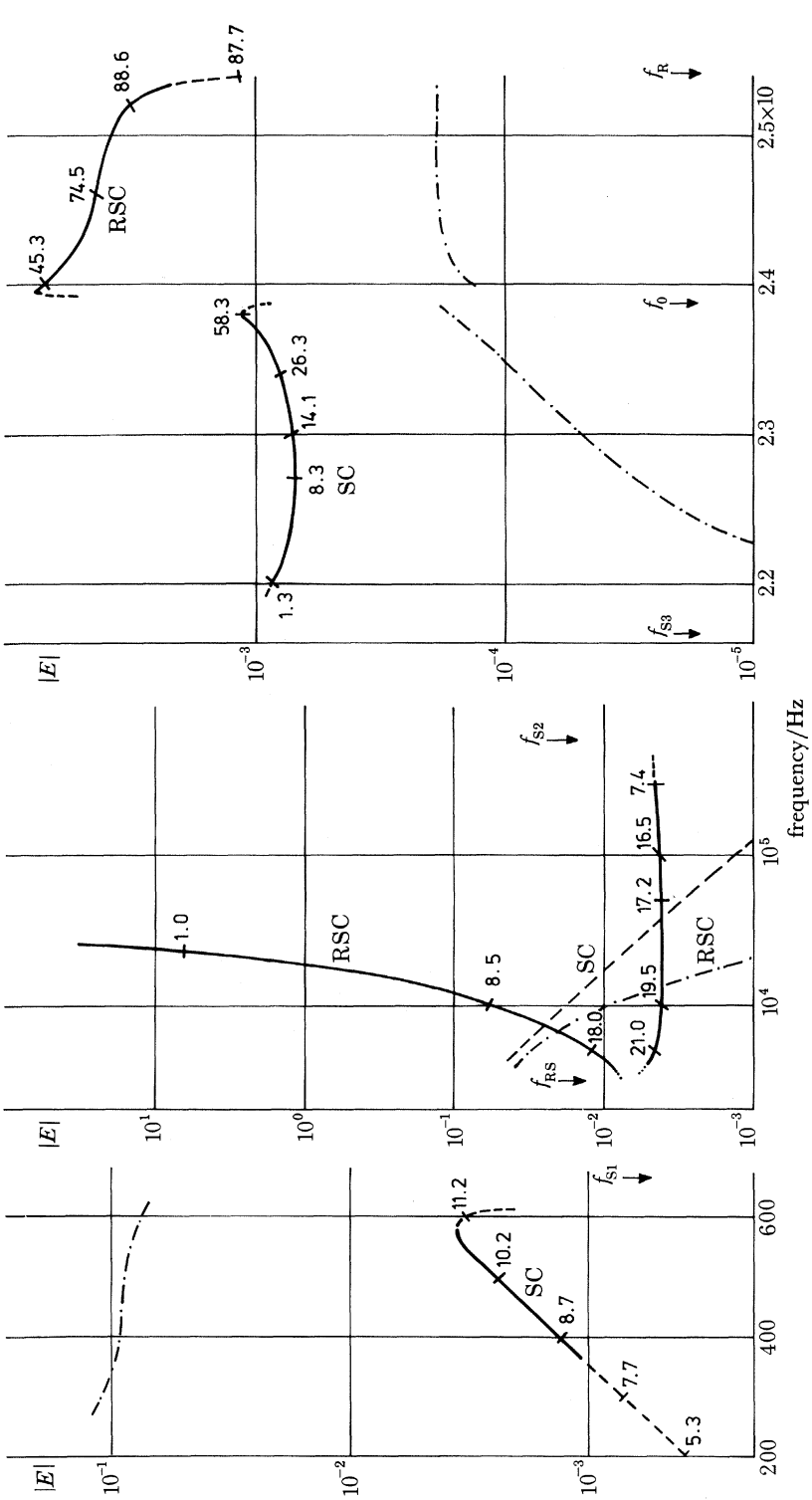

FIGURE 19. Similar to figure 18 and for the same plasma but the $|E|$ values are at the maxima of the Storey cones, marked SC, or the reversed Storey cones, marked RSC. The meaning of the numbers by the curves, the description of the frequency scales, the wave types and the ranges for (*a*), (*b*) and (*c*) are the same as given in the caption of figure 18. The symbols for the transition frequencies are also the same, and in addition f_R, f_S, f_{RS} are used as defined in §9. Comparison values of $|E|$ in free space, equation (118), are shown as chain lines and as a long dash line for SC in (*b*).

PHILOSOPHICAL TRANSACTIONS OF THE ROYAL SOCIETY A MATHEMATICAL, PHYSICAL & ENGINEERING SCIENCES

If the axially enhanced $|E|$ is compared with the free space $|E|$ at $\beta = \beta_v$, the above enhancement factors would have to be multiplied by z/x that is about 2000–3000. The resulting factors are then very large but this is not a property of the plasma. It occurs rather because we happen to have chosen a source dipole that radiates very weakly in free space for directions near to $\boldsymbol{B}$.

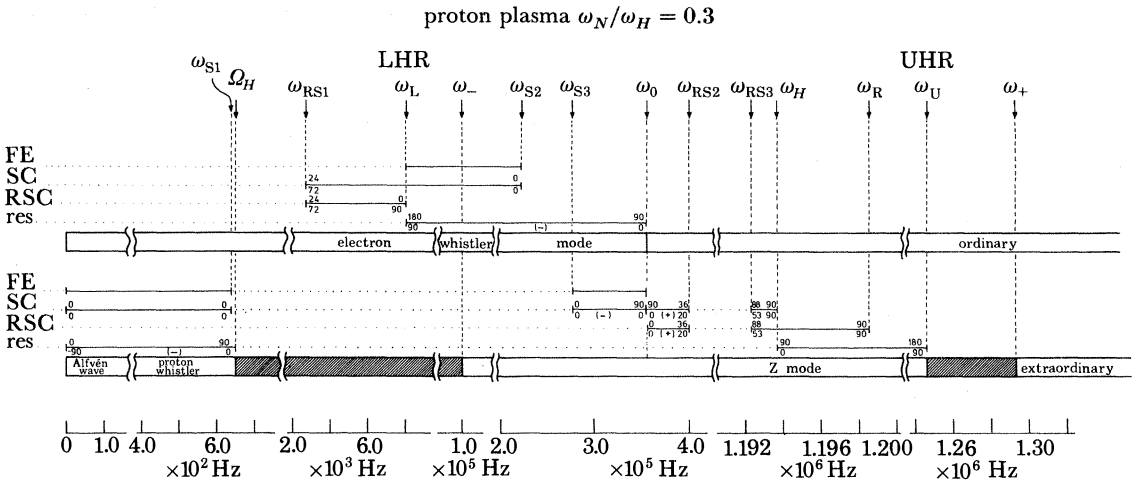

FIGURE 20. Chart similar to figure 15 but for a cold, fully ionized, loss free, proton plasma with $\omega_N/\omega_H = 0.3$.

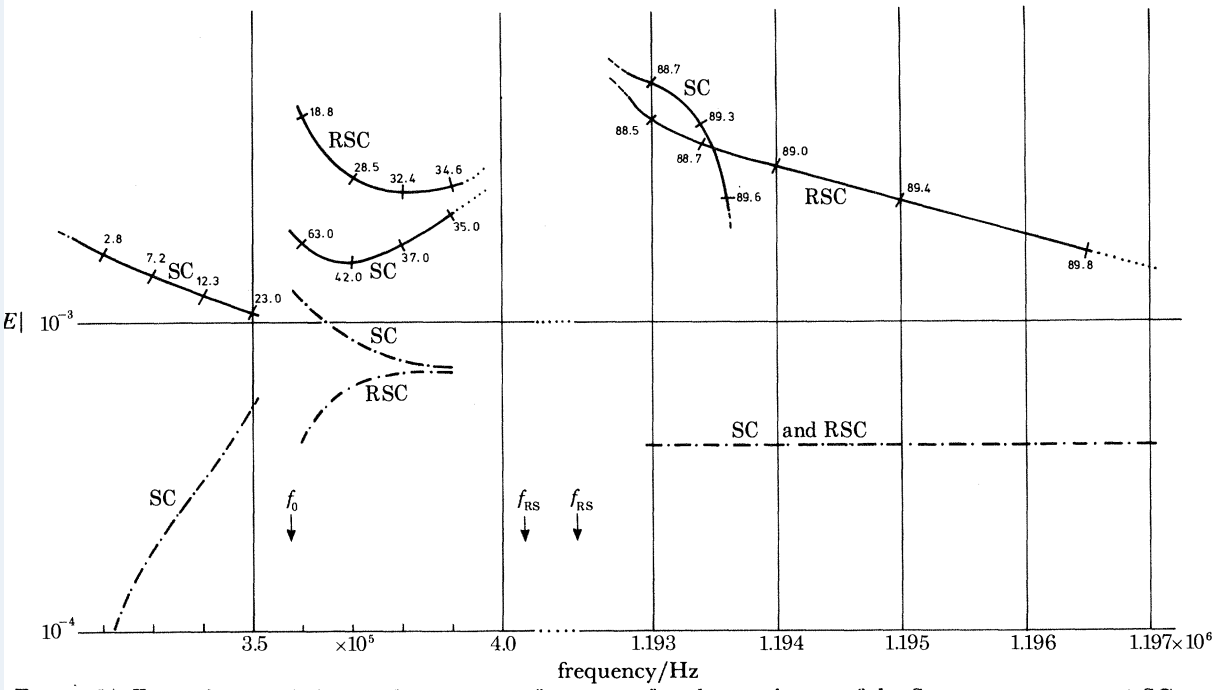

FIGURE 21. Dependence of $|E|$, equation (117), on frequency f at the maximum of the Storey cones, marked SC, and the reversed Storey cones, marked RSC. See legends for figures 16 and 17. These results are for a fully ionized cold proton plasma with $\omega_N/\omega_H = 0.3$ and with $\nu_e = 100\ s^{-1}$. They apply for the extraordinary wave, Z mode. The cones occur in two separate frequency ranges with a gap between them (see figure 20). Where the curves are dotted the formulae are unreliable because too many saddle points of the integrand of (41) are close together. The transition frequencies (see figure 20) beyond the left and right of this figure are $f_S = 2.76 \times 10^5$ Hz and $f_R = 1.1986 \times 10^6$ Hz respectively.

(*b*) *Proton plasma with* $\omega_N/\omega_H = 0.3$

Figure 20 is a chart showing the transition frequencies for this plasma. Comparison with figure 15 shows that there are again three frequency ranges where a resonance or reversed resonance is present. The one for the Alfvén wave, $\omega < \Omega_H$, is the same as in figure 15. For the ordinary wave, electron whistler, the range is now $\omega_L < \omega < \omega_0$ with upper limit ω_0 instead of ω_H. For the reversed resonance in the Z mode the range is $\omega_H < \omega < \omega_U$ with lower limit ω_H instead of ω_0. Apart from these changes there is little difference between the general properties of the resonance and reversed resonance cones for the two plasmas.

Similarly the Storey cone for the Alfvén wave with $\omega < \omega_{S1}$, and the Storey cone and reversed Storey cone for the electron whistler wave, $\omega_{RS1} < \omega < \omega_{S2}$, have similar properties to those for the plasma of §10(*a*). For the Z mode however, figure 20 shows that there are now two separate frequency ranges $\omega_{S3} < \omega < \omega_{RS2}$ containing the window frequency ω_0, and $\omega_{RS3} < \omega < \omega_U$ containing the electron gyrofrequency ω_H where a Storey cone or a reversed Storey cone or both occur. Some results for these cones are shown in figure 21.

11. Results for a fully ionized cold plasma with three positive ion species

In this section we give results similar to those of §10 but for a plasma with three species of positive ion, namely protons, singly charged helium ions and singly charged atomic oxygen ions. It is possible to construct diagrams of C.M.A. type for this plasma similar to figures 13 and 14, to show the various transition frequencies. It is found, however, that transition frequencies less than $\Omega(H^+)$ are almost independent of the electron plasma frequency, equivalently of ω_0. Thus they would appear as nearly horizontal lines in the lower parts of the diagrams. The upper parts of the diagrams are closely similar to figures 13 and 14. Figure 22 is a chart similar to figures 15 and 20 which shows the location of the transition frequencies for the three ion plasma. It is for $\omega_N/\omega_H = 2.0$ but, for those transition frequencies less than $\Omega(H^+)$, it would apply equally well for any other value of ω_N/ω_H in the range 0.1–10.0. It can therefore be used to show where the horizontal transition lines would appear in the lower parts of the C.M.A. type diagrams.

Many of the properties of waves in this plasma are similar to those for the proton plasma, §10. For example curves of $|E|$ against frequency for the maximum of the resonance cone show an amplitude enhancement factor of order 10^2–10^6, but with a decrease as the ends of the frequency range are approached. There is an example in figure 23 as $f \to F(He^+)$. For Storey cones and reversed Storey cones the enhancement is smaller and often less than unity. But for the reversed Storey cone in figure 24 (compare figure 19*b*) it tends to a large value as $f \to f_{L1,2}$ (the smaller ion–ion hybrid frequency), and for the Storey cone in figure 24 it tends to a large value as $f \to F(He^+)$ (the helium gyro frequency).

The new features that appear for this plasma are the two crossover frequencies ω_{cr1} and ω_{cr2}. Figure 22 shows that ω_{cr1} occurs for the ordinary wave and ω_{cr2} for the extraordinary wave. The results now to be given are designed to show the behaviour of the waves for ω near to ω_{cr1}. The behaviour for ω near to ω_{cr2} is very similar.

The properties of the two refractive index surfaces and their $\beta(\theta)$ curves for ω at or near crossover were given in §8(viii). In the present example it is found that, at both crossover frequencies $\epsilon_{xx} + \epsilon_3 < 0$, and this is likely to apply for nearly all multi-ion plasmas encountered in

PHILOSOPHICAL TRANSACTIONS OF THE ROYAL SOCIETY A MATHEMATICAL, PHYSICAL & ENGINEERING SCIENCES

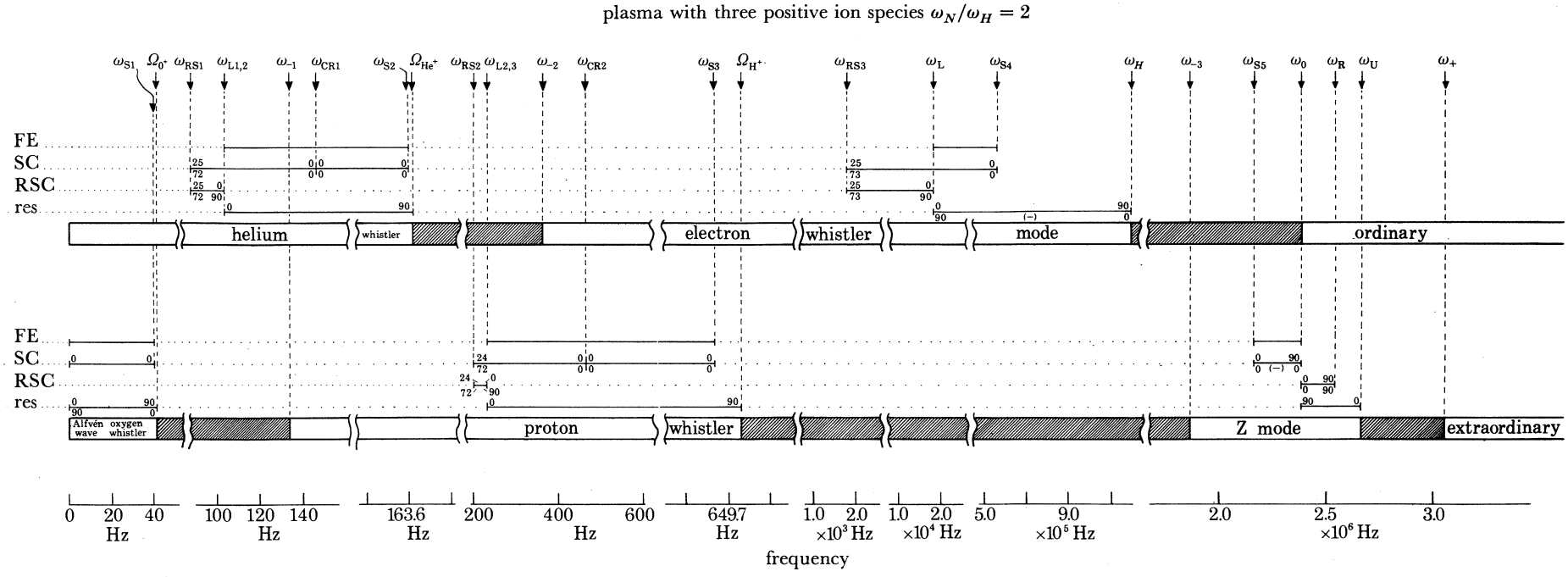

FIGURE 22. Chart similar to figures 15 and 20 to show the transition frequencies for a cold fully ionized plasma with $\omega_N/\omega_H = 2.0$. In this example there are three species of positive ion with concentration ratios C_i (§1) as follows. Protons: $C_1 = 0.5$. He^+ ions: $C_2 = 0.1$. O^+ ions: $C_3 = 0.4$.

practice. Thus the outer refractive index surface has a Storey cone at $\beta = \beta_s$ for ω on either side of ω_{cr}, and $\beta_s \to 0$ when $\omega \to \omega_{cr}$. This surface also has a resonance, and is a hyperboloid at exact crossover. It is associated with field enhancement near the axis, §7, when $\omega \neq \omega_{cr}$. This is confirmed by figure 22; near crossover, the Storey cone, the resonance and the field enhancement occur for the same wave. For this outer surface, at exact crossover, the waves are linearly polarized with the electric vector in the plane ϕ = constant.

The inner refractive index surface is a sphere at exact crossover, and the polarization is then linear with the electric vector perpendicular to the plane $\phi = 0$, and therefore perpendicular to the source dipole which is parallel to the z axis. This wave cannot, therefore, be excited by the source at exact crossover, and the degree of its excitation would be small when ω is near to ω_{cr}.

The equation (34) for finding the saddle points can be expressed as an equation of degree six for n^2 (Budden & Stott 1980). Let

$$Q = \tfrac{1}{2}(\epsilon_+ - \epsilon_-) = -i\epsilon_{xy}. \tag{120}$$

Then, near crossover, Q is very small. If (120) is substituted in the sixth degree equation, and it is then expanded in powers of Q as far as Q^2, the result is, after cancellation of some non-zero factors:

$$\begin{aligned}(n^2-\epsilon_{xx})^5\,(\epsilon_{xx}-\epsilon_3)\,\epsilon_{xx}\{\epsilon_{xx}(n^2-\epsilon_{xx})\cos^2\beta+\epsilon_3(n^2-\epsilon_3)\sin^2\beta\}\\ +(n^2-\epsilon_{xx})^3\,Q^2\{\epsilon_{xx}(n^2-\epsilon_{xx})\cos^2\beta(2n^2\epsilon_{xx}-2\epsilon_3^2-5\epsilon_{xx}^2+3\epsilon_3\epsilon_{xx})\\ +\epsilon_3(n^2-\epsilon_3)\sin^2\beta(5n^2\epsilon_{xx}-n^2\epsilon_3-3\epsilon_{xx}^2-\epsilon_3\epsilon_{xx})\}=0.\end{aligned} \tag{121}$$

There are no odd powers of Q in this expansion. The full expansion contains terms in Q^4 and Q^6 but they are very complicated. The solution $n^2 = \epsilon_{xx}$ of (121) corresponds to the inner and spherical refractive index surface. For this surface, for any value of β, there are three coincident solutions and therefore the integral (32) has three saddle points, which are near together for ω near to ω_{cr}, and coincident at exact crossover. This means that the method of steepest descents as expressed by (39) cannot be used for this inner surface. In the present study with a dipole source parallel to the z axis this is unimportant because the wave is not excited or only weakly excited. For a different source, for example an electric dipole perpendicular to the z axis, the wave is excited and a more elaborate treatment of the integral (32) is needed. This problem has been studied by Stott (1982).

The remaining three solutions of (121) correspond to the outer refractive index surface (104), which has the general shape shown in figure 1*a*. The full sixth degree equation (but not the approximation (121)) shows that two of these solutions are equal when $\beta = 0$, and these two are associated with the field enhancement on the axis, §7. When $\beta \neq 0$ the three solutions are, in general, distinct but two of them move to coincidence when β is on a Storey cone.

The results presented here cover the frequency range 90–163 Hz which is between the gyro frequencies of the oxygen and helium ions. They are designed to show the effect of crossover, at 146.59 Hz, on the resonance cone, figure 23, the Storey cone, figure 24 and the field enhancement on the axis, figure 25. A very small collision frequency was used, $\nu_e = 1.0\,s^{-1}$ with all other collision frequencies equal to zero. At these low frequencies this is sufficient to ensure that (54) was satisfied at resonance for most of the frequency range studied. A range $r = 5000$ km from the source was used so that $kr \approx 9$–17. This was to ensure that the saddle points are sufficiently well separated in the n_ρ plane even when $|\omega - \omega_{cr}|$ is small.

Figure 23 shows how $|E|$ depends on frequency for the maximum of the resonance cone. The values of β, shown by the curve, are very small so that θ is near to 90°. Here the dipole source

radiates strongly. At all frequencies in this range, whether or not they are near crossover, the behaviour near resonance is normal and similar to that shown in figures 16 and 18. There is no deviation of the curve where it passes through the crossover frequency.

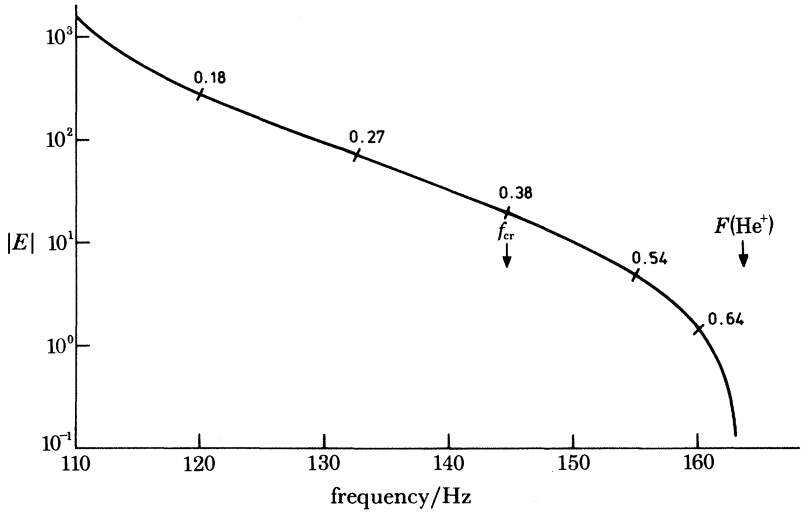

FIGURE 23. Dependence of $|E|$, equation (117), on frequency f at the maxima of resonance cones in the plasma with three positive ion species as described in figure 22. The electron collision frequency is $\nu_e = 1\ s^{-1}$. The range from source to receiver is $r = 5000$ km. Other features are the same as in figure 18. The frequency range used here contains the crossover frequency f_{cr1}.

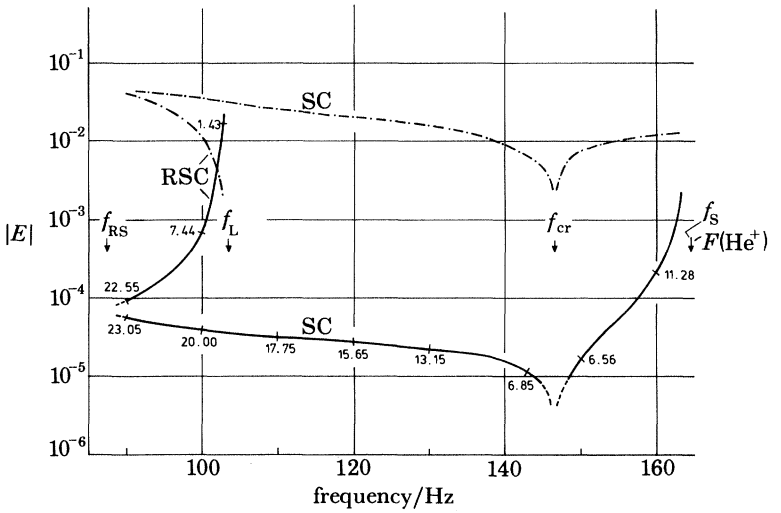

FIGURE 24. Similar to figure 23 and for the same plasma and the same value of r. The $|E|$ values are at the maxima of the Storey cone, marked SC, or the reversed Storey cone, marked RSC. Other features are the same as in figure 18.

Figure 24 shows the frequency dependence of $|E|$ for the Storey cone. There is also a reversed Storey cone for the lower part of the frequency range but this is not near crossover and the behaviour is similar to that already described and shown in figure 19*b*. For the Storey cone the values of β_s and θ_s both approach zero as $|\omega - \omega_{cr}| \to 0$. The dipole radiates only weakly where θ is small and this explains why the signal amplitude is small near crossover. The comparison signal (118) for a dipole source in free space is also shown. This gets small at crossover because there the factor $\sin\beta$ tends to zero.

Figure 25 illustrates the field enhancement near the axis. It shows how $|E|$ depends on distance x from the axis for various frequencies. At exact crossover, where $\epsilon_{xy} = 0$, (86) shows that $n_\rho = n \sin\theta = 0$ so that $\theta = 0$ and the wave is not excited by the source. Thus no curve for exact crossover can appear in figure 25. Curve b is for a frequency very close to crossover and shows that the excitation is small. The other curves show that the excitation gets larger as the frequency gets further away from crossover. Even with this weak excitation the amplitude at the first maximum is enhanced as compared with the signal at the same range for the same dipole in free space in the direction of its maximum radiation. For the curves of figure 25 the enhancement factors are: a, 50; b, 1.3; c, 100; d, 500.

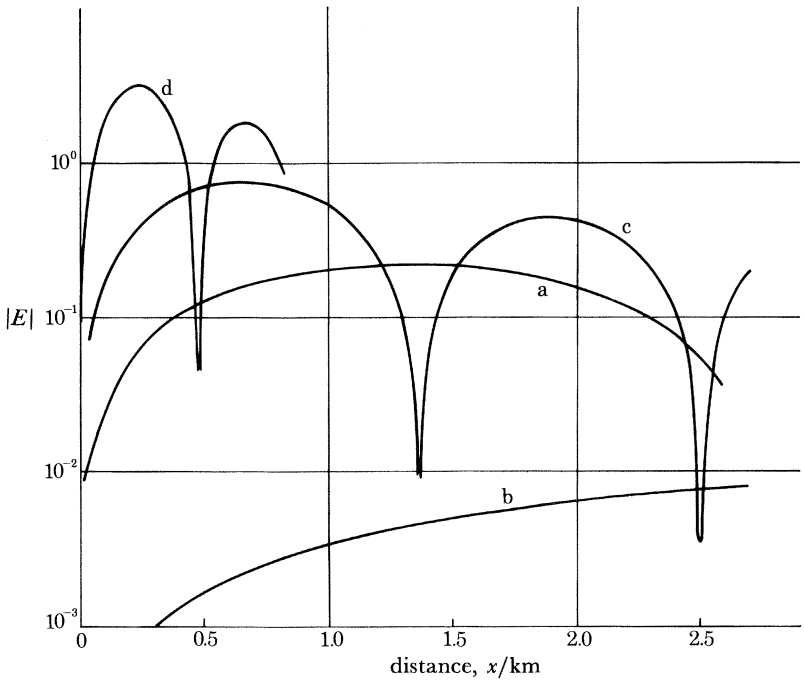

FIGURE 25. Field enhancement near the axis for various frequencies on both sides of the crossover frequency $f_{cr1} = 146.59$ Hz. The plasma is the same as used for figures 23 and 24. The distance z from the source is 5000 km. Other features are the same as for $|E|$ in figures 8 and 9. The frequencies used here are: curve a, 144.90 Hz; curve b, 146.50 Hz; curve c, 152.05 Hz; curve d, 162.31 Hz.

The oscillations of the curves in figure 25 are caused by the Bessel functions that appear in (89) through the factor g_j (28). The argument ξ (26), of these Bessel functions is proportional to n_ρ as given by (86) and gets larger as the frequency f moves away from crossover, so that the period of oscillation gets smaller.

12. Conclusion

In this paper we have tried to illustrate the physical nature of the radiated field from the source dipole, and particularly those features of it which arise from the properties of the plasma itself. The results of outstanding interest are the three types of signal enhancement. These occur in directions and at frequencies which are determined by the plasma and not by the nature of the source. In future work it would be interesting to use other types of source such as a magnetic hertzian dipole, or an electric hertzian dipole perpendicular to the magnetic field, with the

formulae of Appendix B; Stott (1982) has made a start on this. It is also desirable now to extend the theory to deal with situations where three saddle points are close together. This has already been done for another problem (Budden 1976). Its application to the present theory would simply involve the working out of the rather complicated algebra.

The Cambridge authors are indebted to the Cambridge University Computing service. One of them (G.F.S.) was supported by the Science and Engineering Research Council.

Appendix A. Effect of collisions in a cold magnetoplasma containing positive ions and neutral particles

(a) *Object*

This appendix describes how the effect of collisions is incorporated when allowance is made for the relative motion of the various species. It is based on the method described by Al'pert (1980*b*). We study a homogeneous plasma which contains electrons, three species of positive ion, and neutral particles, and their properties are indicated by using subscripts e, 2, 3, 4, n. This is convenient in the matrix operations. Thus we may think of e as the same as 1, and n as the same as 5. The particles have masses m_i, concentrations N_i and velocities $\boldsymbol{v}_i$, where $\boldsymbol{v}_i$ is the average drift velocity of species i caused by the electromagnetic field and by collisional forces. The effective collision frequency of particles i with particles j is ν_{ij} where i, j can be any of e, 2, 3, 4, n. In the actual calculations 2 refers to protons, 3 to singly charged helium ions and 4 to singly charged oxygen ions.

We do not here consider collisions of particles with their own kind. This is a separate effect, sometimes called electron or ion viscosity that requires different treatment (Akhiezher *et al.* 1976; Al'pert 1980*b*).

(b) *Collisional forces*

The average force exerted on one particle of species i through collisions with particles of species j is assumed (Stix 1962) to be

$$-m_i \nu_{ij}(\boldsymbol{v}_i - \boldsymbol{v}_j). \tag{A 1}$$

Thus the rate of transfer of momentum to the particles i in unit volume, from particles j is

$$-N_i m_i \nu_{ij}(\boldsymbol{v}_i - \boldsymbol{v}_j). \tag{A 2}$$

This must be equal and opposite to the rate of transfer of momentum to particles j from particles i, which requires (Stix 1962) that

$$N_i m_i \nu_{ij} = N_j m_j \nu_{ji}. \tag{A 3}$$

In the present study it was thought to be interesting to allow neutral particles to be present, because they can affect the properties of some plasmas, and for very low frequencies their movements are important. This is discussed by Hines (1963).

(c) *Massive ions*

Since the plasma must be neutral, the sum of the concentrations of all the positive ions must equal N_e. It is often assumed that a plasma contains positive ions that are so massive that they cannot move and therefore cannot contribute to the electric permittivity. They serve only as a charge neutralizing background. If their concentration is N_h then neutrality requires that

$$N_e = N_2 + N_3 + N_4 + N_h. \tag{A 4}$$

Let the effective collision frequency for an electron, or ion of species i with a massive ion be ν_{ih}. Then the average force exerted on the ion through collisions is

$$-m_i \nu_{ih} \boldsymbol{v}_i. \tag{A 5}$$

This is simpler than (A 1) because $\boldsymbol{v}_h$ must be zero. It is the same as the expression used in the older theories where relative motions of the particles were ignored. By itself it would lead to the idea of treating collisions by using a complex mass for each particle. This idea is used for most of the results given in the main part of this paper. Thus ν_{eh}, ν_{2h} etc. are the same as ν_e, ν_2 etc. of § 2.

(*d*) *Outline of the method*

We use cartesian coordinates x, y, z. The constant magnetic field $\boldsymbol{B}$ is parallel to the z axis. Each velocity $\boldsymbol{v}_i$ has cartesian components v_{ix}, v_{iy}, v_{iz}. An electric field $\boldsymbol{E}e^{i\omega t}$ is present. It is required to find the electric permittivity tensor $\boldsymbol{\epsilon}$ of the plasma, (1). This is done by finding its three diagonal elements (4) in the complex principal axes. The method is to formulate the linear equations for the velocities $\boldsymbol{v}_i$. These are then transformed to complex principal axis coordinates. In these coordinates the equations for the three sets v_{i-}, v_{i+} and v_{i3} (with $i = e, 2, 3, 4, n$) are separate and independent of each other. Each of them can therefore be solved by matrix inversion. From the solutions the principal axis components P_-, P_+, P_3 of the electric polarization $\boldsymbol{P} = \epsilon_0 (\boldsymbol{\epsilon} - 1) \boldsymbol{E}$ are found. This leads at once to expressions for ϵ_-, ϵ_+, ϵ_3.

(*e*) *Detailed derivation*

The equation of motion of an electron is

$$\begin{aligned} i\omega m_e \boldsymbol{v}_e = {} & -e\boldsymbol{E} - e\boldsymbol{v}_e \wedge \boldsymbol{B} \\ & - m_e\{\nu_{e2}(\boldsymbol{v}_e - \boldsymbol{v}_2) + \nu_{e3}(\boldsymbol{v}_e - \boldsymbol{v}_3) + \nu_{e4}(\boldsymbol{v}_e - \boldsymbol{v}_4) + \nu_{en}(\boldsymbol{v}_e - \boldsymbol{v}_n) + \nu_{eh}\boldsymbol{v}_e\}. \end{aligned} \tag{A 6}$$

The equation of motion of an ion of species i ($= 2, 3$ or 4) is

$$i\omega m_i \boldsymbol{v}_i = e\boldsymbol{E} + e\boldsymbol{v}_i \wedge \boldsymbol{B} - m_i\{\nu_{ie}(\boldsymbol{v}_i - \boldsymbol{v}_e) + \sum_{j \neq i} \nu_{ij}(\boldsymbol{v}_i - \boldsymbol{v}_j) + \nu_{in}(\boldsymbol{v}_i - \boldsymbol{v}_n) + \nu_{ih}\boldsymbol{v}_i\}. \tag{A 7}$$

Finally the equation of motion of a neutral particle is

$$i\omega m_n \boldsymbol{v}_n = -m_n\{\nu_{ne}(\boldsymbol{v}_n - \boldsymbol{v}_e) + \sum_j \nu_{nj}(\boldsymbol{v}_n - \boldsymbol{v}_j) + \nu_{nh}\boldsymbol{v}_n\}. \tag{A 8}$$

These three equations for the vectors $\boldsymbol{v}$ may be written in matrix form by treating the cartesian components v_x, v_y, v_z as a column matrix. The equations then contain matrix products of the form $\boldsymbol{M}\boldsymbol{v}$ where $\boldsymbol{M}$ is 3×3. The matrices $\boldsymbol{M}$ can all be diagonalized by the same unitary transformation (3) to new complex coordinates, called 'principal axis coordinates'. The principal axis values for any $\boldsymbol{v}$ in these coordinates are denoted by v_+, v_-, v_3. Then the required transformation is

$$\begin{bmatrix} v_+ \\ v_- \\ v_3 \end{bmatrix} = \begin{bmatrix} 1/\sqrt{2} & i/\sqrt{2} & 0 \\ 1/\sqrt{2} & -i/\sqrt{2} & 0 \\ 0 & 0 & 1 \end{bmatrix} \begin{bmatrix} v_x \\ v_y \\ v_z \end{bmatrix} = \begin{bmatrix} (v_x + iv_y)/\sqrt{2} \\ (v_x - iv_y)/\sqrt{2} \\ v_z \end{bmatrix}, \tag{A 9}$$

where any subscripts e, 2, 3, 4, n can be used on the quantities v. The same transformation gives the principal axis values E_+, E_-, E_3 of the electric intensity $\boldsymbol{E}$. The cartesian components of the vector $\boldsymbol{v} \wedge \boldsymbol{B}$ are $B(v_y, -v_x, 0)$. Its principal axis components are

$$B \begin{bmatrix} (v_y - iv_x)/\sqrt{2} \\ (v_y + iv_x)/\sqrt{2} \\ 0 \end{bmatrix} = -iB \begin{bmatrix} v_+ \\ -v_- \\ 0 \end{bmatrix}. \tag{A 10}$$

If these results are now put into (A 6), (A 7), (A 8) we obtain three sets of equations, one for the v_+, one for the v_- and one for the v_3. The equations for the v_+ are

$$\begin{aligned} \mathrm{i}\omega m_\mathrm{e} v_{\mathrm{e}+} &= -eE_+ + \mathrm{i}eBv_{\mathrm{e}+} \\ &\quad - m_\mathrm{e}\{\nu_{\mathrm{e}2}(v_{\mathrm{e}+}-v_{2+}) + \nu_{\mathrm{e}3}(v_{\mathrm{e}+}-v_{3+}) + \nu_{\mathrm{e}4}(v_{\mathrm{e}+}-v_{4+}) + \nu_{\mathrm{e}n}(v_{\mathrm{e}+}-v_{\mathrm{n}+}) + \nu_{\mathrm{e}h}v_{\mathrm{e}+}\} \quad \text{(A 11)} \\ \mathrm{i}\omega m_i v_{i+} &= eE_+ - \mathrm{i}eBv_{i+} - m_i\{\nu_{ie}(v_{i+}-v_{\mathrm{e}+}) + \sum_{j\neq i}\nu_{ij}(v_{i+}-v_{j+}) + \nu_{in}(v_{i+}-v_{\mathrm{n}+}) + \nu_{ih}v_{i+}\}, \quad \text{(A 12)} \\ \mathrm{i}\omega m_\mathrm{n} v_{\mathrm{n}+} &= -m_\mathrm{n}\{\nu_{\mathrm{ne}}(v_{\mathrm{n}+}-v_{\mathrm{e}+}) + \sum_j \nu_{\mathrm{n}j}(v_{\mathrm{n}+}-v_{j+}) + \nu_{\mathrm{nh}}v_{\mathrm{n}+}\}, \quad \text{(A 13)} \end{aligned}$$

for $i, j = 2, 3, 4$. From these, the equations for the v_- are obtained by replacing all subscripts $+$ by $-$ and changing the sign of B. The equations for v_3 are obtained by replacing all subscripts $+$ by 3 and omitting the terms containing B.

Now for each $\boldsymbol{v}$ let

$$\boldsymbol{v} = \mathrm{i}\omega \boldsymbol{r}. \quad \text{(A 14)}$$

The same subscripts and superscripts are used on the symbol r as for the symbol v. Divide each equation (A 11)–(A 13) by $-\omega m$ where m has the appropriate subscript. Use

$$eB/m_\mathrm{e} = \Omega_\mathrm{e}, \quad eB/m_i = \Omega_i \quad \text{(angular gyro frequencies)}.$$

Rearrange the equations to obtain

$$\begin{aligned} &r_{\mathrm{e}+}\{\omega - \Omega_\mathrm{e} - \mathrm{i}(\nu_{\mathrm{e}2}+\nu_{\mathrm{e}3}+\nu_{\mathrm{e}4}+\nu_{\mathrm{e}n}+\nu_{\mathrm{e}h})\} + \mathrm{i}\{\nu_{\mathrm{e}2}r_{2+}+\nu_{\mathrm{e}3}r_{3+}+\nu_{\mathrm{e}4}r_{4+}+\nu_{\mathrm{e}n}r_{\mathrm{n}+}) = eE_+/\omega m_\mathrm{e}, \quad \text{(A 15)} \\ &r_{i+}\{\omega + \Omega_i - \mathrm{i}(\nu_{ie} + \sum_{j\neq i}\nu_{ij} + \nu_{in} + \nu_{ih})\} \\ &\qquad + \mathrm{i}\{\nu_{ie}r_{\mathrm{e}+} + \sum_{j\neq i}\nu_{ij}r_{j+} + \nu_{in}r_{\mathrm{n}+}) = -eE_+/\omega m_i \quad \text{for} \quad i, j = 2, 3, 4, \quad \text{(A 16)} \\ &r_{\mathrm{n}+}\{\omega - \mathrm{i}(\nu_{\mathrm{ne}} + \sum_i \nu_{\mathrm{n}i} + \nu_{\mathrm{nh}})\} + \mathrm{i}(\nu_{\mathrm{ne}}r_{\mathrm{e}+} + \sum_i \nu_{\mathrm{n}i}r_{i+}) = 0. \quad \text{(A 17)} \end{aligned}$$

For subscript $-$ reverse the signs of Ω_e, Ω_i. For subscript 3 omit Ω_e and Ω_i.

Equations (A 15)–(A 17) may now be written in matrix form

$$(\boldsymbol{A}_+ + \mathrm{i}\boldsymbol{B})\boldsymbol{c}_+ = (\epsilon_0\omega_N^2 E_+/eN_\mathrm{e}\omega)\,\boldsymbol{d}. \quad \text{(A 18)}$$

Here

$$\omega_N^2 = N_\mathrm{e}e^2/\epsilon_0 m_\mathrm{e} \quad \text{(A 19)}$$

is the square of the angular electron plasma frequency ω_N, $\boldsymbol{A}_+$ is a 5×5 diagonal matrix with elements

$$\omega - \Omega_\mathrm{e}, \quad \omega + \Omega_2, \quad \omega + \Omega_3, \quad \omega + \Omega_4, \quad \omega, \quad \text{(A 20)}$$

$\boldsymbol{c}_+$ is the column with elements $r_{\mathrm{e}+}$, r_{2+}, r_{3+}, r_{4+}, $r_{\mathrm{n}+}$, $\boldsymbol{d}$ is the column with elements 1, $-m_\mathrm{e}/m_2$, $-m_\mathrm{e}/m_3$, $-m_\mathrm{e}/m_4$, 0 and $\boldsymbol{B}$ is the matrix

$$\begin{bmatrix} -(\nu_{\mathrm{e}2}+\nu_{\mathrm{e}3}+\nu_{\mathrm{e}4}+\nu_{\mathrm{e}n}+\nu_{\mathrm{e}h}) & \nu_{\mathrm{e}2} & \nu_{\mathrm{e}3} & \nu_{\mathrm{e}4} & \nu_{\mathrm{e}n} \\ \nu_{2\mathrm{e}} & -(\nu_{2\mathrm{e}}+\nu_{23}+\nu_{24}+\nu_{2\mathrm{n}}+\nu_{2\mathrm{h}}) & \nu_{23} & \nu_{24} & \nu_{2\mathrm{n}} \\ \nu_{3\mathrm{e}} & \nu_{32} & -(\nu_{3\mathrm{e}}+\nu_{32}+\nu_{34}+\nu_{3\mathrm{n}}+\nu_{3\mathrm{h}}) & \nu_{34} & \nu_{3\mathrm{n}} \\ \nu_{4\mathrm{e}} & \nu_{42} & \nu_{43} & -(\nu_{4\mathrm{e}}+\nu_{42}+\nu_{43}+\nu_{4\mathrm{n}}+\nu_{4\mathrm{h}}) & \nu_{4\mathrm{n}} \\ \nu_{\mathrm{ne}} & \nu_{\mathrm{n}2} & \nu_{\mathrm{n}3} & \nu_{\mathrm{n}4} & -(\nu_{\mathrm{ne}}+\nu_{\mathrm{n}2}+\nu_{\mathrm{n}3}+\nu_{\mathrm{n}4}+\nu_{\mathrm{nh}}) \end{bmatrix} \quad \text{(A 21)}$$

PHILOSOPHICAL TRANSACTIONS OF THE ROYAL SOCIETY A MATHEMATICAL, PHYSICAL & ENGINEERING SCIENCES

Similar equations are obtained for $\boldsymbol{c}_-$ and $\boldsymbol{c}_3$. We may therefore temporarily omit the subscripts. Now (A 21) is solved by inversion of the square matrix on the left, to give $\boldsymbol{c}$. If

$$(\boldsymbol{A}+\mathrm{i}\boldsymbol{B})^{-1} = \boldsymbol{X}+\mathrm{i}\boldsymbol{Y}, \tag{A 22}$$

then we have

$$\boldsymbol{X} = (\boldsymbol{A}+\boldsymbol{B}\boldsymbol{A}^{-1}\boldsymbol{B})^{-1}, \quad \boldsymbol{Y} = -\boldsymbol{A}^{-1}\boldsymbol{B}\boldsymbol{X}. \tag{A 23}$$

The electric polarization $\boldsymbol{P}$ in the medium is a vector given by

$$\boldsymbol{P} = e(-N_\mathrm{e}\boldsymbol{r}_\mathrm{e}+N_2\boldsymbol{r}_2+N_3\boldsymbol{r}_3+N_4\boldsymbol{r}_4) = \epsilon_0(\boldsymbol{\epsilon}-1)\,\boldsymbol{E}. \tag{A 24}$$

On taking principal axis components with subscript $+$ we get

$$\epsilon_+ = 1+(\omega_N^2/\omega)\,(-1, N_2/N_\mathrm{e}, N_3/N_\mathrm{e}, N_4/N_\mathrm{e}, 0)\,(\boldsymbol{X}_+ + \mathrm{i}\boldsymbol{Y}_+)\boldsymbol{d}. \tag{A 25}$$

Similar results are obtained for subscript $-$ (reverse signs of Ω_e, Ω_i in (A 20)), and for subscript 3 (omit Ω_e, Ω_i in (A 20)).

Appendix B. Dipole source not parallel to the constant magnetic field

The results in this paper are all for a hertzian dipole source parallel to the superimposed magnetic field $\boldsymbol{B}$, that is to the z axis. They were derived from the integrals given by (27), in which the factor g_j of the integrand was given by the six expressions (28) for the six field components (25). For a dipole source with any other orientation, the same integral (27) can be used for the field components, but the values of the g_j are different. They are now to be given for a dipole source (a) parallel to the x axis, (B 1) and (b) parallel to the y axis (B 2). In all cases the magnetic field $\boldsymbol{B}$ is parallel to the z axis. The fields for a dipole with any other orientation can then be found by first resolving the dipole into components parallel to the x, y, z axes, and then using a corresponding combination of (B 1), (B 2) and (28) to get the total fields. It is here assumed, as was done in the body of the paper, that the coordinates of the receiver are $(x, 0, z) = (r\sin\beta, 0, r\cos\beta)$. The superscript (l) on $n^{(l)}$ is omitted for the reasons given in § 4. The argument ξ in the following Bessel functions is given by (26).

Case (a). Dipole source parallel to x axis

The six g_j in (27) are

$$\left.\begin{aligned}
&\mathrm{i}(n_\rho n_z)^{-1}\{\epsilon_3(\epsilon_{xx}-n_z^2)-n_\rho^2\epsilon_{xx}+\tfrac{1}{2}n_\rho^2(n^2-\epsilon_3)\}J_0(\xi)-\tfrac{1}{2}\mathrm{i}n_\rho n_z^{-1}(n^2-\epsilon_3)J_2(\xi)\\
&\mathrm{i}(n_\rho n_z)^{-1}\epsilon_{xy}(\epsilon_3-n_\rho^2)J_0(\xi)\\
&(n^2-\epsilon_{xx})J_1(\xi)\\
&\tfrac{1}{2}\mathrm{i}\epsilon_{xy}\{n_\rho^{-1}(n_\rho^2-2\epsilon_3)J_0(\xi)-n_\rho J_2(\xi)\}\\
&-\mathrm{i}n_\rho^{-1}\{\tfrac{1}{2}n_\rho^2(\epsilon_3+\epsilon_{xx})+\epsilon_3(n_z^2-\epsilon_{xx})\}J_0(\xi)+\tfrac{1}{2}\mathrm{i}n_\rho(\epsilon_3-\epsilon_{xx})J_2(\xi)\\
&n_z^{-1}\epsilon_{xy}(\epsilon_3-n_\rho^2)J_1(\xi).
\end{aligned}\right\} \tag{B 1}$$

Case (b). Dipole source parallel to y axis

The six g_j in (27) are

$$\left.\begin{aligned}
&-(n_\rho n_z)^{-1}\epsilon_{xy}(\epsilon_3-n_\rho^2)\,J_0(\xi)\\
&\mathrm{i}(n_\rho n_z)^{-1}\{\epsilon_3(\epsilon_{xx}-n_z^2)-n_\rho^2\epsilon_{xx}+\tfrac{1}{2}n_\rho^2(n^2-\epsilon_3)\}J_0(\xi)+\tfrac{1}{2}n_\rho n_z^{-1}(n^2-\epsilon_3)\,J_2(\xi)\\
&-\epsilon_{xy}J_1(\xi)\\
&\mathrm{i}n_\rho^{-1}\{\tfrac{1}{2}n_\rho^2(\epsilon_3+\epsilon_{xx})+\epsilon_3(n_z^2-\epsilon_{xx})\}J_0(\xi)+\tfrac{1}{2}\mathrm{i}n_\rho(\epsilon_3-\epsilon_{xx})\,J_2(\xi)\\
&\tfrac{1}{2}\mathrm{i}\epsilon_{xy}\{n_\rho^{-1}(n_\rho^2-2\epsilon_3)\,J_0(\xi)+n_\rho J_2(\xi)\}\\
&n_z^{-1}(n_\rho^2\epsilon_{xx}+n_z^2\epsilon_3-\epsilon_3\epsilon_{xx})\,J_1(\xi).
\end{aligned}\right\}\qquad\text{(B 2)}$$

Some examples of the use of formulae equivalent to (B 1), (B 2) have been given by Stott (1982).

References

Akhiezer, A. I., Lapshin, V. I. & Stepanov, K. N. 1976 *J. exp. theor. Phys.* **70**, 1. (Engl. trans: *Soviet Phys. JETP* **43**, 42.)

Allis, W. P. 1959 M.I.T. Research Laboratory Electronics Quarterly Progress Report 54.

Al'pert, Ya. L. 1946 *Dokl. Akad. Nauk SSSR* **53**, 19, 708. (In Russian.)

Al'pert, Ya. L. 1948 *Izv. Akad. Nauk SSSR* Ser Phys. **12**, 241. (In Russian.)

Al'pert, Ya. L. 1967 *Space Sci. Rev.* **6**, 781.

Al'pert, Ya. L. 1980*a* *J. atmos. terr. Phys.* **42**, 205.

Al'pert, Ya. L. 1980*b* *J. atmos. terr. Phys.* **42**, 217.

Al'pert, Ya. L. & Moiseyev, B. S. 1980 *J. atmos. terr. Phys.* **42**, 521.

Arbel, E. & Felsen, L. B. 1963 In *Electromagnetic theory and antennas* (ed. E. C. Jordan), part I, p. 421. Oxford: Pergamon Press.

Booker, H. G. 1975 *Phil. Trans. R. Soc. Lond.* A **280**, 57.

Bremmer, H. 1949 *Terrestrial radio waves*. New York: Elsevier.

Budden, K. G. 1961 *Radio waves in the ionosphere*. Cambridge University Press.

Budden, K. G. 1976 *Proc. R. Soc. Lond.* A **350**, 143.

Budden, K. G. 1980 *J. atmos. terr. Phys.* **42**, 287.

Budden, K. G. & Daniell, G. J. 1965 *J. atmos. terr. Phys.* **27**, 395.

Budden, K. G. & Stott, G. S. 1980 *J. atmos. terr. Phys.* **42**, 791.

Bunkin, F. V. 1957 *J. exp. theor. Phys.* **32**, 338. (Engl. trans: *Soviet Phys. JETP* **5**, 277.)

Chester, C., Friedman, B. & Ursell, F. 1957 *Proc. Camb. phil. Soc.* **53**, 599.

Clemmow, P. C. 1963 In *Electromagnetic theory and antennas* (ed. E. C. Jordan), part I, p. 461. Oxford: Pergamon Press.

Clemmow, P. C. 1966 *The plane wave spectrum representation of electromagnetic fields*. Oxford: Pergamon Press.

Clemmow, P. C. & Mullaly, R. F. 1955 In *The physics of the ionosphere*, p. 340. London: The Physical Society.

Hines, C. O. 1963 In *Electromagnetic theory and antennas* (ed. E. C. Jordan), part I, p. 289. Oxford: Pergamon Press.

Kogelnik, H. 1960 *J. Res. natn. Bur. Stand.* D **64**, 515.

Miller, J. C. P. 1946 *The Airy integral*. Brit. Ass. Math. Tables, Part vol. B. Cambridge University Press.

Mittra, R. & Deschamps, G. A. 1963 In *Electromagnetic theory and antennas* (ed. E. C. Jordan), part I, p. 495. Oxford: Pergamon Press.

Morse, P. M. & Feshbach, H. 1953 *Methods of theoretical physics*. New York: McGraw-Hill.

Motz, H. & Kogelnik, H. 1963 In *Electromagnetic theory and antennas* (ed. E. C. Jordan), part I, p. 477. Oxford: Pergamon Press.

Rawer, K. & Suchy, K. 1967 *Handb. Phys.* **49/2**, 1.

Stix, T. H. 1962 *Theory of plasma waves*. New York and London: McGraw-Hill.

Storey, L. R. O. 1953 *Phil. Trans. R. Soc. Lond.* A **246**, 113.

Stott, G. F. 1982 Ph.D. thesis, Cambridge (unpublished).

Suchy, K. 1972 *J. plasma Phys.* **8**, 33.

Walker, A. D. M. 1977*a* *J. plasma Phys.* **17**, 467.

Walker, A. D. M. 1977*b* *J. plasma Phys.* **18**, 339.

Watson, G. N. 1944 *Theory of Bessel functions*. Cambridge University Press.

Westfold, K. C. 1949 *Aust. J. Scient. Res.* **2**, 168.

PHILOSOPHICAL TRANSACTIONS OF THE ROYAL SOCIETY A MATHEMATICAL, PHYSICAL & ENGINEERING SCIENCES